

THERMAL TRANSPORT IN SUPERCONDUCTORS
WITH COEXISTING
SPIN DENSITY WAVE ORDER

by

Sourav Sen Choudhury

A dissertation submitted in partial fulfillment
of the requirements for the degree

of

Doctor of Philosophy

in

Physics

MONTANA STATE UNIVERSITY
Bozeman, Montana

September 2021

©COPYRIGHT

by

Sourav Sen Choudhury

2021

All Rights Reserved

DEDICATION

I dedicate this to the memory of my grandparents, without whom I would have never made it through the turbulent years of my childhood.

ACKNOWLEDGEMENTS

I would like to acknowledge Prof. Anton B. Vorontsov for his patient guidance and support. I have learnt how to do theoretical physics from him: to think critically about a problem, pictorially represent complex calculations, to be aware of possible pitfalls, and to be not satisfied until one has obtained a sensible physical picture that explains the results. This training has been of an inestimable value to me. I would also like to express my gratitude to Prof. Yves Idzerda, Margaret Jarrett, Dr. Sam Mitchell and Donna Neggard for their invaluable support during many difficult times. Finally I would like to acknowledge my parents, without whom I would have never come this far.

TABLE OF CONTENTS

1. INTRODUCTION	1
Conventional Superconductors	1
Unconventional Superconductors	4
Heavy Fermions	6
Cuprates.....	8
Iron based Superconductors	11
Density Waves	12
Coexistence of Superconductivity and Spin Density waves	13
Motivation and Scope of the Thesis	14
Outline of the Thesis	19
2. THE SUPERCONDUCTING STATE	20
Bogoliubov Quasi-particles and Particle-Hole symmetry	20
The Mean-field Hamiltonian.....	20
Particle-Hole Symmetry.....	21
Diagonalization and Bogoliubov quasi-particles	22
The Nambu Matrix Green's Function.....	26
Self-consistent determination of the order parameter $\Delta_{\mathbf{k}}$	27
3. THE SPIN DENSITY WAVE STATE	30
Bogoliubov Quasiparticles in the SDW state.....	30
The Nambu Matrix Green's Function	34
The Self-consistent determination of order parameter M	35
4. BOLTZMANN KINETICS	37
The Boltzmann Equation for Electrons	37
Impurity scattering.....	39
Linearized Boltzmann Equation and the Quasiparticle Relaxation Time	41
Thermal Transport in Normal Metals.....	43
Thermal Transport in Superconductors	44
Thermal Transport in a metal with a Spin Density Wave	49
5. THERMAL TRANSPORT IN SUPERCONDUCTORS WITH COEXIST- ING SPIN DENSITY WAVE ORDER	53
Contribution of Authors and Co-Authors	53

TABLE OF CONTENTS – CONTINUED

Manuscript Information	54
6. CONCLUSION	68
REFERENCES CITED.....	71

LIST OF FIGURES

Figure	Page
1.1 Periodic Table of Superconducting elements from [17].....	2
1.2 Contrast of exterior field pattern (a) thin cylinder or sheet placed parallel to a uniform magnetic field and (b) a sphere in an uniform magnetic field from [90].	3
1.3 $T - P$ phase diagrams of CeRhIn ₅ in zero magnetic field from ac calorimetry (circles), ac susceptibility (triangles), and resistivity (diamonds for T_N and stars for T_c). At low pressure the ground state is antiferromagnetic. Below p_c^* , both antiferromagnetism (AF) and superconductivity (SC) coexists. At p_c^* the AF is suppressed suddenly before the quantum critical point at p_c is reached under pressure. Above p_c^* a purely superconducting ground state appears in zero magnetic field. The dashed line gives the expected pressure dependence of the Néel temperature in absence of superconductivity. Taken from[51].	7
1.4 Schematic phase diagram of n- and p-type cuprates, taken from [6]. The bright green colored area shows the extension of the antiferromagnetic phase in the case of no coexistence of SC and AF. The grey colored area shows the region with coexistence of SC and AF in the cuprates. Which of the these two scenarios is realized is not clearly known.	8
1.5 Doping-Temperature phase diagram of the iron pnictide superconductor Ba(Fe _{1-x} Co _x) ₂ As ₂ , taken from [76].	11
1.6	12
1.7 Schematic phase diagrams of Cuprates and Pnictides on electron or hole doping, taken from [12]. Not all details/phases are shown.	14
2.1 Temperature dependence of $\Delta(T)$ for a $d_{x^2-y^2}$ -wave superconductor	28

LIST OF FIGURES – CONTINUED

Figure	Page
3.1 The solid red curve shows the shapes of the perfectly nested (left panel) and partially nested (right panel) Fermi surfaces. The blue dotted square is the reduced Brillouin zone (RBZ) for $\mathbf{Q} = (\pi, \pi)$ -SDW ordering. When the FS is perfectly nested $\mu = 0$ and $t_2 = 0$ in our model (3.3), the SDW opens a gap along entire FS since the FS overlaps the RBZ completely. When the FS is partially nested $\mu = 0$ and $t_2/t_1 = 0.2$, only those parts of the FS that overlap with the RBZ get gapped with M	31
3.2 The quasiparticle energies in the Brillouin zone along the path $(0, 0) \rightarrow (\pi/2, \pi/2) \rightarrow (\pi, 0) \rightarrow (0, 0)$. The normal state band is depicted by the dashed magenta curve. The two quasi-particle bands $E_{\alpha, \beta}$ in the SDW phase are depicted by orange and blue curves respectively. The parameters are $t_2/t_1 = 0.2, M/t_1 = 0.2$	33
3.3 Temperature dependence of $M(T)$ for a SDW metal.....	36
4.1 Thermal conductivity for SC states: s -, $d_{x^2-y^2}$ - and d_{xy} -wave (dispersion parameters $t_1/2\pi T_C = 100, t_2/2\pi T_C = 10, \mu = 0$)	48
4.2 The solid red curve shows the shape of the FS for the above parameters, the dashed blue lines are a schematic representation of the order parameter profiles for the $d_{x^2-y^2}$ and d_{xy} pairing states.....	48
4.3 Thermal conductivity for a SDW metal (dispersion parameters for a perfectly nested FS are $t_1/2\pi T_{SDW} = 100, t_2/2\pi T_{SDW} = 0$ and for a partially nested FS are $t_1/2\pi T_{SDW} = 100, t_2/2\pi T_{SDW} = 10$)	52
4.4 The solid cyan curve shows the shapes of the partially nested and perfectly nested Fermi Surfaces for the above parameters. The regions of the FS gapped by the SDW order are shaded in orange.....	52

ABSTRACT

In this thesis we study thermal transport in a two-dimensional system with coexisting s - or d -wave Superconducting (SC) and Spin Density Wave (SDW) orders. We analyse the nature of coexistence phase in a tight-binding square lattice with $\mathbf{Q} = (\pi, \pi)$ SDW ordering. The electronic thermal conductivity is computed within the framework of the Boltzmann kinetic theory, using Born approximation for the impurity scattering collision integral. We describe the influence of the Fermi surface (FS) topology, the competition between the SC and SDW order parameters, the presence or absence of zero energy excitations in the coexistence phase, on the low temperature behavior of thermal conductivity of the various pairing states. We present qualitative analytical, and fully numerical results that show that the heat transport signatures of various SC states emerging from collinear SDW order are quite distinct, and depend on the symmetry properties of the SC order parameter under translation by the SDW nesting vector \mathbf{Q} . A combination of (π, π) -SDW and the $d_{x^2-y^2}$ pairing state results in fully gapped excitations, whereas (π, π) -SDW co-existing with either d_{xy} or s -wave pairing states may always have gapless excitations. There appear special stable Dirac nodal points that are not gapped by the SC order in the coexistence phase, resulting in finite residual heat conductivity.

INTRODUCTION

In this chapter we give a brief introduction to elemental superconductors and then move on to describe superconducting materials that are at the forefront of current research. We set up the motivation for the Thesis and give a brief outline of the main chapters that are to follow.

Conventional Superconductors

The phenomenon of Superconductivity was discovered by Heike Kamerlingh Onnes while conducting a series of low temperature experiments at the University of Leiden in 1911. He found that below the transition temperature $T_c = 4.2K$, the resistance in a solid mercury wire immersed in liquid helium suddenly vanished. He noted in his notebook, “ Mercury has passed into a new state, which on account of its extraordinary electrical properties may be called the superconductive state ” [91]. Since then most elements Fig. 1.1 have been found to become superconducting at low temperatures. Superconductors also exhibit the so called Meissner-Ochsenfeld-effect [34, 83] i.e. magnetic fields do not penetrate the bulk of a superconductor. When a superconductor is cooled in a weak magnetic field, at the transition temperature persistent currents arise on the surface and circulate so as to cancel the flux density inside. Superconductors can be classified into two types, the so-called type-I superconductors, where there the effects of fields strong enough to destroy superconductivity depend on the shape of the sample. In the case of a long, thin cylinder or sheet placed parallel to a uniform magnetic field H_a , everywhere along the surface the field is equal to H_a see Fig. 1.2. Therefore superconductivity is destroyed when the applied field reaches the critical value H_c . For other geometries like a sphere, field lines have a higher density

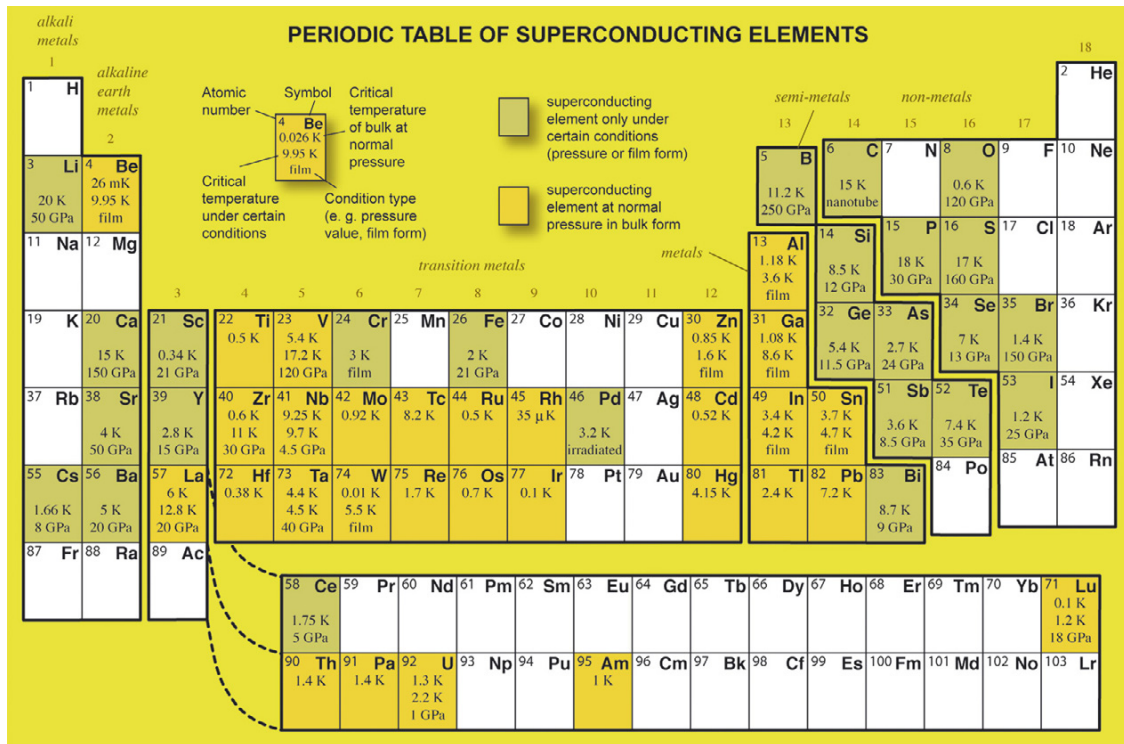


Figure 1.1: Periodic Table of Superconducting elements from [17]

at the equator compared to the poles see Fig. 1.2. Far away from the sphere, where any perturbations caused by it average out, the applied field H_a is lower than at the equator. A natural question arises what happens when the equatorial field reaches the critical value H_c . Clearly H_a at that moment is below H_c and therefore, the whole sphere cannot revert to the normal state. On the other hand, the whole sphere is not permitted to be superconducting either, because the field at the equator has already reached the critical value. This leads to a coexistence of alternating superconducting and normal regions within the sphere called the intermediate state. The intermediate state is expected whenever the applied field lies in the range $1 - n < \frac{H_a}{H_c} < 1$, where n is the demagnetizing factor and depends on the shape of the sample, for example $n = 1/3$ for a sphere. The whole sphere transitions to the normal state once the applied field H_a reaches the critical value H_c everywhere on the sphere.

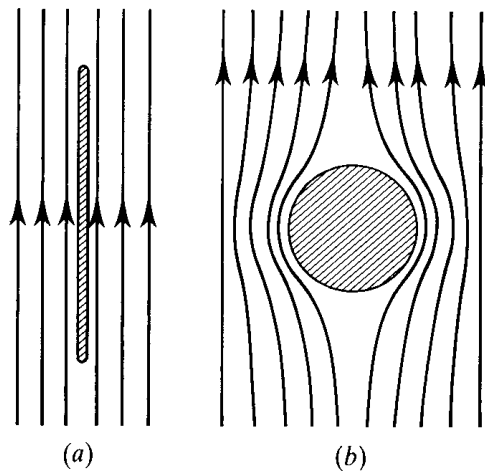


Figure 1.2: Contrast of exterior field pattern (a) thin cylinder or sheet placed parallel to a uniform magnetic field and (b) a sphere in an uniform magnetic field from [90].

In type-II superconductors, there exists a lower critical field H_{c1} above which the magnetic flux lines can penetrate the bulk of the superconductor without destroying the bulk superconductivity and an upper critical field H_{c2} above which the superconductivity is destroyed. Most elemental superconductors are of type-I, while most superconducting alloys and compounds are of type-II.

Further in superconductors there exists an energy gap of size 2Δ for elementary excitations, which can be observed directly and indirectly in many ways, for example the exponential decrease with decreasing temperature of the thermal conductivity of a number of superconductors below $T_c/3$ first found by Goodman in Tin [35].

In 1957, Bardeen, Cooper and Schrieffer formulated the correct microscopic theory of superconductivity, referred to as BCS theory [10]. Further extensions were made by Bogololiubov [16], Gorkov [36] and Eliashberg [27, 28]. The BCS theory with the above extensions could describe all superconductors known at the time.

According to the BCS theory, electrons overcome the Coulomb repulsion via the exchange of phonons. This can be pictured in real space in the following manner: an

electron moving through a lattice of positively charged ions displaces an ion and creates a local excess of positive charge, which attracts the next passing electron. This retarded attraction is possible because the atoms are much heavier than the electrons and therefore move much slower. In momentum space, one electron emits a virtual phonon of momentum $\hbar\mathbf{q}$ which is absorbed by a second electron. This interaction is given by

$$V_{eff}(\mathbf{q}, \omega) = |g_{\mathbf{q}\lambda}|^2 \frac{1}{\omega^2 - \omega_{\mathbf{q}\lambda}^2},$$

where \mathbf{q} and $\omega_{\mathbf{q}\lambda}$ are the wavevector and energy of the phonon and $g_{\mathbf{q}\lambda}$ is the electron-phonon coupling matrix element. A negative V_{eff} means a attractive interaction. In BCS theory $\omega_{\mathbf{q}\lambda}$ is replaced by ω_D the phononic Debye frequency and only electrons within $\pm k_B T$ of the Fermi surface are considered. Thus ω is always much smaller than ω_D at temperatures relevant to conventional superconductivity. The end result is a net attractive effective interaction. Due to this interaction two electrons with opposite spin and momentum form bound states, so-called Cooper pairs, which then build up a phase coherent condensate. The new state is characterized by a gap function or order parameter Δ which is non zero in the superconducting state, only in the vicinity of the Fermi surface.

Unconventional Superconductors

Classification of the superconducting states are based on symmetry properties of the order parameter Δ which are related to the properties of the wave-function of the Cooper pair. In the original BCS formulation the electrons comprising the Cooper pair are in a singlet state having opposite spins. The spin part of the wave-function thus is antisymmetric with respect to particle exchange. This requires the momentum dependent part of the wave-function to be even, which can only happen if the orbital angular momentum (l) of the pair wave-function is even. The gap function for singlet superconductors can be written

as $\Delta(\mathbf{k}) = i\sigma_y\psi(\mathbf{k})$, [87], where the scalar valued function satisfies $\psi(-\mathbf{k}) = \psi(\mathbf{k})$. In the original BCS theory, the angular momentum of the pair wave-function was taken to be zero. Obviously this is not the only possibility, other pairing states are also feasible. For superconductors with an inversion center, Cooper pairs can form either singlets with even orbital angular momentum in $s(l = 0), d(l = 2), \dots$ states, or triplets with odd orbital angular momentum, i.e. $p(l = 1), f(l = 3) \dots$ states. Therefore the functions $\psi(\mathbf{k})$ can be expressed as linear combinations of spherical harmonics [64]

$$\psi_l(\mathbf{k}) = \sum_{m=-l}^l a_{lm} Y_{lm}(\hat{\mathbf{k}}) \quad \text{for } l = 0, 2, 4, \dots \quad (1.1)$$

In an isotropic system which is invariant under all spatial rotations (elements of group $SO(3)$), the irreducible representations are labelled by the value of l and the $2l + 1$ spherical harmonics with given orbital angular momentum l forms the basis of the irreducible representation. Thus in isotropic systems the types of Cooper pairing are in one-to-one correspondence with the irreducible representations of the group of three dimensional rotations. In the case of crystals the superconducting states are classified by the subgroups $H \subset G$ that leave the superconducting order parameter $\Delta(\mathbf{k})$ invariant. The group G is $G = G_c \times T \times U(1)$. Here G contains the symmetry group of the crystal G_c , the operations of time reversal T and gauge transformations $U(1)$, we have assumed there is no spin-orbit coupling [64]. The superconducting states in the crystal are in one to one correspondence with the irreducible representations (IRs) Γ of G . An IR can be represented with a set of basis functions $\Phi_i^\Gamma(\mathbf{k})$ for $1 \geq i \leq d_\Gamma$, where d_Γ is the IR's dimension. Thus in the case of crystals the expansion (1.1) becomes

$$\psi_l(\mathbf{k}) = \sum_{i=1}^{d_\Gamma} \alpha_i \Phi_i^{\Gamma_g}(\hat{\mathbf{k}}) \quad (1.2)$$

where α_i are complex amplitudes for the components of the order parameter and the index g denotes functions even in $\hat{\mathbf{k}}$. The conventional superconducting state has the full point group symmetry of the crystal lattice, i.e. it belongs to the identity representation A_{1g} and is determined by the class $H = G_c \times T$. Unconventional superconductivity is realized whenever $H \neq G_c \times T$ i.e. they do not possess the full point group symmetry of the crystal lattice.

As an example the cuprate superconductors like $\text{La}_{2-x}\text{Ba}_x\text{CuO}_4$ have crystal lattices of tetragonal symmetry i.e. $G_c = D_4 \times I$ where $D_4 = C_n, U_n$ at $n = 0, 1, 2, 3$ comprises of the rotations C_n along the \hat{z} axis by angles $\pi n/2$ and rotations U_n by angle π about the axes $\hat{x} \cos(\frac{\pi n}{4}) + \hat{y} \sin(\frac{\pi n}{4})$, I represents inversion symmetry. Experiments point to the cuprates having an order parameter $\Delta(\hat{\mathbf{k}}) \propto \hat{k}_x^2 - \hat{k}_y^2$. It is called the d -wave state because its angular dependence can be accounted with spherical harmonics at $l = 2$. The order parameter $\Delta(\hat{\mathbf{k}})$ is not invariant under $D_4 \times I$ but instead the symmetry group is $D_4(D_2) \times I$ where $D_4(D_2) = \{C_{2k}, U_{2k}, e^{i\pi}C_{2k+1}, e^{i\pi}U_{2k+1}\}$ at $k = 0, 1$. The phase $e^{i\pi} = 1$ is needed to compensate the sign change of the order parameter under rotations. In the above discussion we have limited ourselves to singlet superconductors since this thesis we only study singlet pairing states. The symmetry classification of triplet states follow along similar lines and can be found in [64]. Unconventional superconductors also differ from superconductors described by BCS theory in that, their pairing mechanism is not derived from electron-phonon interaction [70]. Alternative pairing mechanisms include the Kohn Luttinger mechanism based on renormalized Coloumb interaction or mechanisms based on spin fluctuation exchange, further details can be found in [57, 81, 87].

Heavy Fermions

One of the first discovered families of unconventional superconductors were the heavy Fermion materials, which started with the discovery [88] of the compound CeCu_2Si_2 in 1979. In heavy fermion superconductors the f -electron derived bands yield effective masses up to

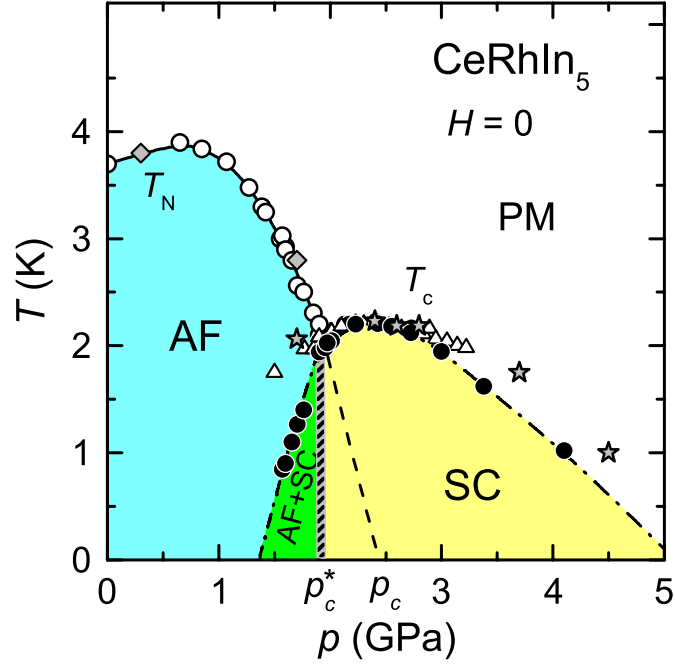


Figure 1.3: $T - P$ phase diagrams of CeRhIn_5 in zero magnetic field from ac calorimetry (circles), ac susceptibility (triangles), and resistivity (diamonds for T_N and stars for T_c). At low pressure the ground state is antiferromagnetic. Below p_c^* , both antiferromagnetism (AF) and superconductivity (SC) coexists. At p_c^* the AF is suppressed suddenly before the quantum critical point at p_c is reached under pressure. Above p_c^* a purely superconducting ground state appears in zero magnetic field. The dashed line gives the expected pressure dependence of the Néel temperature in absence of superconductivity. Taken from [51].

100 times the bare electron mass. The properties of the heavy fermion superconductors include ferromagnetism, antiferromagnetism, and even coexistence of magnetism and superconductivity. As an example for the variety of phases present in the heavy fermion superconductors, the pressure-temperature phase diagram of CeRhIn_5 is shown in Fig 1.3. CeRhIn_5 is antiferromagnetically ordered below $T_N = 3.8\text{K}$ at ambient pressure. It orders in an incommensurate magnetic structure with an ordering vector $\mathbf{Q} = 1/2, 1/2, 0.297$ (see discussion of spin density waves below). In zero magnetic field AF is suppressed rapidly for pressures $p > p_c^* = 1.95\text{ GPa}$ and the ground state is superconducting with probably d -wave symmetry [51]. At p_c the antiferromagnetic transition temperatures (T_N) and the

superconducting transition temperatures (T_C) become the same. When $T_c > T_N$ no long range order magnetic order exists as large parts of the Fermi surface are gapped due to onset of SC. Below p_c^* i.e ($T_n > T_c$) antiferromagnetism and superconductivity coexist. The nature of the superconducting state below p_c^* is a matter of debate [50]. In these materials superconductivity is believed to be mediated by magnetic interactions.

Cuprates

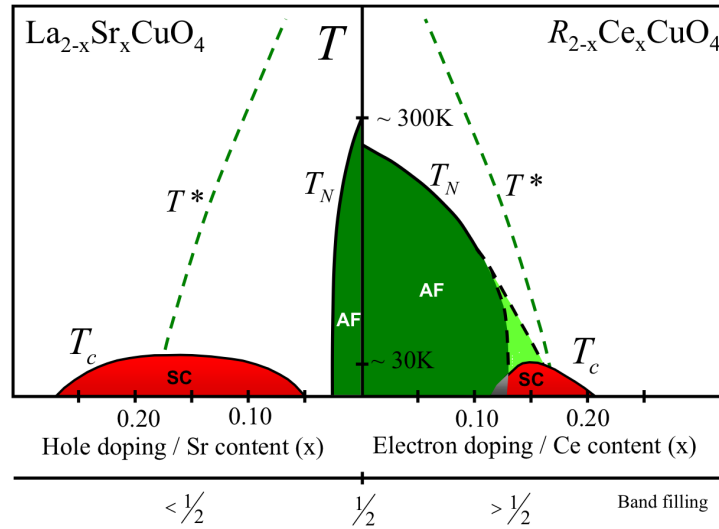


Figure 1.4: Schematic phase diagram of n- and p-type cuprates, taken from [6]. The bright green colored area shows the extension of the antiferromagnetic phase in the case of no coexistence of SC and AF. The grey colored area shows the region with coexistence of SC and AF in the cuprates. Which of these two scenarios is realized is not clearly known.

The next family of high temperature superconductors to be discovered were the Cuprates in 1986 by J. Bednorz and K. Müller [13], for which they won the Nobel prize in 1987. They found superconductivity in the $\text{La}_{2-x}\text{Ba}_x\text{CuO}_4$ system with $T_c \approx 30\text{K}$. Soon the transition temperature tripled with the discovery of the YBCO system with $T_c \approx 90\text{K}$ [93]. The cuprate superconductors are based on ceramic perovskites and have a complex layered structure. The important structural element common to all cuprates is the CuO_2 layers which

are separated by spacer layers containing other atoms. The spacer layer is called the charge reservoir because dopant atoms are usually introduced there, rather than directly into the CuO_2 planes. Thus the spacer layers control the carrier concentration in the CuO_2 planes. The CuO_2 planes are believed to be responsible for the formation of superconductivity in the Cuprates. Therefore in theoretical treatments of the cuprates, usually only models of the two-dimensional CuO_2 layers are considered.

The properties of all cuprates are extremely sensitive to doping. Fig 1.4 shows the general temperature-doping phase diagram of cuprates. One can see that without doping both types of cuprates are antiferromagnetic Mott insulators with Néel temperatures $T_N \approx 250 - 300K$. A Mott insulator is a material that is expected to be a metal as per the predictions of conventional band theories, but instead turn out to be insulators (particularly at low temperatures). In the case of cuprates, if we look at the parent compound La_2CuO_4 , simple electron counting finds that the copper must have valence +2 here, resulting in an outer shell electron configuration $3d^9$. On the other hand Oxygen's valence is -2 , leading to a closed shell configuration $2s^22p^6$. Thus in the CuO_2 planes there is one hole per unit cell, and simple band theory would thus predict the system to be a metal. Instead La_2CuO_4 is an antiferromagnetic insulator. This insulating behaviour is due to strong electron–electron interactions, which are not considered in conventional band theory. Mott transition is a transition from a metal to an insulator, driven by the strong interactions between electrons. One of the simplest models that can capture the Mott transition is the Hubbard model [30]. In this thesis we do not try to model this insulating antiferromagnetic state.

Upon hole-doping the Néel temperature is rapidly falls and the antiferromagnetic phase vanishes completely at about 5 percent of hole doping. At a hole doping of 0.16 an unconventional superconducting phase is found. The maximal T_c is reached at a doping level of 0.16, therefore this doping level is referred to as optimal while smaller and higher hole-doping levels are called under-doped and over-doped, respectively. It is now well

established that the superconducting phase on the hole-doped side of the phase diagram is unconventional, with the superconducting order parameter having $d_{x^2-y^2}$ symmetry [85].

In the over-doped region one finds the usual Fermi liquid behavior. At smaller dopings below a temperature T^* , there exists the so called pseudo-gap region, i. e. the Fermi surface is not simply gapped but folded back and forms a number of disconnected, but closed Fermi pockets [9]. Such a behavior is expected to be realized in the presence of a Spin(Charge) Density Wave [63]. Density waves are broken symmetry states of metals, brought about by electron-phonon or by electron-electron interactions. The ground states are the coherent superposition of electron-hole pairs, and, as the name implies, the charge density or spin density is not uniform but displays a periodic spatial variation. The existence of Density Waves are one possible explanation of the pseudo gap phase [65, 95]. The presence of the pseudo-gap region above the under-doped side of the superconducting dome also raises the question whether the order responsible for the pseudo-gap behavior persists in the superconducting phase. There is a possibility that part of superconducting dome coexists with some kind of Density Wave [18]. In this case the T^* -line in Fig 1.4 would not terminate at T_c , but extend into the superconducting phase and terminate at zero temperature at a doping level of about 0.19. However such a coexistence is still a matter of debate.

We now turn to the electron doped cuprates shown in the right panel of Fig 1.4. As in the hole-doped case there is a superconducting phase around a doping level of about 0.16, but the maximal T_c and the doping width of this phase are significantly smaller. There is no general consensus on the symmetry of the superconducting order parameter. Some experimental evidence indicate $d_{x^2-y^2}$ symmetry as in the hole-doped cuprates, but s-wave symmetry is also considered to be a possibility [6]. Furthermore, since the T_c and T_N lines intersect at non-zero temperatures there is the possibility of coexistence of antiferromagnetism and superconductivity in the electron doped cuprates. There is quite a bit of experimental evidence of superconductivity coexisting with Spin-Density Wave order [3, 6, 45, 53, 59,

86, 94]. The overall situation in cuprates and in particular in electron doped cuprates is complicated, for recent reviews look at [38, 77].

Iron based Superconductors

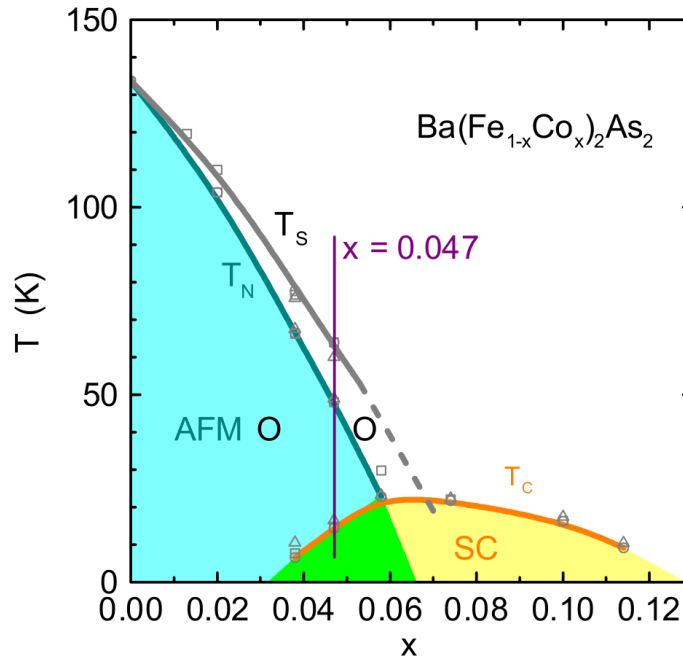


Figure 1.5: Doping-Temperature phase diagram of the iron pnictide superconductor $\text{Ba}(\text{Fe}_{1-x}\text{Co}_x)_2\text{As}_2$, taken from [76].

In 2008, a new class of superconductors was discovered [44] beginning with the alloy $\text{LaFeAsO}_{0.89}\text{F}_{0.11}$. These are the so called iron based superconductors. The iron pnictides are quasi-two-dimensional layered materials containing FePn (Pn refers to pnictogen atom) layers. They exhibit a complex phase diagram, containing phases with spin density wave antiferromagnetism and superconductivity as well as the coexistence of both [72, 76]. As an example the phase diagram of $\text{Ba}(\text{Fe}_{1-x}\text{Co}_x)_2\text{As}_2$ is shown in Fig 1.5.

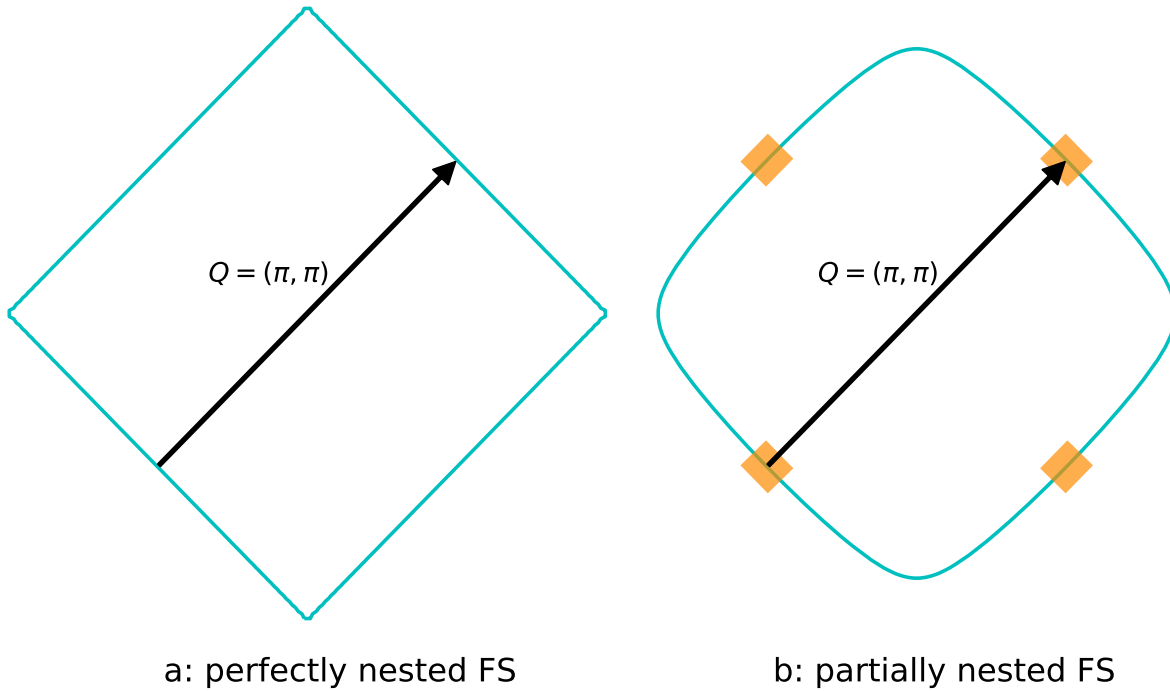
Density Waves

Figure 1.6

There are two types of density waves that are relevant in superconducting materials, Charge Density Waves (CDW) and Spin Density Waves (SDW). Charge density waves were introduced by Peierls in 1930 [74]. He showed that a one dimensional electron system coupled to a lattice is unstable with respect to the formation of a periodic modulation of the electron density and an associated periodic distortion of the lattice [40]. A Spin-Density Wave (SDW) is conceptually similar to a CDW and was introduced by Overhauser in 1962 [71]. In the case of an SDW, the modulated density is the spin density, which results in antiferromagnetic behavior of such a state [29]. Density waves form due to the existence of nesting vectors in the materials' Fermi surface (FS). The concept of a nesting vector is illustrated in the Fig 1.6. A nested Fermi surface has parallel regions connected by a nesting vector \mathbf{Q} . For a perfectly nested Fermi Surface all points on the FS are connected by \mathbf{Q} , whereas for an

partially nested Fermi surface, only points belonging to the parallel parts of the FS (shown by the orange shaded regions in Fig 1.6) are connected by \mathbf{Q} . The real-space periodicity of the resulting spin-density wave is given by $2\pi/\mathbf{Q}$. If the new periodicity is a rational fraction or multiple of the lattice constant, the density wave is said to be commensurate, otherwise the density wave is termed incommensurate.

In general due to an enhanced tendency of Fermi surface nesting CDW's and SDW's form preferably in low dimensional materials. Examples for quasi one-dimensional materials known to have a Charge Density Wave phase are NbSe_3 and $\text{K}_{0.3}\text{MoO}_3$ [40]. Several quasi-2D systems, including layered transition metal dichalcogenides [61], undergo Peierls transitions to form quasi-2D CDWs. These result from multiple nesting wavevectors coupling different flat regions of the Fermi surface [52]. The most prominent example of a SDW material is Cr [29], which transitions from a paramagnetic to SDW state at a Néel temperature of 311K. Cr is a body-centered cubic metal whose Fermi surface features many parallel boundaries between electron pockets and is therefore susceptible to the nesting instability. Unlike in a superconductor where electrons with opposite momentum and spin pair up, in density waves the pairing takes place between electrons and holes with momentum differing by the fixed momentum Q . The momentum Q is the momentum of the density modulation. If this momentum is related to the reciprocal lattice vectors by a simple rational number, the Density Wave is referred to as commensurate, otherwise as incommensurate. In this thesis we will only consider commensurate Spin Density Waves.

Coexistence of Superconductivity and Spin Density waves

As discussed before the electronic phase diagrams of many highly correlated systems are complex, with multiple broken symmetry phases appearing with similar ordering temperatures as dopant concentration is varied over wide ranges. For example, in Fig 1.7 we see the that there is a proximate antiferromagnetic (AF) state in the schematic phase

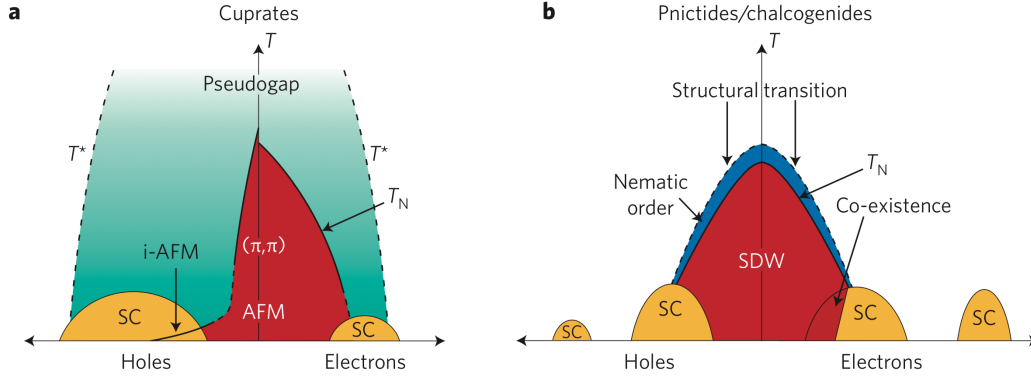


Figure 1.7: Schematic phase diagrams of Cuprates and Pnictides on electron or hole doping, taken from [12]. Not all details/phases are shown.

diagrams of superconductors such as cuprates and iron pnictides [12]. Theoretically this problem has been studied for several decades from a large number of different perspectives, [8, 15, 23, 39, 43, 46, 47, 48, 54, 55, 56, 62, 65, 67, 68, 69, 73, 80, 92]. These studies all indicate that the superconducting state emerging out of an antiferromagnetic background is highly non-trivial. The presence of the SDW can influence the momentum dependence and nodal structure of the gap [15, 43, 46, 80]. The structure and properties of the superconducting gap in the presence of coexisting antiferromagnetic order is a rich problem and there are many possibilities based on material specific models of cuprates, pnictides and heavy fermions. One of the aims of this thesis is to shed light on this topic by studying a very general model that captures the essential physics of superconductivity coexisting with spin density wave antiferromagnetic order and therefore is relevant to the materials mentioned above.

Motivation and Scope of the Thesis

As mentioned before the problem of superconductivity(SC) coexisting with antiferromagnetic(AF) order has been studied quite extensively. Early studies [8, 78] focused on generalizing the Abrikosov-Gorkov theory for pairbreaking in superconductors due to a dilute

concentration of magnetic impurities, to the case when the magnetic ions are present in a large concentration or on a regular lattice. The case in which the magnetic ions undergo a transition to an antiferromagnetic phase was considered and the strong influence of AF on SC was explained through Fermi Surface(FS) nesting [78]. These studies were aimed at explaining coexistence of AF and SC in compounds that contain a lattice of magnetic rare earth ions [60]. The theory of coexistence of SC and SDW's, where both the orders were treated on an equal footing under the mean field approximation, was worked out by Machida and his collaborators in a series of papers in the 1980's [46, 47, 54, 55, 56]. On the basis of an imperfect-nesting-band model in two dimensions it was shown that anisotropic pairing states can be categorized into two classes: less-competitive and competitive states according to the combined symmetry of the SC order parameter (parity and translational symmetry determined by the nesting vector). The materials of interest for these studies were the heavy fermion superconductors. Based on the same mean field theory of antiferromagnetic superconductors several authors also studied thermodynamics, impurity and spin fluctuation effects [67, 68, 71]. It was shown that the temperature dependence of the order parameter $\Delta(T)$, specific heat $C(T)$ and the critical field $H_c(T)$ deviate markedly from BCS theory. The interplay between antiferromagnetism and superconductivity was studied for specific heavy Fermion superconductors in particular CeCoIn₅ in [48]. It was shown that the near-perfect nesting of the quasiparticle pockets created by Zeeman pair-breaking near the nodal regions creates the conditions for the antiferromagnetic instability even when the normal state Fermi surface is not nested. In earlier studies [4, 42] it was shown that the amplitude modulation of the superconducting order parameter, $\Delta(\mathbf{r})$, is essential and drives a spin density wave(SDW). Studies concentrating on coexistence of SDW and SC in Cuprates have also received attention. In [69] properties of a spin-density-wave antiferromagnetic mean-field ground state with d -wave superconducting correlations was discussed, whereas in [15] the perturbative stability of zero energy nodal points in the quasiparticle spectrum

of d -wave superconductors in the presence of coexisting commensurate orders was studied. Coexistence of SDW and SC in multiband metals like the Iron based superconductors have also been investigated by several authors [43, 73, 80, 92]. These studies have focused on elucidating the unconventional structure of the order parameter and the superconducting phase diagram.

However, much less is known about thermal transport in superconductors with coexisting SDW order. Previous studies with models specific to cuprates have shown [26, 82] that, in d -wave superconductors heat transport by nodal quasiparticles shows an impurity-independent, universal, limit at low temperatures [25, 37]. This is experimentally observed in many materials [84, 89]. Therefore theoretical investigations of thermal transport in “superconductor + density wave order” systems [15, 26, 82] have focused on the issue of how the CDW or SDW order influences the $T \rightarrow 0$ limit of thermal conductivity in $d_{x^2-y^2}$ superconductors. These calculations indicated that the robustness of the universal limit of thermal conductivity of $d_{x^2-y^2}$ superconductors depends on direction of the ordering vector, and the type of the coexisting order (CDW or SDW).

The transport calculations were carried out in $2D$, within Kubo linear response theory using the Green’s function technique, where impurity effects were included only through non-self-consistent energy broadening parameter. The CDW or SDW were also incorporated non-self-consistently, as an additional tunable small order on top of the SC state, and neither the nature of the co-existence, nor its temperature dependence, was investigated. Another study [19] looked at the changes in zero-temperature heat transport across continuous SC to SC+SDW transition for $d_{x^2-y^2}$ superconductor, employing the same non-self-consistent treatments of impurities and SDW order, assumed to be controlled by doping. These calculations show that thermal conductivity behaves very differently depending whether emerging SDW is commensurate or incommensurate. For a commensurate SDW the SC \rightarrow SC+SDW transition results in a gradual drop in thermal conductivity as a function

of growing SDW order, whereas incommensurate SDW results in a sharp drop across the transition [19].

As described above correlated electronic materials which exhibit unconventional superconductivity (SC), have phase diagrams that are intrinsically complex. Multiple distinct broken-symmetry phases appear as parameters such as composition, pressure, and magnetic field are varied. Our focus in this thesis has been on unconventional superconductors (materials such as cuprates, iron pnictides, and heavy fermions) which have regions in their phase diagrams where SC and SDW orders coexist. However, this is just the tip of the iceberg, various other orders like charge-density wave (CDW), nematicity, pair-density wave (PDW) and possibly other forms of symmetry-breaking order—also occur with comparable onset temperatures in a wide range of material parameters [32]. It has become common in literature to describe such ordering tendencies as “competing orders”. Even if we limit ourselves to describing multiple coexisting orders at the level of the mean field approximation, there are non trivial effects that come from the “intertwining” of these orders. In other words the interplay of these multiple orders leads to new features that would be absent if they operated independently of one another. One purpose of this thesis is to emphasize the effects that arise from interplay of different orders, taking the coexistence SC and the SDW orders as a case study. Previous studies on the coexistence of superconductivity(SC) and antiferromagnetic(AF) order have not clearly addressed this aspect of the problem - in particular the nature of the quasiparticle excitations in different coexistence states arising from the interplay between the SDW order and SC pairing states of s -wave, $d_{x^2-y^2}$ and d_{xy} symmetry. We find that a combination of (π, π) -SDW and the $d_{x^2-y^2}$ pairing state results in fully gapped excitations, whereas (π, π) -SDW coexisting with either d_{xy} or s -wave pairing states may always have gapless excitations. There appear special stable Dirac nodal points that are not gapped by the SC order in the coexistence phase. The existence of these Dirac points has been reported for the first time in this thesis. Therefore we can see that the

“intertwining” of SC and SDW orders can have a significant impact on the very nature of the quasiparticle excitations of the system. This would in turn have a non trivial impact on the thermodynamic and transport properties of such systems.

The study of thermal transport in superconductors with coexisting SDW order is an important subject because, most unconventional superconductors have a nodal gap structure i.e there exist points on the Fermi surface (FS) called nodes, where the superconducting gap is zero. As the energy gap is small around the nodes, the nodal quasiparticles can be easily excited and they dominate the heat transport properties of such superconductors. Therefore the behaviour of the thermal conductivity is heavily influenced by the nature of the low energy quasiparticles in the coexistence state. As a result thermal conductivity measurements can reveal the gap structure of unconventional superconductors [58, 84]. Therefore in this thesis we look at the impact of the “intertwining” of SC and SDW orders on the temperature behavior of the thermal conductivity of several pairing states: s -wave, $d_{x^2-y^2}$ and d_{xy} symmetry. The main focus of previous works [19, 25, 82] on thermal transport in superconductors with coexisting SDW order has been the $T = 0$ limit investigation of thermal conductivity when a phenomenologically introduced SDW state covers the nodes of the $d_{x^2-y^2}$ SC order parameter. In this thesis we investigate full temperature range and microscopically evaluate co-existence of SDW and SC orders, with SC order appearing out of SDW background. We also treat other SC pairing states, like s -wave or d_{xy} orders and self-consistently compute all order parameters, as well as the impurity scattering rates. The different heat transport signatures of the various SC states emerging from the SDW background is the main result of this thesis, which has not been addressed in any previous work. As has been stated before, coexistent magnetic and superconducting states have been discovered in cuprates, iron-based superconductors, and heavy-fermion superconductors, therefore this theoretical study may be useful for identifying order parameter symmetry of such compounds.

Outline of the Thesis

The thesis is organized as follows. In chapter 2 the basic properties of the superconducting state are summarized. The Bogoliubov quasiparticles and the particle-hole symmetry of the mean field Hamiltonian is described. The self consistent equation for the order parameter is derived using the Nambu Green's function.

In chapter 3 the spin density wave state is discussed. The discussion is along similar lines as the previous chapter showing the unity of the methods used. The focus is again on the Bogoliubov quasiparticles and self consistent determination of the mean field order parameter.

In chapter 4 thermal transport in normal metals, superconductors and spin density wave metals is studied within the formalism of the Boltzmann transport theory.

Chapters 2, 3, 4 are meant to provide the necessary background for chapter 5 where the manuscript "*Thermal transport in superconductors with coexisting spin density wave order*" by Sen Choudhury and Vorontsov -*Phys. Rev. B* **103**, 104501 (2021) is reproduced.

In Chapter 6 the most important results are summarized.

THE SUPERCONDUCTING STATE

Bogoliubov Quasi-particles and Particle-Hole symmetry

In this section the quasi-particle method for superconductivity is reviewed. The aim is to explain how the superconducting state can be described in terms of appropriately defined quasi-particles.

The Mean-field Hamiltonian

The mean-field Hamiltonian that describes the superconducting state can be written in the most general form as

$$\begin{aligned}
 H &= H_0 + H_{SC}, \\
 H_0 &= \sum_{\mathbf{k}, s_1, s_2} \xi_{s_1, s_2}(\mathbf{k}) c_{\mathbf{k}s_1}^\dagger c_{\mathbf{k}s_2}, \\
 H_{SC} &= \frac{1}{2} \sum_{\mathbf{k}, s_1, s_2} \Delta_{s_1, s_2}(\mathbf{k}) \left(c_{\mathbf{k}s_1}^\dagger c_{-\mathbf{k}s_2}^\dagger + h.c. \right).
 \end{aligned} \tag{2.1}$$

where $c_{\mathbf{k}s}(c_{\mathbf{k}s}^\dagger)$ is the annihilation(creation) operator of the electron with momentum \mathbf{k} and spin s , and $\xi_{s_1, s_2}(\mathbf{k})$ is the band Hamiltonian which gives the momentum and spin dependent band energy and can be viewed as a 2×2 matrix in spin space. The mean field order parameter is given by

$$\Delta_{s's'}(\mathbf{k}) = - \sum_{\mathbf{k}', s_3, s_4} g_{s, s', s_3, s_4}(\mathbf{k}, \mathbf{k}') \langle c_{-\mathbf{k}', s_3} c_{\mathbf{k}', s_4} \rangle \tag{2.2}$$

where $g_{s, s', s_3, s_4}(\mathbf{k}, \mathbf{k}')$ is the pairing interaction responsible for forming Cooper pairs. We do not confine our analysis to any particular pairing mechanism, only requiring $g_{s, s', s_3, s_4}(\mathbf{k}, \mathbf{k}')$ to satisfy the following conditions coming from the anti-symmetry of fermionic

annihilation(creation) $c_{\mathbf{k}s}$ ($c_{\mathbf{k}s}^\dagger$) operators.

$$\begin{aligned}
g_{s_1, s_2, s_3, s_4}(\mathbf{k}, \mathbf{k}') &= -g_{s_2, s_1, s_3, s_4}(-\mathbf{k}, \mathbf{k}') \\
&= -g_{s_1, s_2, s_4, s_3}(\mathbf{k}, -\mathbf{k}') \\
&= g_{s_4, s_3, s_2, s_1}(\mathbf{k}, \mathbf{k}')
\end{aligned} \tag{2.3}$$

It is convenient to recast (2.1) into 4×4 matrix constructed from spin up-down and particle-hole spaces

$$\begin{aligned}
H &= \frac{1}{2} \sum_{\mathbf{k}, s_1, s_2} \begin{pmatrix} c_{\mathbf{k}s_1}^\dagger & c_{-\mathbf{k}s_1} \end{pmatrix} \mathcal{H}_{4 \times 4}(\mathbf{k}) \begin{pmatrix} c_{\mathbf{k}s_2} \\ c_{-\mathbf{k}, s_2}^\dagger \end{pmatrix} \\
\mathcal{H}_{4 \times 4}(\mathbf{k}) &= \begin{pmatrix} \xi_{s_1, s_2}(\mathbf{k}) & \Delta_{s_1, s_2}(\mathbf{k}) \\ \Delta_{s_1, s_2}^\dagger(-\mathbf{k}) & -\xi_{s_1, s_2}^T(-\mathbf{k}) \end{pmatrix}
\end{aligned} \tag{2.4}$$

Note that the spin indices make $\xi_{s_1, s_2}(\mathbf{k})$ and $\Delta_{s_1, s_2}(\mathbf{k})$ to be 2×2 matrices in spin space, thus $\begin{pmatrix} c_{\mathbf{k}s_1}^\dagger & c_{\mathbf{k}s_1} \end{pmatrix}$ is a four component vector $\begin{pmatrix} c_{\mathbf{k}\uparrow}^\dagger, c_{\mathbf{k}\downarrow}^\dagger, c_{-\mathbf{k}\uparrow}, c_{-\mathbf{k}\downarrow} \end{pmatrix}$.

Particle-Hole Symmetry

The matrix form of the Hamiltonian (2.4) is anti-symmetric under the particle-hole transformation

$$\begin{aligned}
\mathcal{C} \mathcal{H}_{4 \times 4}(\mathbf{k}) \mathcal{C}^{-1} &= -\mathcal{H}_{4 \times 4}(-\mathbf{k}), \\
\mathcal{C} &= \tau_1 \otimes 1_\sigma K
\end{aligned} \tag{2.5}$$

The Pauli matrices $\sigma_{x, y, z}$ and $\tau_{1, 2, 3}$ act on the spin up-down and particle-hole spaces respectively. K is complex conjugation. Here one should keep in mind the relation $\Delta_{s_1, s_2}(\mathbf{k}) = -\Delta_{s_2, s_1}(-\mathbf{k})$ coming from the Fermi statistics of $c_{\mathbf{k}s}$ and $c_{\mathbf{k}s}^\dagger$ operators. The mean-field Hamiltonian is diagonalized by the eigenvectors $(u_s(\mathbf{k}), v_s^*(-\mathbf{k}))^T$ of the eigenvalue

equation

$$\mathcal{H}_{4 \times 4}(\mathbf{k}) \begin{pmatrix} u_s(\mathbf{k}) \\ v_s^*(-\mathbf{k}) \end{pmatrix} = E(\mathbf{k}) \begin{pmatrix} u_s(\mathbf{k}) \\ v_s^*(-\mathbf{k}) \end{pmatrix} \quad (2.6)$$

Again $\begin{pmatrix} u_s(\mathbf{k}) \\ v_s^*(-\mathbf{k}) \end{pmatrix}$ stands for the four component vector $\begin{pmatrix} u_\uparrow(\mathbf{k}) \\ u_\downarrow(\mathbf{k}) \\ v_\uparrow^*(-\mathbf{k}) \\ v_\downarrow^*(-\mathbf{k}) \end{pmatrix}$ in the full spin up-down and particle-hole and spaces. Particle-hole symmetry imposes a relation between the solutions of (2.6), namely using (2.5) one can rewrite (2.6) as

$$\mathcal{H}_{4 \times 4}(\mathbf{k}) \begin{pmatrix} v_s(\mathbf{k}) \\ u_s^*(-\mathbf{k}) \end{pmatrix} = -E(-\mathbf{k}) \begin{pmatrix} v_s(\mathbf{k}) \\ u_s^*(-\mathbf{k}) \end{pmatrix} \quad (2.7)$$

Therefore each eigenfunction $\begin{pmatrix} u_s(\mathbf{k}) \\ v_s^*(-\mathbf{k}) \end{pmatrix}$ of the Hamiltonian (2.1) at energy $E(\mathbf{k}) > 0$ has a counterpart $\begin{pmatrix} v_s(\mathbf{k}) \\ u_s^*(-\mathbf{k}) \end{pmatrix}$ at $-E(-\mathbf{k})$.

Diagonalization and Bogoliubov quasi-particles

In this subsection we describe the diagonalization of the Hamiltonian (2.1) in considerable detail, since we use the same procedure in [21], which contains the main findings of this thesis. In the following we consider H_0 in (2.1) to be spin independent, i.e. $\xi_{s_1 s_2}(\mathbf{k}) = \xi(\mathbf{k})\sigma_0$ where σ_0 is the identity matrix in spin up-down space. The matrix (2.1) can be diagonalized by a unitary Bogoliubov transformation $B(\mathbf{k})$ whose columns are

the eigenvectors of the Hamiltonian matrix $\mathcal{H}(\mathbf{k})$

$$\mathcal{H}_{4 \times 4}(\mathbf{k})\hat{B}(\mathbf{k}) = \hat{B}(\mathbf{k})\hat{\mathcal{E}}_{4 \times 4}(\mathbf{k}) \quad (2.8)$$

where

$$\hat{\mathcal{E}}_{4 \times 4}(\mathbf{k}) = \begin{pmatrix} \hat{E}(\mathbf{k}) & 0 \\ 0 & -\hat{E}(-\mathbf{k}) \end{pmatrix} \quad (2.9)$$

and

$$\hat{B}_{4 \times 4}(\mathbf{k}) = \begin{pmatrix} \hat{u}(\mathbf{k}) & \hat{v}(\mathbf{k}) \\ \hat{v}^*(-\mathbf{k}) & \hat{u}^*(-\mathbf{k}) \end{pmatrix} \quad (2.10)$$

with $B(\mathbf{k})B^\dagger(\mathbf{k}) = B^\dagger(\mathbf{k})B(\mathbf{k}) = 1$. The 2×2 matrices $\hat{E}(\mathbf{k})$ are

$$\hat{E}_{2 \times 2}(\mathbf{k}) = \begin{pmatrix} E_1(\mathbf{k}) & 0 \\ 0 & E_2(\mathbf{k}) \end{pmatrix} \quad (2.11)$$

To find the transformation $\hat{B}(\mathbf{k})$ we need more information about the structure of the matrix $\Delta_{s_1, s_2}(\mathbf{k})$. We consider $\Delta_{s_1, s_2}(\mathbf{k})$ to be unitary, i.e the product $\hat{\Delta}(\mathbf{k})\hat{\Delta}^\dagger(\mathbf{k})$ is proportional to the unit matrix σ_0 . Pairing in the singlet channel ($\hat{\Delta}_{singlet}(\mathbf{k}) = i\sigma_y\Delta(\mathbf{k})$, $\Delta(-\mathbf{k}) = \Delta(\mathbf{k})$) satisfies the unitary condition since $\hat{\Delta}_{singlet}(\mathbf{k})\hat{\Delta}_{singlet}^\dagger(\mathbf{k}) = |\Delta(\mathbf{k})|^2\sigma_0$ where $|\Delta(\mathbf{k})|^2 = \frac{1}{2}Tr[\hat{\Delta}(\mathbf{k})\hat{\Delta}^\dagger(\mathbf{k})]$, therefore we specialize to singlet pairing from now on. The Bogoliubov transformation (2.8) gives two matrix equations

$$\begin{aligned} \hat{u}(\mathbf{k})\left(\hat{E}(\mathbf{k}) - \xi(\mathbf{k})\sigma_0\right) &= \hat{\Delta}(\mathbf{k})\hat{v}^*(-\mathbf{k}) \\ \hat{v}^*(-\mathbf{k})\left(\hat{E}(\mathbf{k}) + \xi(\mathbf{k})\sigma_0\right) &= \hat{\Delta}^\dagger(\mathbf{k})\hat{u}(\mathbf{k}) \end{aligned} \quad (2.12)$$

Eliminating $v^*(-\mathbf{k})$ from (2.12) and using the unitarity condition we arrive at the simple

solution

$$\hat{E}^2(\mathbf{k}) = \left(\xi^2(\mathbf{k}) + |\Delta(\mathbf{k})|^2 \right) \sigma_0 \quad (2.13)$$

Taking the trace of the above matrix equation we see that the spectrum is doubly degenerate

$$E_1(\mathbf{k}) = E_2(\mathbf{k}) = \sqrt{\xi^2(\mathbf{k}) + |\Delta(\mathbf{k})|^2} \quad (2.14)$$

The $\hat{u}(\mathbf{k})$ and $\hat{v}(\mathbf{k})$ matrices comprising the Bogoliubov transformation can also be determined from the eigenvalue problem

$$\begin{pmatrix} \xi(\mathbf{k})\sigma_0 & i\sigma_y\Delta(\mathbf{k}) \\ -i\sigma_y\Delta^*(\mathbf{k}) & -\xi(\mathbf{k})\sigma_0 \end{pmatrix} \begin{pmatrix} u_s(\mathbf{k}) \\ v_s^*(-\mathbf{k}) \end{pmatrix} = E(\mathbf{k}) \begin{pmatrix} u_s(\mathbf{k}) \\ v_s^*(-\mathbf{k}) \end{pmatrix} \quad (2.15)$$

with the normalization condition

$$|u_s(\mathbf{k})|^2 + |v_s(\mathbf{k})|^2 = 1 \quad (2.16)$$

Again we have specialized to singlet pairing: $\hat{\Delta}_{singlet}(\mathbf{k}) = i\sigma_y\Delta(\mathbf{k})$, $\Delta(-\mathbf{k}) = \Delta(\mathbf{k})$. In terms of 4×4 notation the equation (2.15) can be written as

$$\begin{pmatrix} \xi(\mathbf{k}) & 0 & 0 & \Delta(\mathbf{k}) \\ 0 & \xi(\mathbf{k}) & -\Delta(\mathbf{k}) & 0 \\ 0 & -\Delta^*(\mathbf{k}) & -\xi(\mathbf{k}) & 0 \\ \Delta^*(\mathbf{k}) & 0 & 0 & -\xi(\mathbf{k}) \end{pmatrix} \begin{pmatrix} u_\uparrow(\mathbf{k}) \\ u_\downarrow(\mathbf{k}) \\ v_\uparrow^*(-\mathbf{k}) \\ v_\downarrow^*(-\mathbf{k}) \end{pmatrix} = E(\mathbf{k}) \begin{pmatrix} u_\uparrow(\mathbf{k}) \\ u_\downarrow(\mathbf{k}) \\ v_\uparrow^*(-\mathbf{k}) \\ v_\downarrow^*(-\mathbf{k}) \end{pmatrix} \quad (2.17)$$

The diagonalization of the above 4×4 matrix is equivalent to that of (1, 4) and (2, 3) submatrices for particular spin orientations $s = \pm 1(\uparrow, \downarrow)$. The upper and lower signs correspond

to the (1, 4) and (2, 3) sub-matrices corresponding to the two possible pairing schemes of time reversed electron states: (\mathbf{k}, \uparrow) with $(-\mathbf{k}, \downarrow)$ and (\mathbf{k}, \downarrow) with $(-\mathbf{k}, \uparrow)$ respectively,

$$\begin{pmatrix} \xi(\mathbf{k}) & s\Delta(\mathbf{k}) \\ s\Delta^*(\mathbf{k}) & -\xi(\mathbf{k}) \end{pmatrix} \begin{pmatrix} u_s(\mathbf{k}) \\ v_{-s}(\mathbf{k}) \end{pmatrix} = E(\mathbf{k}) \begin{pmatrix} u_s(\mathbf{k}) \\ v_{-s}^*(-\mathbf{k}) \end{pmatrix} \quad (2.18)$$

The eigenvalue equation is identical for both spin orientations $s = \pm 1(\uparrow, \downarrow)$, and is given by $(\xi(\mathbf{k}) - E(\mathbf{k}))(-\xi(\mathbf{k}) - E(\mathbf{k})) - |\Delta(\mathbf{k})|^2 = 0$ which yields a positive branch of the spectrum $E(\mathbf{k}) = \sqrt{\xi(\mathbf{k})^2 + |\Delta(\mathbf{k})|^2}$. The eigen-vectors can be easily determined from the second row of either (2.18) and the normalization condition (2.16) to obtain

$$\begin{aligned} u_s(\mathbf{k}) &= \frac{E(\mathbf{k}) + \xi(\mathbf{k})}{\sqrt{\left(E(\mathbf{k}) + \xi(\mathbf{k})\right)^2 + |\Delta(\mathbf{k})|^2}} \equiv u(\mathbf{k}) \\ v_{-s}(\mathbf{k}) &= \frac{s\Delta^*(\mathbf{k})}{\sqrt{\left(E(\mathbf{k}) + \xi(\mathbf{k})\right)^2 + |\Delta(\mathbf{k})|^2}} \equiv sv(\mathbf{k}) \end{aligned} \quad (2.19)$$

Now we have enough information to write the Bogoliubov transformation matrix $B_{4 \times 4}(\mathbf{k})$ -

$$B_{4 \times 4}(\mathbf{k}) = \begin{pmatrix} u(\mathbf{k}) & 0 & 0 & -v^*(\mathbf{k}) \\ 0 & u(\mathbf{k}) & v^*(\mathbf{k}) & 0 \\ 0 & -v(\mathbf{k}) & u(\mathbf{k}) & 0 \\ v(\mathbf{k}) & 0 & 0 & u(\mathbf{k}) \end{pmatrix} = \begin{pmatrix} \sigma_0 u(\mathbf{k}) & -i\sigma_y v^*(\mathbf{k}) \\ -i\sigma_y v(\mathbf{k}) & \sigma_0 u(\mathbf{k}) \end{pmatrix} \quad (2.20)$$

The first two columns are the eigenvectors for the positive branch of the spectrum $E(\mathbf{k}) = \sqrt{\xi(\mathbf{k})^2 + |\Delta(\mathbf{k})|^2}$ for the two spin orientations. The last two columns are the eigenvectors of the negative branch of the spectrum $E(-\mathbf{k}) = -\sqrt{\xi(\mathbf{k})^2 + |\Delta(\mathbf{k})|^2}$ for the two spin orientations. They are related by particle-hole symmetry as described before. Therefore $a_{\mathbf{k}s}(a_{\mathbf{k}s}^\dagger)$ - the annihilation(creation) operators for the Bogoliubov quasi-particles in the

superconducting state are defined as

$$\begin{pmatrix} a_{\mathbf{k}s} \\ a_{-\mathbf{k},s}^\dagger \end{pmatrix} = \begin{pmatrix} \sigma_0 u(\mathbf{k}) & -i\sigma_y v^*(\mathbf{k}) \\ -i\sigma_y v(\mathbf{k}) & \sigma_0 u(\mathbf{k}) \end{pmatrix} \begin{pmatrix} c_{\mathbf{k}s'} \\ c_{-\mathbf{k},s'}^\dagger \end{pmatrix} \quad (2.21)$$

The Nambu Matrix Green's Function

In this section we give a brief introduction to the Green's function method [83] for superconductivity. In the Nambu formalism one introduces the two vectors

$$\Psi_{\mathbf{k}s} = \begin{pmatrix} c_{\mathbf{k}s} \\ c_{-\mathbf{k}-s}^\dagger \end{pmatrix} ; \quad \Psi_{\mathbf{k}s}^\dagger = (c_{\mathbf{k}s}^\dagger, c_{-\mathbf{k}-s}) \quad (2.22)$$

Then the Hamiltonian (2.1) for each spin orientation $s = \pm 1(\uparrow, \downarrow)$ can be written as (we have again assumed singlet pairing)

$$\begin{aligned} H^{(s)} &= \frac{1}{2} \sum_{\mathbf{k} \in FBZ} \Psi_{\mathbf{k}s}^\dagger \mathcal{H}_{\mathbf{k}}^{(s)} \Psi_{\mathbf{k}s} \\ \mathcal{H}_{\mathbf{k}}^{(s)} &= \begin{pmatrix} \xi(\mathbf{k}) & s\Delta(\mathbf{k}) \\ s\Delta^*(-\mathbf{k}) & -\xi(\mathbf{k}) \end{pmatrix} \end{aligned} \quad (2.23)$$

To keep things simple lets work with $s = 1$. We define the Nambu greens function to be the following 2×2 matrix,

$$\hat{G}(\mathbf{k}, \tau)_{ab} \equiv \begin{pmatrix} G_{\uparrow\uparrow}(\mathbf{k}, \tau) & F_{\uparrow\downarrow}^*(\mathbf{k}, \tau) \\ F_{\downarrow\uparrow}(\mathbf{k}, \tau) & G_{\downarrow\downarrow}^*(\mathbf{k}, \tau) \end{pmatrix} = -\langle T \Psi_{\mathbf{k}s,a}(\tau) \Psi_{\mathbf{k}s,b}^\dagger(0) \rangle \quad (2.24)$$

The indices a, b represent the components of the nambu vector $\Psi_{\mathbf{k}s}^\dagger = (c_{\mathbf{k}\uparrow}^\dagger, c_{-\mathbf{k}\downarrow})$. The equation of motion of $\hat{G}(\mathbf{k}, \tau)$ in the frequency domain satisfies the following algebraic

equation

$$\begin{aligned} \hat{G}(\mathbf{k}, \omega_n)_{ab} &\equiv \begin{pmatrix} G_{\uparrow\uparrow}(\mathbf{k}, \omega_n) & F_{\downarrow\uparrow}^*(\mathbf{k}, \omega_n) \\ F_{\downarrow\uparrow}(\mathbf{k}, \omega_n) & G_{\downarrow\downarrow}^*(\mathbf{k}, \omega_n) \end{pmatrix} = (i\omega_n - \hat{\mathcal{H}}_{\mathbf{k}})_{ab}^{-1} \\ &= \frac{1}{(i\omega_n)^2 - E_{\mathbf{k}}^2} \begin{pmatrix} i\omega_n + \xi(\mathbf{k}) & \Delta(\mathbf{k}) \\ \Delta^*(-\mathbf{k}) & i\omega_n - \xi(\mathbf{k}) \end{pmatrix} \end{aligned} \quad (2.25)$$

where as before $E_{\mathbf{k}}^2 = \xi^2(\mathbf{k}) + |\Delta(\mathbf{k})|^2$ and $\omega_n = 2\pi T(n + \frac{1}{2})$ are the Matsubara frequencies.

The Green's function can also be written in a manner which makes the poles explicit

$$\begin{aligned} \hat{G}(\mathbf{k}, \omega_n)_{ab} &= \frac{1}{(E(\mathbf{k}) - i\omega_n)} \begin{pmatrix} u(\mathbf{k})^2 & u(\mathbf{k})v(\mathbf{k}) \\ u(\mathbf{k})v(\mathbf{k}) & v(\mathbf{k})^2 \end{pmatrix} \\ &+ \frac{1}{(-E(\mathbf{k}) - i\omega_n)} \begin{pmatrix} v(\mathbf{k})^2 & -u(\mathbf{k})v(\mathbf{k}) \\ -u(\mathbf{k})v(\mathbf{k}) & u(\mathbf{k})^2 \end{pmatrix} \end{aligned} \quad (2.26)$$

which shows that the Green's function has poles at $\pm E(\mathbf{k})$.

Self-consistent determination of the order parameter $\Delta_{\mathbf{k}}$

The self consistent equation that determines the temperature dependence of the order parameter $\Delta(T)$ can be derived from the above Nambu Green's function. For the case of singlet pairing, the mean field order parameter defined in (2.2) is given by

$$\Delta_{\mathbf{k}} = \sum_{\mathbf{k}'} g(\mathbf{k}, \mathbf{k}') \langle c_{-\mathbf{k}'\downarrow} c_{\mathbf{k}'\uparrow} \rangle \quad (2.27)$$

The above equation can be written in terms of the Greens functions defined in (2.24),

$$\Delta_{\mathbf{k}} = - \sum_{\mathbf{k}'} g(\mathbf{k}, \mathbf{k}') F_{\downarrow\uparrow}^*(\mathbf{k}, \tau = 0^+) \quad (2.28)$$

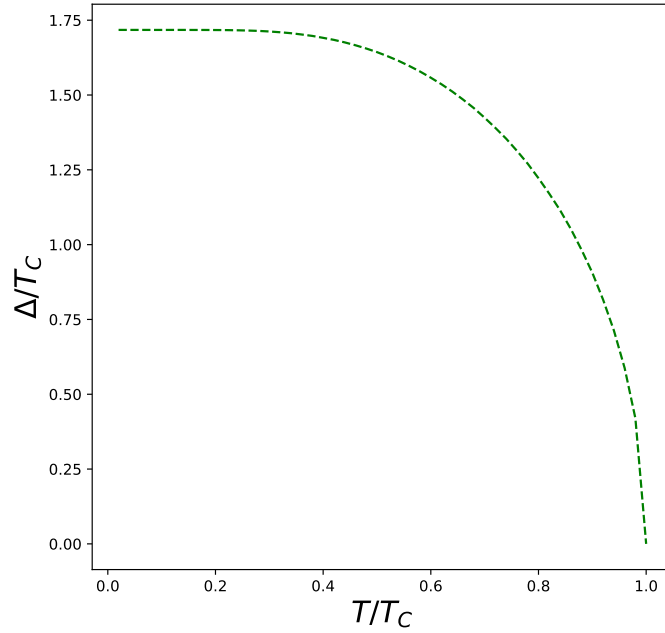


Figure 2.1: Temperature dependence of $\Delta(T)$ for a $d_{x^2-y^2}$ -wave superconductor

Writing $F_{\downarrow\uparrow}^*(\mathbf{k}, \tau = 0^+)$ as a Fourier transform with Matsubara frequencies ω_n the above equation is

$$\begin{aligned} \Delta_{\mathbf{k}} &= -T \sum_{\mathbf{k}'} \sum_{\omega_n} g(\mathbf{k}, \mathbf{k}') F_{\downarrow\uparrow}^*(\mathbf{k}', \omega_n) \\ &= T \sum_{\mathbf{k}'} \sum_{\omega_n} g(\mathbf{k}, \mathbf{k}') \frac{\Delta_{\mathbf{k}'}}{\omega_n^2 + E_{\mathbf{k}'}} \end{aligned} \quad (2.29)$$

We take the pairing interaction to be of the form $g(\mathbf{k}, \mathbf{k}') = g\eta(\mathbf{k})\eta(\mathbf{k}')$, $\eta(\mathbf{k})$ being a basis function compatible with the symmetry of the lattice and g is the effective attractive

interaction. The above equation reduces to the following gap equation

$$\frac{1}{g} = T \sum_{\mathbf{k}} \sum_{\omega_n} \frac{\eta^2(\mathbf{k})}{\omega_n^2 + \xi^2(\mathbf{k}) + |\Delta(\mathbf{k})|^2} \quad (2.30)$$

The above equation has to be solved numerically. In Fig. 2.1 we show the solution for a $d_{x^2-y^2}$ -wave superconductor for which $\eta(\mathbf{k}) = \frac{1}{2}(\cos k_x - \cos k_y)$. For the choice of $\xi(\mathbf{k})$, we considered the following tight binding dispersion relation $\xi(\mathbf{k}) = -t_1(\cos k_x + \cos k_y) - t_2 \cos k_x \cos k_y - \mu$ with $t_2/t_1 = 10, \mu = 0$.

THE SPIN DENSITY WAVE STATE

Bogoliubov Quasiparticles in the SDW state

In this section we briefly summarize the Bogoliubov quasiparticles in the SDW state. The SDW instability occurs if there are parts of the Fermi surface that satisfies a nesting condition- $\xi(\mathbf{k} + \mathbf{Q}) = -\xi(\mathbf{k})$, where \mathbf{Q} is the SDW ordering momentum. Geometrically this means that there are parallel segments of the Fermi surface that are connected by the ordering vector \mathbf{Q} . The mean field Hamiltonian is given by

$$\begin{aligned}
 H &= H_0 + H_{SDW} \\
 H_0 &= \sum_{\mathbf{k}, \sigma} \xi(\mathbf{k}) c_{\mathbf{k}\sigma}^\dagger c_{\mathbf{k}\sigma}, \\
 H_{SDW} &= \frac{1}{2} \sum_{\mathbf{k}, \sigma} \sigma M \left(c_{\mathbf{k}\sigma}^\dagger c_{\mathbf{k}+\mathbf{Q}\sigma} + h.c. \right)
 \end{aligned} \tag{3.1}$$

The mean field order parameter M is defined by the following self consistent equation

$$M = -\frac{U}{2} \sum_{\mathbf{k}, \sigma} \sigma \langle c_{\mathbf{k}+\mathbf{Q}\sigma}^\dagger c_{\mathbf{k}\sigma} \rangle, \tag{3.2}$$

where U is the repulsive on-site Coulomb interaction which leads to the SDW formation [41]. In this thesis we consider a collinear sinusoidal SDW where the spatial magnetization oscillates as $\mathbf{m}(\mathbf{r}) = 2M\hat{\mathbf{z}} \cos(\mathbf{Q} \cdot \mathbf{r})$. We consider an inversion-symmetric dispersion relation, $\xi(\mathbf{k}) = \xi(-\mathbf{k})$.

$$\xi(\mathbf{k}) = -t_1(\cos k_x + \cos k_y) - t_2 \cos k_x \cos k_y - \mu \tag{3.3}$$

It describes the nearest neighbour ($t_1 > 0$) and next-nearest neighbour ($t_2 > 0$) hopping on a 2D square lattice with lattice spacing $a = 1$. We set the chemical potential to zero, and therefore for $t_2 > 0$ the electron filling is slightly less than half. This results in a Fermi

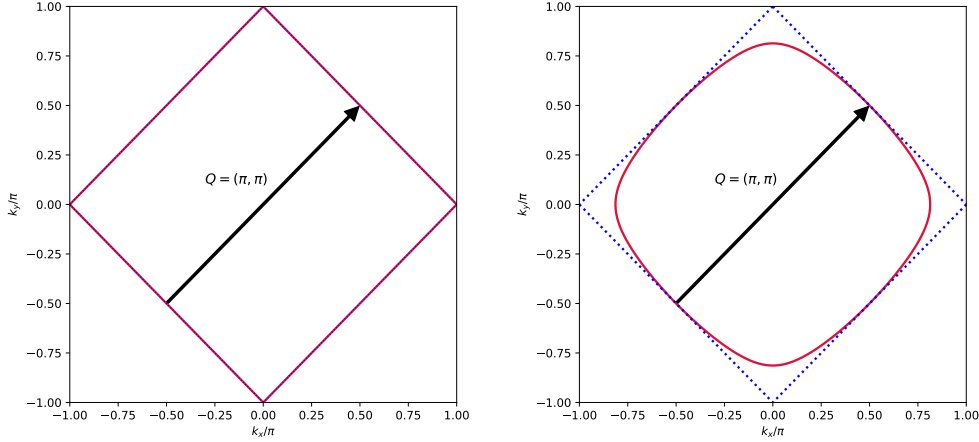


Figure 3.1: The solid red curve shows the shapes of the perfectly nested (left panel) and partially nested (right panel) Fermi surfaces. The blue dotted square is the reduced Brillouin zone (RBZ) for $\mathbf{Q} = (\pi, \pi)$ -SDW ordering. When the FS is perfectly nested $\mu = 0$ and $t_2 = 0$ in our model (3.3), the SDW opens a gap along entire FS since the FS overlaps the RBZ completely. When the FS is partially nested $\mu = 0$ and $t_2/t_1 = 0.2$, only those parts of the FS that overlap with the RBZ get gapped with M .

surface that is not perfectly nested and therefore potentially susceptible to SDW formation. The perfect nesting limit is given by setting $t_2 = 0$. We show the Fermi surfaces for $t_2 > 0$ and $t_2 = 0$ in Fig. 3.1. It is convenient to recast (3.1) into 2×2 matrix for each spin orientation $\sigma = \pm 1(\uparrow, \downarrow)$

$$H = \frac{1}{2} \sum_{\substack{\mathbf{k} \in FBZ \\ \sigma}} \left(c_{\mathbf{k}\sigma}^\dagger, c_{\mathbf{k}+\mathbf{Q}\sigma}^\dagger \right) \mathcal{H}_{2 \times 2}^\sigma(\mathbf{k}) \begin{pmatrix} c_{\mathbf{k}\sigma} \\ c_{\mathbf{k}+\mathbf{Q},\sigma} \end{pmatrix} \quad (3.4)$$

$$\mathcal{H}_{2 \times 2}^\sigma(\mathbf{k}) = \begin{pmatrix} \xi(\mathbf{k}) & \sigma M \\ \sigma M & \xi(\mathbf{k} + \mathbf{Q}) \end{pmatrix}$$

where where $\Phi_{\mathbf{k}\sigma}^\dagger = \left(c_{\mathbf{k}\sigma}^\dagger, c_{\mathbf{k}+\mathbf{Q}\sigma}^\dagger \right)$ represents the Nambu vector. We have ‘folded’ the normal

state band into the reduced Brillouin zone appropriate for the $\mathbf{Q} = (\pi, \pi)$ -SDW unit cell. The $1/2$ in front comes from the the $\mathbf{k}, \mathbf{k} + \mathbf{Q}$ doubling of the bands for the SDW. The reduced anti-ferromagnetic Brillouin zone is defined by

$$RBZ = \{(k_x, k_y) \mid |k_x| + |k_y| \leq \pi\} \quad (3.5)$$

It is given by the area inside the dotted blue diamond in the right panel of Fig 3.1

Using definitions $\xi_{\mathbf{k}}^{\pm} = \frac{1}{2}(\xi_{\mathbf{k}} \pm \xi_{\mathbf{k}+\mathbf{Q}})$ and $\Pi_{\mathbf{k}} = \sqrt{(\xi_{\mathbf{k}}^-)^2 + M^2}$, the eigenvalues of $\mathcal{H}_{2 \times 2}^{\sigma}(\mathbf{k})$ can be written as

$$E_{\alpha}(\mathbf{k}) = \xi_{\mathbf{k}}^+ + \Pi_{\mathbf{k}} \quad , \quad E_{\beta}(\mathbf{k}) = \xi_{\mathbf{k}}^+ - \Pi_{\mathbf{k}} \quad (3.6)$$

In Fig. 3.2 we show the structure of the two distinct (spin degenerate) quasiparticle bands in the SDW phase when the FS is not perfectly nested, leaving a hole pocket $E_{\beta}(\mathbf{k}) = 0$ around $(\pi, 0)$.

The matrix in (3.4) can be diagonalized by a unitary Bogoliubov transformation $B(\mathbf{k})$ whose columns are the eigenvectors of the Hamiltonian matrix $\mathcal{H}_{2 \times 2}^{\sigma}(\mathbf{k})$

$$\mathcal{H}_{2 \times 2}^{\sigma}(\mathbf{k}) \hat{B}^{\sigma}(\mathbf{k}) = \hat{B}^{\sigma}(\mathbf{k}) \hat{\mathcal{E}}_{2 \times 2}(\mathbf{k}) \quad (3.7)$$

where

$$\hat{\mathcal{E}}_{2 \times 2}(\mathbf{k}) = \begin{pmatrix} E_{\alpha}(\mathbf{k}) & 0 \\ 0 & E_{\beta}(\mathbf{k}) \end{pmatrix} \quad (3.8)$$

and

$$\hat{B}_{2 \times 2}^{\sigma}(\mathbf{k}) = \begin{pmatrix} \mathcal{U}(\mathbf{k}) & -\sigma \mathcal{V}(\mathbf{k}) \\ \sigma \mathcal{V}(\mathbf{k}) & \mathcal{U}(\mathbf{k}) \end{pmatrix} \quad (3.9)$$

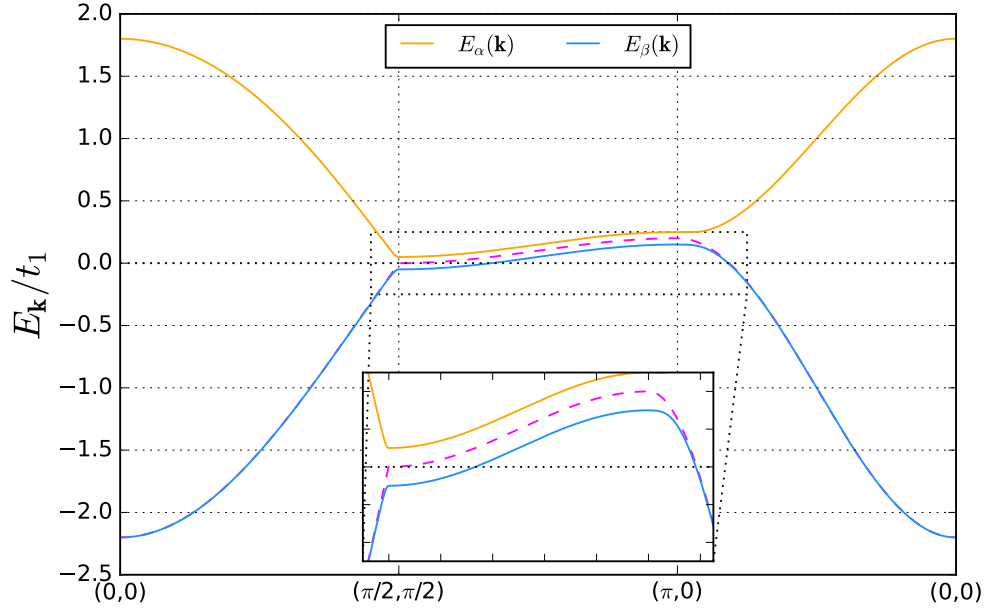


Figure 3.2: The quasiparticle energies in the Brillouin zone along the path $(0,0) \rightarrow (\pi/2, \pi/2) \rightarrow (\pi, 0) \rightarrow (0,0)$. The normal state band is depicted by the dashed magenta curve. The two quasi-particle bands $E_{\alpha,\beta}$ in the SDW phase are depicted by orange and blue curves respectively. The parameters are $t_2/t_1 = 0.2$, $M/t_1 = 0.2$.

with $B(\mathbf{k})B^\dagger(\mathbf{k}) = B^\dagger(\mathbf{k})B(\mathbf{k}) = 1$. The expressions for $u(\mathbf{k}), v(\mathbf{k})$ are

$$\begin{aligned} \mathcal{U}(\mathbf{k}) &= \sqrt{\frac{1}{2} \left(1 + \frac{\xi_k^-}{\Pi_{\mathbf{k}}} \right)} \\ \mathcal{V}(\mathbf{k}) &= \sqrt{\frac{1}{2} \left(1 - \frac{\xi_k^-}{\Pi_{\mathbf{k}}} \right)} \end{aligned} \quad (3.10)$$

Therefore $f_{\mathbf{k}\sigma}(f_{\mathbf{k}\sigma}^\dagger)$ - the annihilation(creation) operators for the Bogoliubov quasi-particles in the SDW state are defined as

$$\begin{pmatrix} f_{\mathbf{k}\sigma} \\ f_{\mathbf{k}+\mathbf{Q},\sigma} \end{pmatrix} = \begin{pmatrix} \mathcal{U}(\mathbf{k}) & -\sigma\mathcal{V}(\mathbf{k}) \\ \sigma\mathcal{V}(\mathbf{k}) & \mathcal{U}(\mathbf{k}) \end{pmatrix} \begin{pmatrix} c_{\mathbf{k}\sigma} \\ c_{\mathbf{k}+\mathbf{Q},\sigma} \end{pmatrix} \quad (3.11)$$

The Nambu Matrix Green's Function

As in the superconducting case one introduces the two Nambu vectors

$$\Phi_{\mathbf{k}\sigma} = \begin{pmatrix} c_{\mathbf{k}\sigma} \\ c_{\mathbf{k}+\mathbf{Q}\sigma} \end{pmatrix} ; \quad \Phi_{\mathbf{k}\sigma}^\dagger = \left(c_{\mathbf{k}\sigma}^\dagger, c_{\mathbf{k}+\mathbf{Q}\sigma}^\dagger \right) \quad (3.12)$$

Then the Hamiltonian (3.1) for each spin orientation $\sigma = \pm 1(\uparrow, \downarrow)$ can be written as

$$H^{(\sigma)} = \frac{1}{2} \sum_{\mathbf{k} \in FBZ} \Phi_{\mathbf{k}\sigma}^\dagger \mathcal{H}_{\mathbf{k}}^{(\sigma)} \Phi_{\mathbf{k}\sigma} \quad (3.13)$$

$$\mathcal{H}_{\mathbf{k}}^{(\sigma)} = \begin{pmatrix} \xi(\mathbf{k}) & \sigma M \\ \sigma M & \xi(\mathbf{k} + \mathbf{Q}) \end{pmatrix}$$

We define the Nambu Green's function to be the following 2×2 matrix,

$$\hat{G}(\mathbf{k}, \tau)_{mn} \equiv \begin{pmatrix} G(\mathbf{k}, \tau) & F(\mathbf{k}, \tau) \\ F(\mathbf{k} + \mathbf{Q}, \tau) & G(\mathbf{k} + \mathbf{Q}, \tau) \end{pmatrix} = -\langle T \Phi_{\mathbf{k}\sigma, m}(\tau) \Phi_{\mathbf{k}\sigma, n}^\dagger(0) \rangle \quad (3.14)$$

The indices m, n denote the components of the Nambu vector $\Phi_{\mathbf{k}\sigma}^\dagger = (c_{\mathbf{k}\sigma}^\dagger, c_{\mathbf{k}+\mathbf{Q}\sigma}^\dagger)$. The equation of motion of $\hat{G}(\mathbf{k}, \tau)$ in the frequency domain satisfies the following algebraic equation

$$\begin{aligned} \hat{G}(\mathbf{k}, \omega_n)_{mn} &= (i\omega_n - \hat{\mathcal{H}}_{\mathbf{k}})_{mn}^{-1} \\ &= \frac{1}{\begin{pmatrix} i\omega_n - \xi(\mathbf{k}) \\ i\omega_n - \xi(\mathbf{k} + \mathbf{Q}) \end{pmatrix} \begin{pmatrix} i\omega_n - \xi(\mathbf{k} + \mathbf{Q}) \\ i\omega_n - \xi(\mathbf{k}) \end{pmatrix} - M^2} \begin{pmatrix} i\omega_n - \xi(\mathbf{k} + \mathbf{Q}) & \sigma M \\ \sigma M & i\omega_n - \xi(\mathbf{k}) \end{pmatrix} \end{aligned} \quad (3.15)$$

where as before $\omega_n = 2\pi T(n + \frac{1}{2})$ are the Matsubara frequencies. The Green's function can also be written in a manner which makes the poles explicit

$$\begin{aligned} \hat{G}(\mathbf{k}, \omega_n)_{mn} = & \frac{1}{(E_\alpha(\mathbf{k}) - i\omega_n)} \begin{pmatrix} \mathcal{U}(\mathbf{k})^2 & \sigma\mathcal{U}(\mathbf{k})\mathcal{V}(\mathbf{k}) \\ \sigma\mathcal{U}(\mathbf{k})\mathcal{V}(\mathbf{k}) & \mathcal{V}(\mathbf{k})^2 \end{pmatrix} \\ & + \frac{1}{(E_\beta(\mathbf{k}) - i\omega_n)} \begin{pmatrix} \mathcal{V}(\mathbf{k})^2 & -\sigma\mathcal{U}(\mathbf{k})\mathcal{V}(\mathbf{k}) \\ -\sigma\mathcal{U}(\mathbf{k})\mathcal{V}(\mathbf{k}) & \mathcal{U}(\mathbf{k})^2 \end{pmatrix} \end{aligned} \quad (3.16)$$

which shows that the Green's function has poles at $E_\alpha(\mathbf{k})$ and $E_\beta(\mathbf{k})$.

The Self-consistent determination of order parameter M

The self consistent equation that determines the temperature dependence of the order parameter $M(T)$ can be derived from the above Nambu Green's function. The mean field order parameter defined in (3.2) is given by

$$M = -\frac{U}{2} \sum_{\mathbf{k}, \sigma} \sigma \langle c_{\mathbf{k}+\mathbf{Q}\sigma}^\dagger c_{\mathbf{k}\sigma} \rangle \quad (3.17)$$

The above equation can be written in terms of the Greens functions defined in (3.14),

$$M = -\frac{U}{2} \sum_{\mathbf{k}, \sigma} \sigma F^\dagger(\mathbf{k} + \mathbf{Q}, \tau = 0^+) \quad (3.18)$$

Writing $F^\dagger(\mathbf{k} + \mathbf{Q}, \tau = 0^+)$ as a Fourier transform with Matsubara frequencies ω_n the

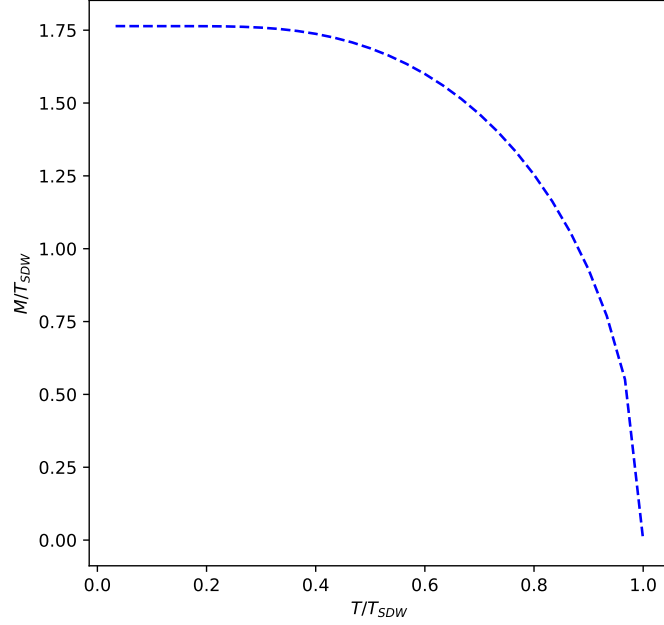


Figure 3.3: Temperature dependence of $M(T)$ for a SDW metal.

above equation is

$$\begin{aligned}
 M &= -\frac{UT}{2} \sum_{\mathbf{k}, \sigma} \sum_{\omega_n} \sigma F^\dagger(\mathbf{k} + \mathbf{Q}, \omega_n) \\
 &= \frac{UT}{2} \sum_{\mathbf{k}, \sigma} \sum_{\omega_n} \frac{\sigma^2 M}{\omega_n^2 + \xi^2(\mathbf{k}) + M^2}
 \end{aligned} \tag{3.19}$$

where as we have used $\xi(\mathbf{k} + \mathbf{Q}) = -\xi(\mathbf{k})$, since the SDW gaps only those parts of the Fermi surface where the nesting condition is obeyed. This simplifies to

$$\frac{1}{U} = T \sum_{\mathbf{k}} \sum_{\omega_n} \frac{1}{\omega_n^2 + \xi^2(\mathbf{k}) + M^2} \tag{3.20}$$

The above equation has to be solved numerically and produces a similar profile like the pure superconducting $\Delta(T)$ as shown in Fig. 3.3.

BOLTZMANN KINETICS

The Boltzmann Equation for Electrons

In this section we give a brief discussion of the Boltzmann kinetic equation for electrons. Let's consider an electron gas slightly out of equilibrium. We know that after some time it will equilibrate. We introduce the distribution function $f(\mathbf{k})$ which measures the average number of electrons with wave vector \mathbf{k} i.e the number density of electrons is given by

$$n(\mathbf{r}) = 2 \int \frac{d^3k}{(2\pi)^3} f(\mathbf{k}) \quad (4.1)$$

The factor of 2 comes from each spin orientation (\uparrow, \downarrow). In order to describe the equilibration process, we need the evolution equation for $f(\mathbf{k})$. The equilibration happens due to collisions and therefore the evolution equation can be written as

$$\frac{df(\mathbf{k})}{dt} = I^{coll}[\mathbf{k}] \quad (4.2)$$

where $I^{coll}(\mathbf{k})$ is the collision integral which incorporates the effect of collisions. The total derivative on the right hand side can be written as a sum of partial derivatives, giving the Boltzmann equation [64]

$$\frac{\partial f(\mathbf{k})}{\partial t} + \frac{\partial E}{\partial \mathbf{k}} \nabla f(\mathbf{k}) - \nabla E \frac{\partial f(\mathbf{k})}{\partial \mathbf{k}} = I^{coll}(\mathbf{k}) \quad (4.3)$$

The collision integral describes transitions between the states with different \mathbf{k} due to collisions. It can be specified if one knows the collision probability $W(\mathbf{k}, \mathbf{k}')$ - the probability of a particle in a state with momentum \mathbf{k} to scatter to a state with momentum \mathbf{k}' . The change of the distribution function induced by the collisions is

$$\begin{aligned}
\text{decrease : } & - \sum_{\mathbf{k}'} W(\mathbf{k} \rightarrow \mathbf{k}') f(\mathbf{k}) [1 - f(\mathbf{k}')] \\
\text{increase : } & \sum_{\mathbf{k}'} W(\mathbf{k}' \rightarrow \mathbf{k}) f(\mathbf{k}') [1 - f(\mathbf{k})]
\end{aligned} \tag{4.4}$$

The first term describes the scattering processes in which the electron leaves the state with momentum \mathbf{k} and scatters into a state of momentum \mathbf{k}' , while the second one describes the processes where an electron comes in to the state with momentum \mathbf{k} after being scattered out of a state with momentum \mathbf{k}' . The factors $[1 - f(\mathbf{k})]$ takes account of the Pauli principle. Therefore

$$I^{coll}[\mathbf{k}] = \sum_{\mathbf{k}'} W(\mathbf{k}' \rightarrow \mathbf{k}) f(\mathbf{k}') [1 - f(\mathbf{k})] - \sum_{\mathbf{k}'} W(\mathbf{k} \rightarrow \mathbf{k}') f(\mathbf{k}) [1 - f(\mathbf{k}')] \tag{4.5}$$

For any elastic scattering, the time reversal symmetry demands

$$W(\mathbf{k} \rightarrow \mathbf{k}') = W(-\mathbf{k}' \rightarrow -\mathbf{k}) \tag{4.6}$$

If in addition we have the inversion symmetry (in the first Born approximation we always do) then

$$W(\mathbf{k} \rightarrow \mathbf{k}') = W(-\mathbf{k}' \rightarrow -\mathbf{k}) = W(\mathbf{k}' \rightarrow \mathbf{k}) \tag{4.7}$$

Therefore the collision integral becomes

$$I^{coll}[\mathbf{k}] = \sum_{\mathbf{k}'} W(\mathbf{k} \rightarrow \mathbf{k}') [f(\mathbf{k}') - f(\mathbf{k})] \tag{4.8}$$

In this thesis we do not discuss what happens when there is no inversion symmetry.

This topic is discussed in [14]. The Boltzmann equation can be deduced from non-equilibrium Green's function theory. This is discussed in [49],[79]. There are several scattering mechanisms that can contribute to transport processes. They are electron-phonon, electron-electron and impurity scattering. As the superconducting transition temperatures are much smaller than characteristic Debye temperatures for metals, electron-phonon scattering becomes negligible at very low temperatures. The electron-electron scattering for energies within $k_B T$ of the Fermi energy is relatively unimportant. This is because of a combination of two requirements- Pauli exclusion principle and the conservation of energy and momentum, see [7] for further details. Therefore scattering by impurities is the dominant collision mechanism at low temperatures.

Impurity scattering

The Boltzmann equation becomes rather complicated if we have to compute $W(\mathbf{k}, \mathbf{k}')$ beyond the Born approximation. Fortunately, the Born approximation is sufficient for many problems (but not all). Under this approximation, the scattering probability for impurities is

$$\begin{aligned} W(\mathbf{k}, \mathbf{k}') &= \frac{2\pi}{\hbar} |\langle \mathbf{k}' | \hat{V}_{imp} | \mathbf{k} \rangle|^2 \delta(E(\mathbf{k}) - E(\mathbf{k}')) \\ &= \frac{2\pi}{\hbar} |V(\mathbf{k}, \mathbf{k}')|^2 \delta(E(\mathbf{k}) - E(\mathbf{k}')) \end{aligned} \tag{4.9}$$

where $V(\mathbf{k}, \mathbf{k}')$ is the matrix elements of the impurity potential

$$V(\mathbf{r}) = \sum_i \mathcal{V}(\mathbf{r} - \mathbf{R}_i) \tag{4.10}$$

which is the sum of the potentials \mathcal{V} of the individual impurities between the Bloch states

$$\frac{1}{\sqrt{vol}} e^{i\mathbf{k}\mathbf{r}} u_{\mathbf{k}}(\mathbf{r}) \quad (4.11)$$

Substituting (4.10) into the expression for matrix elements we get,

$$\begin{aligned} V(\mathbf{k}, \mathbf{k}') &= \frac{1}{vol} \sum_i \int \mathcal{V}(\mathbf{r} - \mathbf{R}_i) e^{i(\mathbf{k}-\mathbf{k}')\cdot\mathbf{r}} u_{\mathbf{k}'}^*(\mathbf{r}) u_{\mathbf{k}}(\mathbf{r}) d\mathbf{r}^3 \\ &= \frac{1}{vol} \sum_i e^{i(\mathbf{k}-\mathbf{k}')\cdot\mathbf{R}_i} \int \mathcal{V}(\mathbf{r}) e^{i(\mathbf{k}-\mathbf{k}')\cdot\mathbf{r}} u_{\mathbf{k}'}^*(\mathbf{r}) u_{\mathbf{k}}(\mathbf{r}) d\mathbf{r}^3 \\ &= \frac{1}{vol} \sum_i e^{i(\mathbf{k}-\mathbf{k}')\cdot\mathbf{R}_i} \mathcal{V}_{\mathbf{k}\mathbf{k}'} \end{aligned} \quad (4.12)$$

Here we have assumed all the impurity atoms be of the same kind and their positions in the primitive cells are equivalent. So we have shifted the origin of the frame of reference for each cell by an appropriate lattice vector. Now we can calculate the scattering probability (4.9).

We get

$$W(\mathbf{k}, \mathbf{k}') = \frac{2\pi}{\hbar} \frac{1}{vol} |\mathcal{V}_{\mathbf{k},\mathbf{k}'}|^2 \delta(E(\mathbf{k}) - E(\mathbf{k}')) \sum_{i,j} e^{i(\mathbf{k}-\mathbf{k}')\cdot(\mathbf{R}_i - \mathbf{R}_j)} \quad (4.13)$$

The last sum can be simplified because the positions of the impurities are random and the distance between them is much greater than inter-atomic spacing a . So we can average over their impurity positions and the only terms important are the ones with $i = j$ (the others oscillate strongly, their contribution being very small). As a result,

$$\overline{\sum_{i,j} e^{i(\mathbf{k}-\mathbf{k}')\cdot(\mathbf{R}_i - \mathbf{R}_j)}} = N_{imp} \quad (4.14)$$

where N_{imp} is the number of impurities. Finally, we get the following for the scattering probability

$$W(\mathbf{k}, \mathbf{k}') = n_{imp} \frac{2\pi}{\hbar} |\mathcal{V}_{\mathbf{k}, \mathbf{k}'}|^2 \delta(E(\mathbf{k}) - E(\mathbf{k}')) \quad (4.15)$$

where we introduced the impurity concentration as $n_i = N_{imp}/vol$

Linearized Boltzmann Equation and the Quasiparticle Relaxation Time

We follow the usual process of linearizing the left hand side of (4.3) in the presence of a thermal gradient, by writing $f(\mathbf{k}) = f^0(\mathbf{k}) + \delta f(\mathbf{k})$, where $f^0(\mathbf{k}) = \frac{1}{e^{E(\mathbf{k})/T} + 1}$ is the equilibrium Fermi-Dirac distribution function. $\delta f(\mathbf{k})$ is the deviation from the equilibrium value caused by the presence of the stationary thermal gradient. The linearization yields [64],

$$\frac{\partial \delta f(\mathbf{k})}{\partial t} - E(\mathbf{k}) \mathbf{v}(\mathbf{k}) \frac{\nabla T}{T} \frac{\partial f^0(\mathbf{k})}{\partial E} = I^{coll}(\mathbf{k}) \quad (4.16)$$

The quasiparticle velocity is defined as

$$\mathbf{v}(\mathbf{k}) = \nabla_{\mathbf{k}} E(\mathbf{k}) \quad (4.17)$$

For a stationary thermal gradient the first term is zero. The collision integrals in the case of weak disorder is obtained by multiplying the contribution of a single impurity by their concentration N_{imp} . Therefore (4.16) becomes

$$E(\mathbf{k}) \mathbf{v}(\mathbf{k}) \frac{\nabla T}{T} \frac{\partial f^0(\mathbf{k})}{\partial E} = -N_{imp} \int \frac{d^3 k'}{(2\pi)^3} \left[W(\mathbf{k}, \mathbf{k}') \left(\delta f(\mathbf{k}') - \delta f(\mathbf{k}) \right) \right] \quad (4.18)$$

We can rewrite (4.18) for $\delta f_n(\mathbf{k})$ as

$$E(\mathbf{k})\mathbf{v}(\mathbf{k})\frac{\nabla T}{T}\frac{\partial f^0(\mathbf{k})}{\partial E} = -N_{imp}\left[\int\frac{d^3k'}{(2\pi)^3}\left(W(\mathbf{k},\mathbf{k}')\delta f(\mathbf{k}')\right)\right] + \left(\frac{1}{\tau(\mathbf{k})}\right)\delta f(\mathbf{k}) \quad (4.19)$$

where we have defined the quasiparticle relaxation time as

$$\tau^{-1}(\mathbf{k}) = N_{imp}\int\frac{d^3k'}{(2\pi)^3}W(\mathbf{k},\mathbf{k}') \quad (4.20)$$

The right hand side is odd under spatial inversion since $\mathbf{v}(-\mathbf{k}) = -\mathbf{v}(\mathbf{k})$, whereas the quasiparticle relaxation time is even under spatial inversion $\tau^{-1}(-\mathbf{k}) = \tau^{-1}(\mathbf{k})$ due to symmetry $W(-\mathbf{k}, -\mathbf{k}') = W(\mathbf{k}, \mathbf{k}')$, which implies that $\delta f_n(\mathbf{k})$ is odd under $\mathbf{k} \rightarrow -\mathbf{k}$. Thus the first terms on the right in (4.19) are integrals of odd functions over a symmetric region of integration and therefore go to zero: $[\dots] = 0$. Therefore

$$\delta f(\mathbf{k}) = \tau(\mathbf{k})E(\mathbf{k})\mathbf{v}(\mathbf{k})\frac{\nabla T}{T}\frac{\partial f_1^0(\mathbf{k})}{\partial E_1} \quad (4.21)$$

The expression of the total heat current carried by the quasiparticles is given by

$$\mathbf{j}_E = 2\int\frac{d^3k}{(2\pi)^3}E(\mathbf{k})\mathbf{v}(\mathbf{k})\delta f(\mathbf{k}) \quad (4.22)$$

In the above expression we do the momentum integration over the Brillouin zone. The factor of two takes care of the spin degeneracy. The thermal conductivity tensor is the proportionality coefficient between the heat current and temperature gradient.

$$(\mathbf{j}_E)_i = -\kappa_{ij}\nabla_j T \quad (4.23)$$

which results in the following expression for the thermal conductivity tensor,

$$(\kappa)_{ij} = -\frac{2}{T} \int \frac{d^3k}{(2\pi)^3} E^2(\mathbf{k}) v_i(\mathbf{k}) v_j(\mathbf{k}) \frac{\partial f^0(\mathbf{k})}{\partial E} \tau(\mathbf{k}) \quad (4.24)$$

where the quasiparticle $\tau(\mathbf{k})$ relaxation time is defined in (4.20).

Thermal Transport in Normal Metals

In a metal the energy of the quasiparticles measured from the chemical potential μ is given by $E(\mathbf{k}) = \xi(\mathbf{k}) = \epsilon(\mathbf{k}) - \mu$. Assume for simplicity that the dispersion $\epsilon(\mathbf{k})$ is quadratic, $\epsilon(\mathbf{k}) = \frac{\hbar|\mathbf{k}|^2}{2m}$, i.e. the velocities are independent of the directions of \mathbf{k} .

$$v_i(\mathbf{k}) = v(\epsilon) \hat{k}_i \quad (4.25)$$

The thermal conductivity given by (4.24) becomes

$$(\kappa)_{ij} = -\frac{2}{T} \int \frac{d\Omega_{\hat{k}}}{4\pi} \hat{k}_i \hat{k}_j \int_{-\mu}^{\infty} d\epsilon N(\epsilon) (\epsilon - \mu)^2 v^2(\epsilon) \frac{\partial f^0(\epsilon)}{\partial E} \tau(\epsilon) \quad (4.26)$$

Changing from ϵ to ξ as the integration variable and recognizing that only quasiparticles close to the Fermi surface participate in thermal transport, we get

$$\begin{aligned} (\kappa)_{ij} &= -\frac{2v_F^2}{3T^2} N(0) \tau_F \delta_{ij} \int_0^{\infty} d\xi \xi^2 \frac{e^{\xi/T}}{(e^{\xi/T} + 1)^2} \\ &= \frac{2v_F^2 T}{3} N(0) \tau_F \delta_{ij} \int_0^{\infty} dx \frac{x^2 e^x}{(e^x + 1)^2} \\ &= \frac{2v_F^2 T}{3} N(0) \tau_F \delta_{ij} \frac{\pi^2}{6} \end{aligned} \quad (4.27)$$

where $N(0) = \frac{mk_F}{2\pi^2\hbar^2}$ is the density of states at the Fermi level. The velocities are $\mathbf{v}(\epsilon) \approx v_F \hat{\mathbf{k}}$, v_F being the Fermi velocity. τ_F is the quasiparticle relaxation time due to scattering channels close to the Fermi surface. Using the relation $N(0)v_F^2 = \frac{3n}{m}$, where n is the quasiparticle density. Therefore we can write

$$(\kappa)_{ij} = \frac{nT\pi^2\tau_F}{3m}\delta_{ij} \quad (4.28)$$

Thus in the normal state the thermal conductivity is linear in T . We now give a simple expression for the quasiparticle relaxation time scattering rate (4.20) in the normal state by considering the case of an isotropic scattering amplitude $\mathcal{V}(\mathbf{k}, \mathbf{k}') = U = \text{const}$. In this simple case the scattering rate becomes

$$\tau^{-1}(\mathbf{k}) = n_{imp}U^2\frac{2\pi}{\hbar} \int \frac{d^3k'}{(2\pi)^3}\delta(\xi(\mathbf{k}) - \xi(\mathbf{k}')) = n_{imp}U^2\frac{2\pi}{\hbar}N(\xi_{\mathbf{k}}) \quad (4.29)$$

where $N(\xi)$ is the density of states for the normal metal. Therefore τ_F is given by

$$\tau_F^{-1} = n_{imp}U^2\frac{2\pi}{\hbar}N(0) \quad (4.30)$$

where $N(0) = \frac{mk_F}{2\pi^2\hbar^2}$ is the density of states at the Fermi level.

Thermal Transport in Superconductors

The kinetic formulation was also first applied to explain the effects that conventional superconductivity has on the thermal conductivity by Bardeen and collaborators [11, 33]. We follow this method to show how the thermal conductivity of a superconductor is calculated within the Boltzmann formulation. We start with the expression (4.24) for the thermal

conductivity tensor specialized for a 2D system

$$(\kappa)_{ij} = -\frac{2}{T} \int \frac{d^2k}{(2\pi)^2} E^2(\mathbf{k}) v_i(\mathbf{k}) v_j(\mathbf{k}) \frac{\partial f^0(\mathbf{k})}{\partial E} \tau(\mathbf{k}) \quad (4.31)$$

In a superconductor we have a quasiparticle branch and a quasihole branch both of which give identical contributions to the heat current. Therefore we only consider the particle branch. Therefore in the superconducting state the quasiparticle dispersion is $E(\mathbf{k}) = \sqrt{\xi^2(\mathbf{k}) + |\Delta(\mathbf{k})|^2}$ and the quasiparticle velocity is $\mathbf{v}(\mathbf{k}) = \nabla_{\mathbf{k}} E(\mathbf{k})$. The equilibrium Fermi distribution is $f_n^0(\mathbf{k}) = \frac{1}{e^{E_n(\mathbf{k})/T} + 1}$. The quasiparticle relaxation time in the Born approximation for an isotropic scattering U is [64].

$$\tau^{-1}(\mathbf{k}) = N_{imp} U^2 \frac{2\pi}{\hbar} \int \frac{d^2k'}{(2\pi)^2} |C(\mathbf{k}, \mathbf{k}')|^2 \delta(E(\mathbf{k}) - E(\mathbf{k}')) \quad (4.32)$$

where $C(\mathbf{k}, \mathbf{k}')$ contains the coherence factors coming from the Bogoliubov transformation between the normal and ordered states. The coherence factors $C(\mathbf{k}, \mathbf{k}')$ can be computed numerically, by first writing the impurity scattering Hamiltonian in the same Nambu basis (2.22) as

$$\begin{aligned} H_{imp} &= U \sum_{\mathbf{k}, \mathbf{k}', s} c_{\mathbf{k}'s}^\dagger c_{\mathbf{k}s} \\ &= \frac{U}{2} \sum_{\mathbf{k}, \mathbf{k}' \in FBZ} \Psi_{\mathbf{k}'s}^\dagger \mathcal{S}_{ab} \Psi_{\mathbf{k}s} \end{aligned} \quad (4.33)$$

$$\mathcal{S}_{ab} = \begin{pmatrix} 1 & 0 \\ 0 & -1 \end{pmatrix}$$

where the factor $\frac{1}{2}$ comes from particle-hole doubling for SC. Upon performing the Bogoliubov transformation (defined in (2.20) and (2.21)) on the Nambu vectors, for either spin

orientations $s = \pm 1(\uparrow, \downarrow)$, we get,

$$H_{imp} = \frac{U}{2} \sum_{\mathbf{k}, \mathbf{k}' \in FBZ} A_{\mathbf{k}'a}^\dagger D_{ab}(\mathbf{k}, \mathbf{k}') A_{\mathbf{k},b} \quad (4.34)$$

where $A_{\mathbf{k}}^\dagger = (a_{\mathbf{k}s}^\dagger, a_{-\mathbf{k}s})$ and the matrix $\hat{D}(\mathbf{k}, \mathbf{k}')$ from which we get the coherence factors

$$\hat{D}(\mathbf{k}, \mathbf{k}') = \hat{B}^\dagger(\mathbf{k}') \hat{\mathcal{S}} \hat{B}(\mathbf{k}) \quad (4.35)$$

The \mathbf{k} dependence in $\hat{D}(\mathbf{k}, \mathbf{k}')$ comes from $\Delta(\mathbf{k})$ and $\xi(\mathbf{k})$ through the eigenvectors of $\hat{\mathcal{H}}_{\mathbf{k}}$.

From the ordering of the $A_{\mathbf{k}}^\dagger$ -vector, the coherence factor is given by

$$\begin{aligned} C(\mathbf{k}, \mathbf{k}') &= D_{11}(\mathbf{k}, \mathbf{k}') \\ |C(\mathbf{k}, \mathbf{k}')|^2 &= \frac{1}{2} \left(1 + \frac{\xi_{\mathbf{k}} \xi_{\mathbf{k}'} - \Delta_{\mathbf{k}} \Delta_{\mathbf{k}'}}{E(\mathbf{k}) E(\mathbf{k}')} \right) \end{aligned} \quad (4.36)$$

Using (4.36) in (4.32) the quasiparticle relaxation time can be calculated. For both the s and d wave superconductors, the $\xi_{\mathbf{k}} \xi_{\mathbf{k}'}$ terms vanish after \mathbf{k}' integration in equation (4.32), due to cancellation of positive and negative $\xi_{\mathbf{k}'}$ contributions. This leaves for the s -wave state

$$\tau^{-1}(\mathbf{k}) = \tau_N^{-1} \frac{N(E(\mathbf{k}))}{N_0} \left(1 - \frac{\Delta^2}{E^2(\mathbf{k})} \right) \quad \text{for } s\text{-wave} \quad (4.37)$$

For the d -wave states also the $\Delta_{\mathbf{k}} \Delta_{\mathbf{k}'}$ terms vanish on integrating over the directions of \mathbf{k}' in equation (4.32), resulting in

$$\tau^{-1}(\mathbf{k}) = \tau_N^{-1} \frac{N(E(\mathbf{k}))}{N_0} \quad \text{for } d_{x^2-y^2} \text{ and } d_{xy} \quad (4.38)$$

$N(E(\mathbf{k}))$ denotes the density of SC states with energies $E(\mathbf{k})$, and N_0 being the normal state density of states at the Fermi level. Using the above expressions for the quasiparticle

relaxation times the thermal conductivity (4.24) can be calculated. Below we present some numerical results [21] for a tight binding Fermi surface given by

$$\xi(\mathbf{k}) = -t_1(\cos k_x + \cos k_y) - t_2 \cos k_x \cos k_y - \mu \quad (4.39)$$

In Fig. 4.1 the temperature profiles of the thermal conductivity for s -, $d_{x^2-y^2}$ - and d_{xy} states are shown. The thermal conductivity for the s -wave superconductor shows a sharp fall and the well known exponential low- T behaviour [11] resulting from the gapping of the entire Fermi surface by the SC order. The general behavior of $\kappa(T)/T$ for the d_{xy} and $d_{x^2-y^2}$ states can be explained explained on the basis of nodal quasiparticles, which dominate the heat transport in the low - T regime, producing the finite residual κ/T . If the FS is circular κ_{xx} is the same for the d_{xy} and $d_{x^2-y^2}$ states [5]. In the case of our anisotropic FS the two states result in very different values of heat conductivity. The $d_{x^2-y^2}$ pairing has nodes on flat parts of the FS with large Fermi velocity and smaller DOS. By gapping the corners of the FS with large DOS, the scattering rate is significantly reduced, producing longer-lived high-velocity nodal quasiparticles that result in heat conductivity exceeding that of the normal state. The d_{xy} state, on the other hand, has nodes where Fermi velocity is small, resulting in much lower κ/T .

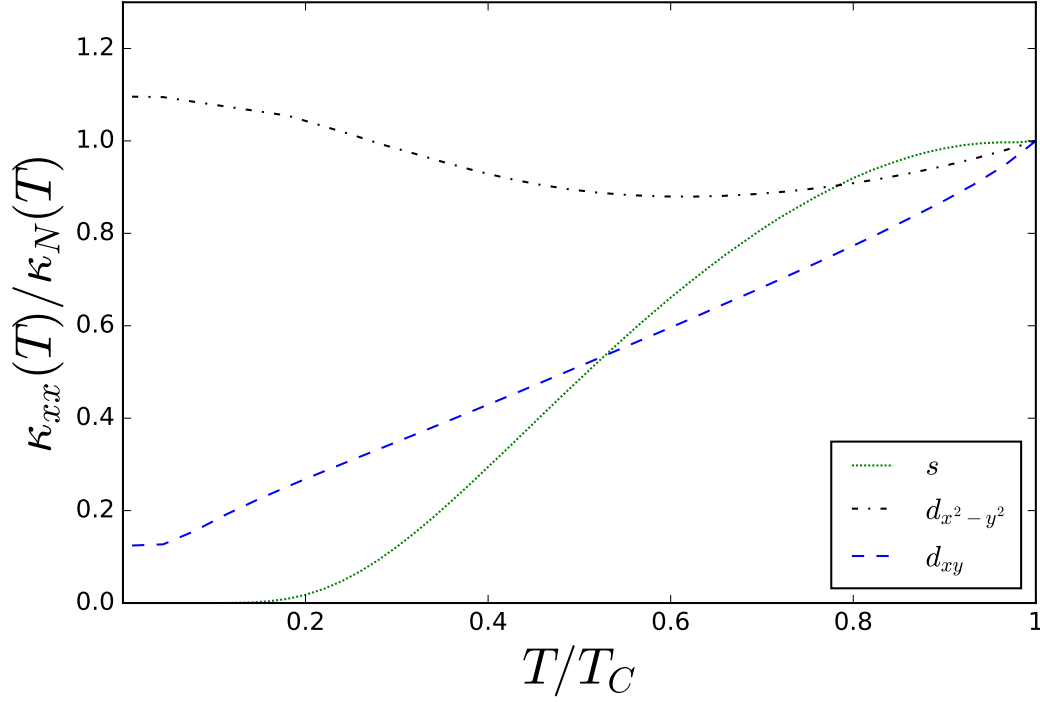


Figure 4.1: Thermal conductivity for SC states: s -, $d_{x^2-y^2}$ - and d_{xy} -wave (dispersion parameters $t_1/2\pi T_C = 100$, $t_2/2\pi T_C = 10$, $\mu = 0$)

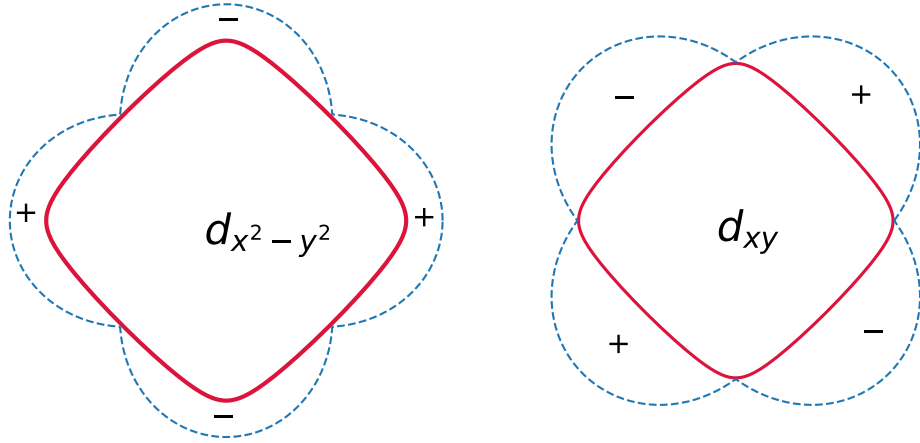


Figure 4.2: The solid red curve shows the shape of the FS for the above parameters, the dashed blue lines are a schematic representation of the order parameter profiles for the $d_{x^2-y^2}$ and d_{xy} pairing states.

Thermal Transport in a metal with a Spin Density Wave

The above method for calculating the thermal conductivity tensor can be generalized to the case of an metal with a Spin Density Wave. We again consider a metal with $2D$ Fermi surface defined by the dispersion (4.39). In the SDW state the total heat current is carried by two quasiparticle branches with energies $E_{1,2}(\mathbf{k}) = \xi^+(\mathbf{k}) \pm \sqrt{(\xi^-(\mathbf{k}))^2 + M^2}$, with the definitions $\xi_{\mathbf{k}}^\pm = \frac{1}{2}(\xi_{\mathbf{k}} \pm \xi_{\mathbf{k}+\mathbf{Q}})$. The thermal conductivity tensor in this case is given by [21],

$$\begin{aligned} \kappa_{ij} &= (\kappa_1)_{ij} + (\kappa_2)_{ij} \\ (\kappa_1)_{ij} &= -\frac{2}{T} \int \frac{d^2k}{8\pi^2} E_1^2(\mathbf{k}) v_{1i}(\mathbf{k}) v_{1j}(\mathbf{k}) \frac{\partial f_1^0(\mathbf{k})}{\partial E_1} \left(\frac{1}{\tau_{11}} + \frac{1}{\tau_{12}} \right)^{-1} \\ (\kappa_2)_{ij} &= -\frac{2}{T} \int \frac{d^2k}{8\pi^2} E_2^2(\mathbf{k}) v_{2i}(\mathbf{k}) v_{2j}(\mathbf{k}) \frac{\partial f_2^0(\mathbf{k})}{\partial E_2} \left(\frac{1}{\tau_{22}} + \frac{1}{\tau_{21}} \right)^{-1} \end{aligned} \quad (4.40)$$

In the above expression we integrate momentum over the FBZ, double-counting the states, and therefore requires an extra factor of 2 in denominator: $2 \times 4\pi^2$. The quasiparticle velocities are $\mathbf{v}_n(\mathbf{k}) = \nabla_{\mathbf{k}} E_n(\mathbf{k})$ and the the equilibrium Fermi distribution is $f_n^0(\mathbf{k}) = \frac{1}{e^{E_n(\mathbf{k})/T} + 1}$. The quasiparticle relaxation times in the Born approximation are [21]

$$\tau_{nm}^{-1}(\mathbf{k}) = N_{imp} \frac{2\pi}{\hbar} U^2 \int \frac{d^2k'}{(2\pi)^2} |C_{nm}(\mathbf{k}, \mathbf{k}')|^2 \delta(E_n(\mathbf{k}) - E_m(\mathbf{k}')) \quad (4.41)$$

where $C(\mathbf{k}, \mathbf{k}')$ contains the coherence factors coming from the Bogoliubov transformation between the normal and ordered states. The coherence factors $C_{nm}(\mathbf{k}, \mathbf{k}')$ are again computed

by first writing the impurity scattering Hamiltonian in the same Nambu basis (3.12) as

$$\begin{aligned}
H_{imp} &= U \sum_{\mathbf{k}, \mathbf{k}', \sigma} c_{\mathbf{k}'\sigma}^\dagger c_{\mathbf{k}\sigma} \\
&= \frac{U}{2} \sum_{\mathbf{k}, \mathbf{k}' \in FBZ} \Phi_{\mathbf{k}'\sigma}^\dagger \mathcal{S}_{ab} \Phi_{\mathbf{k}\sigma} \\
\mathcal{S}_{ab} &= \begin{pmatrix} 1 & 0 \\ 0 & 1 \end{pmatrix}
\end{aligned} \tag{4.42}$$

where the factor $\frac{1}{2}$ comes from $(\mathbf{k}, \mathbf{k} + \mathbf{Q})$ doubling for the SDW. Upon performing the Bogoliubov transformation defined in (3.11) for either spin orientations $\sigma = \pm 1(\uparrow, \downarrow)$, we get,

$$H_{imp} = \frac{U}{2} \sum_{\mathbf{k}, \mathbf{k}' \in FBZ} F_{\mathbf{k}'a}^\dagger D_{ab}(\mathbf{k}, \mathbf{k}') F_{\mathbf{k},b} \tag{4.43}$$

where $F_{\mathbf{k}}^\dagger = (f_{\mathbf{k}\sigma}^\dagger, f_{\mathbf{k}+\mathbf{Q}\sigma}^\dagger)$ and the matrix $\hat{D}(\mathbf{k}, \mathbf{k}')$ from which we get the coherence factors

$$\hat{D}(\mathbf{k}, \mathbf{k}') = \hat{B}^\dagger(\mathbf{k}') \hat{\mathcal{S}} \hat{B}(\mathbf{k}) \tag{4.44}$$

The intra-band coherence factors are

$$C_{11}(\mathbf{k}, \mathbf{k}') = D_{11}(\mathbf{k}, \mathbf{k}') , \quad C_{22}(\mathbf{k}, \mathbf{k}') = D_{22}(\mathbf{k}, \mathbf{k}') ,$$

and the inter-band coherence factors are

$$C_{12}(\mathbf{k}, \mathbf{k}') = D_{12}(\mathbf{k}, \mathbf{k}') , \quad C_{21}(\mathbf{k}, \mathbf{k}') = D_{21}(\mathbf{k}, \mathbf{k}')$$

The analytic expression for the coherence factors are given by,

$$|C_{11}|^2 = |C_{22}|^2 = \frac{1}{2} \left(1 + \frac{\xi_{\mathbf{k}}^- \xi_{\mathbf{k}'}^- + M^2}{\Pi_{\mathbf{k}} \Pi_{\mathbf{k}'}} \right), \quad (4.45)$$

$$|C_{12}|^2 = |C_{21}|^2 = \frac{1}{2} \left(1 - \frac{\xi_{\mathbf{k}}^- \xi_{\mathbf{k}'}^- + M^2}{\Pi_{\mathbf{k}} \Pi_{\mathbf{k}'}} \right) \quad (4.46)$$

where $\Pi_{\mathbf{k}} = \sqrt{(\xi_{\mathbf{k}}^-)^2 + M^2}$. In Fig. 4.3 we show thermal conductivities for a SDW metal. When the FS is perfectly nested $\mu = 0$ and $t_2 = 0$ in our model (4.39), the SDW opens a gap along entire FS (sketched in Fig. 4.4a) causing the sharp fall in the thermal conductivity seen in Fig. 4.3. When the FS is partially nested $\mu = 0$ and $t_2/t_1 = 0.1$ in our model (4.39), a part of the FS gets gapped with M which is indicated by the regions shaded in orange sketched in Fig. 4.4b. The thermal conductivity $\kappa(T)$ drops, but gets saturated at a finite value due to the remaining FS, shown by the cyan lines, which gives a weaker-than-normal metallic state.

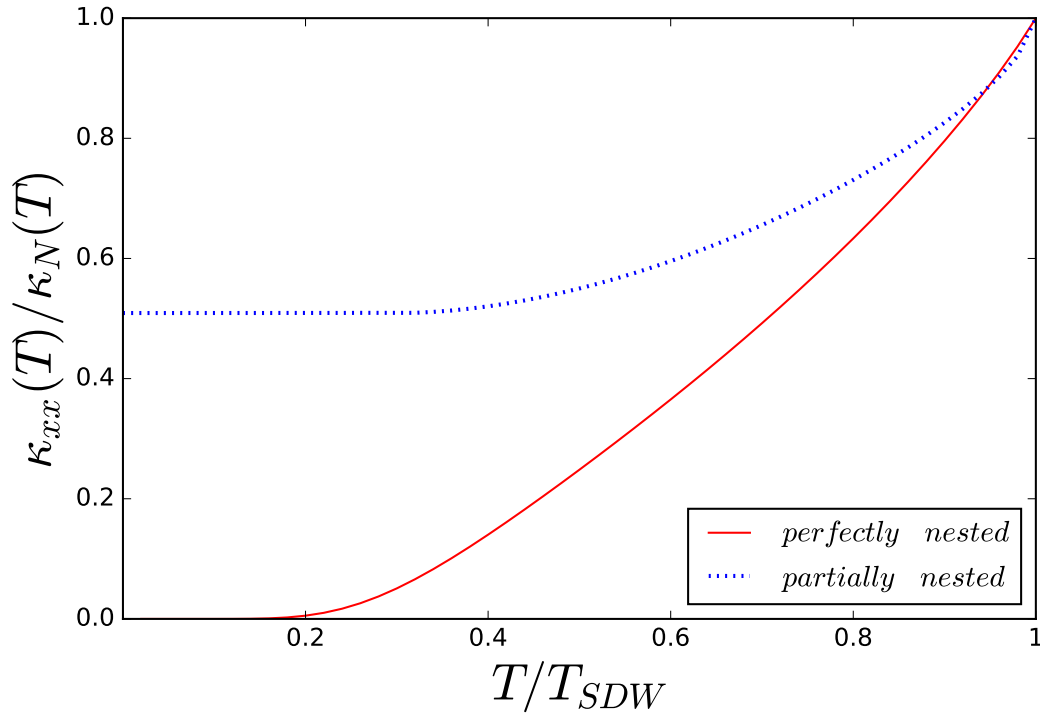


Figure 4.3: Thermal conductivity for a SDW metal (dispersion parameters for a perfectly nested FS are $t_1/2\pi T_{SDW} = 100$, $t_2/2\pi T_{SDW} = 0$ and for a partially nested FS are $t_1/2\pi T_{SDW} = 100$, $t_2/2\pi T_{SDW} = 10$)

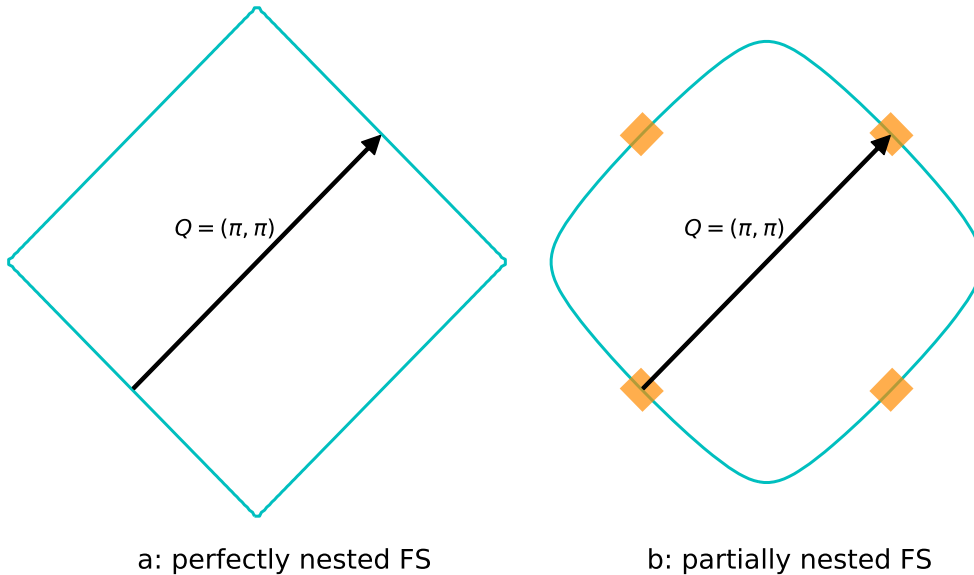


Figure 4.4: The solid cyan curve shows the shapes of the partially nested and perfectly nested Fermi Surfaces for the above parameters. The regions of the FS gapped by the SDW order are shaded in orange.

THERMAL TRANSPORT IN SUPERCONDUCTORS WITH COEXISTING SPIN
DENSITY WAVE ORDER

Contribution of Authors and Co-Authors

Manuscript in following chapter

Author: [Sourav Sen Choudhury]

Contributions: [Carried out all numerical and analytical calculations and analysed the results. Produced the first draft of the manuscript, and jointly wrote the final manuscript with A.B.V.]

Author: [Anton B. Vorontsov]

Contributions: [Analysed the results and jointly wrote the final manuscript with S.S.C.]

Manuscript Information

[Sourav Sen Choudhury and Anton B. Vorontsov]

[Physical Review B]

Status of Manuscript:

Prepared for submission to a peer-reviewed journal

Officially submitted to a peer-reviewed journal

Accepted by a peer-reviewed journal

Published in a peer-reviewed journal

[American Physical Society]

[14 November 2020]

[1 March 2021]

[Physical Review B **103**, 104501 (2021)]

[10.1103/PhysRevB.103.104501]

Thermal transport in superconductors with coexisting spin density wave order

Sourav Sen Choudhury  and Anton B. Vorontsov 

Department of Physics, Montana State University, Bozeman, Montana 59717, USA



(Received 14 November 2020; revised 21 January 2021; accepted 16 February 2021; published 1 March 2021)

We study thermal transport in a two-dimensional system with coexisting s - or d -wave superconducting (SC) and spin density wave (SDW) orders. We analyze the nature of coexistence phase in a tight-binding square lattice with $\mathbf{Q} = (\pi, \pi)$ SDW ordering. The electronic thermal conductivity is computed within the framework of the Boltzmann kinetic theory, using Born approximation for the impurity scattering collision integral. We describe the influence of the Fermi surface (FS) topology, the competition between the SC and SDW order parameters, and the presence or absence of zero energy excitations in the coexistence phase, on the low temperature behavior of thermal conductivity of the various pairing states. We present qualitative analytical and fully numerical results that show that the heat transport signatures of various SC states emerging from collinear SDW order are quite distinct and depend on the symmetry properties of the SC order parameter under translation by the SDW nesting vector \mathbf{Q} . A combination of (π, π) -SDW and the $d_{x^2-y^2}$ pairing state results in fully gapped excitations, whereas (π, π) -SDW coexisting with either d_{xy} or s -wave pairing states may always have gapless excitations. There appear special stable Dirac nodal points that are not gapped by the SC order in the coexistence phase, resulting in finite residual heat conductivity.

DOI: [10.1103/PhysRevB.103.104501](https://doi.org/10.1103/PhysRevB.103.104501)

I. INTRODUCTION

In normal metals, at low temperatures transport properties are primarily determined by scattering of electrons by impurities. The thermal conductivity $\kappa_N(T)$ has a linear T dependence, which is well understood within the framework of semiclassical transport theory based on the Boltzmann kinetic equation [1]. The kinetic formulation was also successfully used to explain the effects that conventional superconductivity has on the thermal conductivity [2,3]. With the discoveries of heavy fermion [4], cuprate [5–8], and iron based [9–11] superconductors, new questions have arisen with regards to the low temperature transport properties of superconductors. The behavior of the thermal conductivity at low temperatures for these unconventional superconductors is not at all like that of the fully-gapped conventional type superconductors. One reason is that most unconventional superconductors have a nodal gap structure, i.e., there exist points on the Fermi surface (FS), nodes, where the superconducting gap is zero. As the energy gap is small around the nodes, the nodal quasiparticles can be easily excited and they dominate the heat transport properties of such superconductors. This problem has been studied by a number of authors at various levels of complexity [12–17], and thermal conductivity measurements became a very useful probe of superconductivity as it can reveal the gap structure of unconventional superconductors [18,19].

Another characteristic feature of many unconventional superconductors is the proximity of magnetic and superconducting orders in these materials [20–24]. The electronic phase diagrams of many highly correlated systems are complex, with multiple broken symmetry phases appearing with similar ordering temperatures as material properties, such as

dopant concentration, varied over wide ranges. For example, there is a proximate antiferromagnetic (AF) state in the phase diagrams of superconductors such as cuprates [22], iron pnictides [24], and heavy fermion superconductors [21,23].

However much less is known about thermal transport in superconductors with coexisting orders (spin-density wave (SDW), charge-density wave (CDW)). Previous studies have addressed mainly one aspect of the heat conductivity in coexisting phases like superconducting (SC) and CDW or SC and SDW [25,26], with cuprates as an application. In d -wave superconductors heat transport by nodal quasiparticles shows impurity-independent, *universal*, limit at low temperatures [16,17], seen in many materials [19,27]. Theoretical investigations of thermal transport in “superconductor + density wave order” systems [25,26] attacked the issue of CDW or SDW order influencing the $T \rightarrow 0$ limit of thermal conductivity by nodal quasiparticles in $d_{x^2-y^2}$ superconductors, in particular how the nodes get gapped by the additional order. The transport calculations were carried out in 2D, within Kubo linear response theory using Green’s function technique, where impurity effects were included only through non-self-consistent energy broadening parameter. The CDW or SDW were also incorporated non-self-consistently, as an additional tunable small order on top of the SC state, and neither the nature of the coexistence, nor its temperature dependence, was investigated. These calculations indicated that the robustness of the universal limit of thermal conductivity of $d_{x^2-y^2}$ superconductors depends on the direction of the ordering vector and the type of the coexisting order (CDW or SDW). Additional order displaces the nodes in k space. For example, the nodal quasiparticles become gapped by the SDW once the d -SC nodes are separated by exactly the ordering \mathbf{Q}

vector [26]. Another study [28] looked at the changes in zero-temperature heat transport across continuous SC to SC+SDW transition for $d_{x^2-y^2}$ superconductor, employing the same non-self-consistent treatments of impurities and SDW order, assumed to be controlled by doping. These calculations show that thermal conductivity behaves very differently depending whether emerging SDW is commensurate or incommensurate. For a commensurate SDW the SC \rightarrow SC+SDW transition results in a gradual drop in κ as a function of growing SDW order, whereas incommensurate SDW results in a sharp drop across the transition [28].

To complement previous studies and provide a different approach, in this paper we look at the thermal transport properties of a number of different superconducting states in which the SC order coexists with the antiferromagnetic spin density wave (SDW) order in the full temperature range. For transport calculation we use quasiparticle Boltzmann equation which is physically more transparent than the Green's function or quasiclassical techniques. The goal is to understand the nature of the different coexistence states arising from the interplay between the SC and SDW order parameters and its impact on the temperature behavior of the thermal conductivity of several pairing states: s -wave, $d_{x^2-y^2}$, and d_{xy} symmetry. The choice of the d -wave states is motivated by the fact that it is a prototypical unconventional pairing state, with sign-changing order parameter and nodal quasiparticles, applicable to heavy fermion and cuprate superconductors [6]. In this paper we calculate the thermal conductivity in which scattering of quasiparticles by nonmagnetic impurities is the dominant process. Within Boltzmann theory, we only consider the case of small phase shifts, i.e., the Born approximation for weak interaction of electrons with impurities. The impurity scattering is the dominant mechanism at lower temperatures, and at higher temperatures the scattering rates can be augmented to incorporate temperature-dependent inelastic scattering [29,30], to reflect the growth of thermal conductivity below T_c , seen in, e.g., CeCoIn₅ [23], or UPt₃ [31].

The organization of the paper is as follows. In Secs. II A–II C, we discuss the model Hamiltonian, symmetries of the SC order parameter, and the topology of the Fermi surface. Self-consistent approach to determining coexisting SDW and SC order parameters is presented in Sec. II E. Kinetic formalism is described in Sec. II F. Numerical results for heat conductivity is discussed in Sec. III. Section IV is a brief conclusion.

II. MODEL AND FORMALISM

A. Hamiltonian

For our model we start with a tight-binding normal state Hamiltonian

$$H_0 = \sum_{\mathbf{k}, \sigma = \pm 1} \xi(\mathbf{k}) c_{\mathbf{k}\sigma}^\dagger c_{\mathbf{k}\sigma}, \quad (1)$$

where

$$\xi(\mathbf{k}) = -t_1(\cos k_x + \cos k_y) - t_2 \cos k_x \cos k_y - \mu$$

is the inversion-symmetric dispersion relation, $\xi(\mathbf{k}) = \xi(-\mathbf{k})$. It describes the nearest neighbor ($t_1 > 0$) and next-nearest neighbor ($t_2 > 0$) hopping on a 2D square lattice with lattice

spacing $a = 1$. We set the chemical potential to zero, and therefore for $t_2 > 0$ the electron filling is slightly less than half. This results in a Fermi surface that is not perfectly nested and therefore potentially susceptible to coexistence of SC and SDW order parameters. The perfect nesting limit is given by setting $t_2 = 0$. The coexistence of SC and SDW orders in models of this type have been previously studied by Machida [32–34]. We wish to look at heat transport in these models across the SDW \rightarrow SC transition. The full mean-field Hamiltonian for a system with intertwined SC and SDW order is given by [34]

$$\begin{aligned} H &= H_0 + H_{\text{SDW}} + H_{\text{SC}}, \\ H_{\text{SDW}} &= \frac{1}{2} \sum_{\mathbf{k}, \sigma} \sigma M (c_{\mathbf{k}\sigma}^\dagger c_{\mathbf{k}+\mathbf{Q}\sigma} + \text{H.c.}), \\ H_{\text{SC}} &= \frac{1}{2} \sum_{\mathbf{k}, \sigma} \sigma \Delta_{\mathbf{k}} (c_{\mathbf{k}\sigma}^\dagger c_{-\mathbf{k}-\sigma}^\dagger + \text{H.c.}) \end{aligned} \quad (2)$$

The mean field order parameters are defined by the following self-consistent equations

$$\begin{aligned} M &= -\frac{U}{2} \sum_{\mathbf{k}, \sigma} \sigma \langle c_{\mathbf{k}+\mathbf{Q}\sigma}^\dagger c_{\mathbf{k}\sigma} \rangle, \\ \Delta_{\mathbf{k}} &= -\sum_{\mathbf{k}'} g(\mathbf{k}, \mathbf{k}') \langle c_{-\mathbf{k}', \downarrow}^\dagger c_{\mathbf{k}', \uparrow}^\dagger \rangle, \end{aligned} \quad (3)$$

where U is the repulsive onsite Coulomb interaction which leads to the SDW formation [35]. We consider a collinear sinusoidal SDW with spatial magnetization $\mathbf{m}(\mathbf{r}) = 2M\hat{z} \cos(\mathbf{Q} \cdot \mathbf{r})$. The SDW couples electron states with parallel spins and momenta differing by the nesting vector \mathbf{Q} , i.e., $(\mathbf{k} \uparrow)$ with $(\mathbf{k} + \mathbf{Q} \uparrow)$ and $(\mathbf{k} \downarrow)$ with $(\mathbf{k} + \mathbf{Q} \downarrow)$ (this is schematically represented by dashed lines in Fig. 1). As for the SC pairing interaction, we consider the singlet channel and assume the interaction to be of the form $g(\mathbf{k}, \mathbf{k}') = g\eta(\mathbf{k})\eta(\mathbf{k}')$, $\eta(\mathbf{k})$ being a basis function compatible with the square symmetry of the 2D lattice. The SC order parameter combines time-reversed electron states with opposite momenta and antiparallel spins, i.e., $(-\mathbf{k} \downarrow)$ with $(\mathbf{k} \uparrow)$ and $(-\mathbf{k} - \mathbf{Q} \downarrow)$ with $(\mathbf{k} + \mathbf{Q} \uparrow)$ (this is schematically represented by dotted lines in Fig. 1). For our purposes we consider the case where the pure SDW transition temperature T_{SDW} is greater than the pure SC transition temperature T_{C0} , i.e., the ratio

$$p = \frac{T_{\text{C0}}}{T_{\text{SDW}}} < 1.$$

B. Symmetry classes of the SC order parameters

The coexistence problem critically depends on the symmetry properties of the SC order parameter and also on the topology of the FS. If we consider the case of a commensurate SDW with nesting vector $\mathbf{Q} = (\pi, \pi)$, i.e., $2\mathbf{Q} = \mathbf{G} = (2\pi, 2\pi)$ —the diagonal reciprocal lattice vectors for the 2D square lattice—then the various SC pairing states can be classified [36] based on the combined symmetry operations of parity, $\Delta_{-\mathbf{k}} = \pm\Delta_{\mathbf{k}}$ (even or odd), and translation by the nesting vector, $\Delta_{\mathbf{k}+\mathbf{Q}} = \pm\Delta_{\mathbf{k}}$ (even or odd). The symmetry classification of the pairing states ($\Delta_{\mathbf{k}} = \Delta\eta(\mathbf{k})$) are

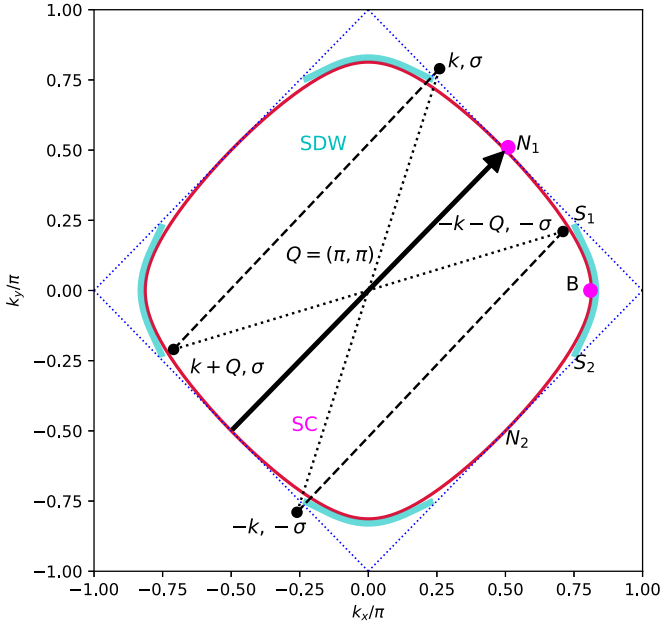


FIG. 1. The FS of the normal state (solid red curve) and in the SDW phase (cyan curve). The parameters are $t_2/t_1 = 0.2$, $M/t_1 = 0.1$ (this value is taken for illustration purposes, the typical value in the calculations are $M/t_1 \sim 10^{-3}$). $\mathbf{Q} = (\pi, \pi)$ is the nesting vector. The dashed blue square indicates the boundary of the reduced Brillouin zone (RBZ).

summarized in Table I. This classification has important consequences for the coexistence problem [34]: The SC states in the (E, E) class are competitive with the SDW, whereas states in the (E, O) class are less competitive with the SDW and the two orders can naturally coexist. The difference in the nature of the coexistence problem in these two distinct symmetry classes has an obvious impact on the thermal transport properties of the system across the SDW \rightarrow SC transition. One of the aims of this paper is to establish the relation between the nature of the SC-SDW coexistence and its signatures in the electronic thermal transport.

C. Topology of the Fermi surface

In Fig. 1 we show the Fermi surface for our model. In the normal state the FS is indicated by the solid red curve. The

$$H = \frac{1}{4} \sum_{\mathbf{k} \in \text{FBZ}} \Psi_{\mathbf{k}}^\dagger \mathcal{H}_{\mathbf{k}, \mathbf{Q}} \Psi_{\mathbf{k}} \mathcal{H}_{\mathbf{k}, \mathbf{Q}} = \left(\begin{array}{cc|cc} \xi_{\mathbf{k}} & \Delta_{\mathbf{k}}(i\sigma_y) & \mathbf{M}_{\mathbf{Q}}^* \sigma & 0 \\ -\Delta_{-\mathbf{k}}^*(i\sigma_y) & -\xi_{-\mathbf{k}} & 0 & -\mathbf{M}_{\mathbf{Q}}^* \sigma^* \\ \mathbf{M}_{\mathbf{Q}} \sigma & 0 & \xi_{\mathbf{k}+\mathbf{Q}} & \Delta_{\mathbf{k}+\mathbf{Q}}(i\sigma_y) \\ 0 & -\mathbf{M}_{\mathbf{Q}} \sigma^* & -\Delta_{-\mathbf{k}-\mathbf{Q}}^*(i\sigma_y) & -\xi_{-\mathbf{k}-\mathbf{Q}} \end{array} \right), \quad (4)$$

where we ‘folded’ the normal state band into the reduced Brillouin zone appropriate for the (π, π) -SDW unit cell. The $1/4$ in front comes from the particle-hole doubling of the bands for superconductivity and the $\mathbf{k}, \mathbf{k} + \mathbf{Q}$ doubling for SDW. We do our analysis in the full Brillouin zone (FBZ) primarily to take advantage of the particle-hole symmetry, which simplifies the calculation of scattering rates in Sec. F.

TABLE I. The symmetry classification of the various pairing states and the corresponding basis functions. First letter (E —even, O —odd) corresponds to parity symmetry $\Delta_{-\mathbf{k}} = \pm \Delta_{\mathbf{k}}$, and the second letter is for SDW translations $\Delta_{\mathbf{k}+\mathbf{Q}} = \pm \Delta_{\mathbf{k}}$.

Symmetry class	Pairing state	SC basis function
I or (E, O)	$d_{x^2-y^2}$	$\eta(\mathbf{k}) = \frac{1}{2}(\cos k_x - \cos k_y)$
II or (E, E)	d_{xy} s wave	$\eta(\mathbf{k}) = \sin k_x \sin k_y$, $\eta(\mathbf{k}) = 1$

SDW with the ordering vector $\mathbf{Q} = (\pi, \pi)$ doubles the lattice cell size reducing the Brillouin zone to the dotted blue square (RBZ). For this SDW ordering all four flat sides of the normal FS are nested, and become gapped, leaving zero energy excitations only at the corners—the FS in the SDW state is indicated by the solid cyan curve. As the SDW gap grows from zero and reaches its maximum value the FS continuously shrinks from the $N_1 - N_2$ section to the $S_1 - S_2$ section. Points N_1 and B denote location of the nodes of the $d_{x^2-y^2}$ and d_{xy} pairing states, respectively, they are indicated by the magenta dots. Since SDW gaps region around point N_1 , appearance of the $d_{x^2-y^2}$ SC gap completely removes the low-energy excitations. In the case of the d_{xy} pairing state the low-energy excitations remain since the nodal line crosses Fermi pocket at point B , which is not gapped by the SDW. Further, in the case of the d_{xy} - and s -wave pairing states, we show that unusual zero energy excitations remain on the boundary of the RBZ near points $S_{1,2}$, even when the SC order starts to grow inside the SDW state. The stability of these zero energy excitations is related to the even symmetry of the d_{xy} - and s -wave states under translations by the nesting vector \mathbf{Q} . We explain this in more detail in the following section. The relative positions of the nodes for the two d -wave pairing states, and the extra zero energy excitations in the coexistence phase of the d_{xy} state leads to their different thermal conductivity $\kappa(T)$ behavior.

D. Diagonalization of the model Hamiltonian

The more general form for Hamiltonian (2), corresponding to SDW magnetization $\mathbf{m}(\mathbf{r}) = \text{Re}(\mathbf{M}_{\mathbf{Q}} e^{i\mathbf{Q}\mathbf{r}})$ is an 8×8 matrix

The Nambu state vector is

$$\Psi_{\mathbf{k}}^\dagger = (c_{\mathbf{k}\alpha_1}^\dagger, c_{-\mathbf{k}\alpha_2}, c_{\mathbf{k}+\mathbf{Q}\alpha_3}^\dagger, c_{-\mathbf{k}-\mathbf{Q}\alpha_4}), \quad \alpha_{1,2,3,4} = \uparrow, \downarrow.$$

Each outlined block represents a 4×4 matrix constructed from spin up-down and particle-hole spaces, represented by Pauli matrices $\sigma_{x,y,z}$ and $\tau_{1,2,3}$ correspondingly. Diagonal blocks in the full matrix represent the ‘folded’

superconducting bands, while off-diagonal 4×4 blocks appear as result of SDW mixing of the electron states with momenta \mathbf{k} and $\mathbf{k} + \mathbf{Q}$ on ‘folded’ bands. With this ‘folded’ space we associate Pauli matrices $\rho_{1,2,3}$. The Hamiltonian is (anti)symmetric under particle-hole transformation by the construction due to superconductivity doubling (K is complex conjugation)

$$\mathcal{C}\mathcal{H}_{\mathbf{k},\mathbf{Q}}\mathcal{C}^{-1} = -\mathcal{H}_{-\mathbf{k},-\mathbf{Q}}, \quad \mathcal{C} = 1_\rho \otimes \tau_1 \otimes 1_\sigma K. \quad (5)$$

Also, while the time-reversal symmetry is definitely broken in the SDW state, because transformation $\mathcal{T} = 1_\rho \otimes 1_\tau \otimes (i\sigma_y)K$ reverses the magnetization direction $\mathbf{M} \rightarrow -\mathbf{M}$, a combination of time reversal and a ‘gauge’ transformation $c_{\mathbf{k}+\mathbf{Q}} \rightarrow -c_{\mathbf{k}+\mathbf{Q}}$, given by ρ_3 , can still be a symmetry

$$\mathcal{T}_\pi \mathcal{H}_{\mathbf{k},\mathbf{Q}} \mathcal{T}_\pi^{-1} = \mathcal{H}_{-\mathbf{k},-\mathbf{Q}}, \quad \mathcal{T}_\pi = \rho_3 \otimes 1_\tau \otimes (i\sigma_y)K \quad (6)$$

provided $\xi_{\mathbf{p}} = \xi_{-\mathbf{p}}$, $\Delta_{\mathbf{p}}^* = \Delta_{\mathbf{p}}$ and $\mathbf{M}_{-\mathbf{Q}} = \mathbf{M}_{\mathbf{Q}}^*$. (The gauge transformation establishes an arbitrary phase φ between states \mathbf{k} and $\mathbf{k} + \mathbf{Q}$: $c_{\mathbf{k}+\mathbf{Q}} \rightarrow e^{i\varphi} c_{\mathbf{k}+\mathbf{Q}}$, which results in a ‘slide’ of the SDW profile $\mathbf{m}(\mathbf{r}) \propto \text{Re}(\langle c_{\mathbf{k}+\mathbf{Q}}^\dagger c_{\mathbf{k}} \rangle e^{-i\mathbf{Q}\cdot\mathbf{r}})$: $\mathbf{M} \cos(\mathbf{Q} \cdot \mathbf{r}) \rightarrow \mathbf{M} \cos(\mathbf{Q} \cdot \mathbf{r} + \varphi)$, signifying arbitrariness of the coordinate origin. Shift by half wavelength of SDW order, for $\varphi = \pi$, reverses the magnetization direction, canceling the time reversal.)

With real $\Delta_{\mathbf{k}}$, M and inversion-symmetric $\xi_{\mathbf{k}}$, both charge conjugation and ‘time-gauge’ symmetries are present, so we split the full Hamiltonian into two independent 4×4 blocks for particular spin orientations $\sigma = \pm 1(\uparrow, \downarrow)$,

$$H^{(\sigma)} = \frac{1}{4} \sum_{\mathbf{k} \in \text{FBZ}} \Psi_{\mathbf{k}\sigma}^\dagger \mathcal{H}_{\mathbf{k}}^{(\sigma)} \Psi_{\mathbf{k}\sigma}$$

$$\mathcal{H}_{\mathbf{k}}^{(\sigma)} = \begin{pmatrix} \xi_{\mathbf{k}} & \sigma \Delta_{\mathbf{k}} & \sigma M & 0 \\ \sigma \Delta_{-\mathbf{k}} & -\xi_{-\mathbf{k}} & 0 & \sigma M \\ \sigma M & 0 & \xi_{\mathbf{k}+\mathbf{Q}} & \sigma \Delta_{\mathbf{k}+\mathbf{Q}} \\ 0 & \sigma M & \sigma \Delta_{-\mathbf{k}-\mathbf{Q}} & -\xi_{-\mathbf{k}-\mathbf{Q}} \end{pmatrix}, \quad (7)$$

where $\Psi_{\mathbf{k}\sigma}^\dagger = (c_{\mathbf{k}\sigma}^\dagger, c_{-\mathbf{k}-\sigma}^\dagger, c_{\mathbf{k}+\mathbf{Q}\sigma}^\dagger, c_{-\mathbf{k}-\mathbf{Q}-\sigma}^\dagger)$ represents partial Nambu vector. Hamiltonian (7) is diagonalized by the Bogoliubov transformation

$$\Psi_{\mathbf{k}\sigma} = \begin{pmatrix} c_{\mathbf{k}\sigma} \\ c_{-\mathbf{k}-\sigma}^\dagger \\ c_{\mathbf{k}+\mathbf{Q}\sigma} \\ c_{-\mathbf{k}-\mathbf{Q}-\sigma}^\dagger \end{pmatrix} = \hat{B}_\sigma(\mathbf{k}) \begin{pmatrix} a_{1\mathbf{k}} \\ a_{3\mathbf{k}}^\dagger \\ a_{2\mathbf{k}} \\ a_{4\mathbf{k}}^\dagger \end{pmatrix} \quad (8)$$

with the matrix $\hat{B}_\sigma(\mathbf{k})$, whose columns are the eigenvectors of the Hamiltonian matrix

$$\mathcal{H}_{\mathbf{k}}^{(\sigma)} \hat{B}_\sigma(\mathbf{k}) = \hat{B}_\sigma(\mathbf{k}) \hat{E}_\sigma(\mathbf{k}) \quad (9)$$

where

$$\hat{E}_\sigma(\mathbf{k}) = \begin{pmatrix} E_1^\sigma(\mathbf{k}) & 0 & 0 & 0 \\ 0 & -\tilde{E}_1^\sigma(\mathbf{k}) & 0 & 0 \\ 0 & 0 & E_2^\sigma(\mathbf{k}) & 0 \\ 0 & 0 & 0 & -\tilde{E}_2^\sigma(\mathbf{k}) \end{pmatrix}. \quad (10)$$

The $-\sigma$ spin sector is diagonalized in a similar way, and we obtain another matrix $\hat{B}_{-\sigma}(\mathbf{k})$, and the quasiparticle

creation-annihilation operators

$$\Psi_{\mathbf{k}-\sigma} = \hat{B}_{-\sigma}(\mathbf{k})(a_{1\mathbf{k}}, a_{3\mathbf{k}}^\dagger, a_{2\mathbf{k}}, a_{4\mathbf{k}}^\dagger)^T \quad (11)$$

$$\mathcal{H}_{\mathbf{k}}^{(-\sigma)} \hat{B}_{-\sigma}(\mathbf{k}) = \hat{B}_{-\sigma}(\mathbf{k}) \hat{E}_{-\sigma}(\mathbf{k}). \quad (12)$$

The two spin sectors are connected by the present symmetries. For example, the particle-hole transformation connects $\mathcal{C}\mathcal{H}_{\mathbf{k}}^{(\sigma)}\mathcal{C}^{-1} = -\mathcal{H}_{-\mathbf{k}}^{(-\sigma)}$ and we can identify $\hat{E}_{1,2}^\sigma(\mathbf{k}) = \hat{E}_{1,2}^{-\sigma}(-\mathbf{k})$, relating eigenvectors $\hat{B}_{-\sigma}(-\mathbf{k}) = \mathcal{C}\hat{B}_\sigma(\mathbf{k})$ and the quasiparticle branches $3\mathbf{k} = 1'(-\mathbf{k})$, $4\mathbf{k} = 2'(-\mathbf{k})$, etc. The time-reversal + gauge combination reduces distinct energy levels further, by requiring $E_{1,2}^\sigma(\mathbf{k}) = E_{1,2}^{-\sigma}(-\mathbf{k})$, leaving just two different energy values for four quasiparticle branches.

Using definitions $\xi_{\mathbf{k}}^\pm = \frac{1}{2}(\xi_{\mathbf{k}} \pm \xi_{\mathbf{k}+\mathbf{Q}})$ and $\Delta_{\mathbf{k}}^\pm = \frac{1}{2}(\Delta_{\mathbf{k}} \pm \Delta_{\mathbf{k}+\mathbf{Q}})$, these eigenvalues of $\hat{\mathcal{H}}_{\mathbf{k}}$ can be written as [37,38]

$$E_1^2(\mathbf{k}) = \Gamma_{\mathbf{k}} + 2\Lambda_{\mathbf{k}}, \quad E_2^2(\mathbf{k}) = \Gamma_{\mathbf{k}} - 2\Lambda_{\mathbf{k}}$$

$$\Gamma_{\mathbf{k}} = (\xi_{\mathbf{k}}^+)^2 + (\xi_{\mathbf{k}}^-)^2 + (\Delta_{\mathbf{k}}^+)^2 + (\Delta_{\mathbf{k}}^-)^2 + M^2$$

$$\Lambda_{\mathbf{k}} = [(\xi_{\mathbf{k}}^+ \xi_{\mathbf{k}}^- + \Delta_{\mathbf{k}}^+ \Delta_{\mathbf{k}}^-)^2 + M^2((\xi_{\mathbf{k}}^+)^2 + (\Delta_{\mathbf{k}}^+)^2)]^{\frac{1}{2}}. \quad (13)$$

In the pure SDW state ($\Delta = 0$) we get $E_{1,2}^2(\mathbf{k}) = (\xi_{\mathbf{k}}^\pm \pm \sqrt{(\xi_{\mathbf{k}}^\mp)^2 + M^2})^2$ and we assign specific roots to the SDW branches as $E_{\alpha,\beta} = \xi_{\mathbf{k}}^\pm \pm \sqrt{(\xi_{\mathbf{k}}^\mp)^2 + M^2}$ (Greek indices refer to signs $\alpha(+)$, $\beta(-)$). In Fig. 2(a) we show the structure of the two distinct (spin degenerate) quasiparticle bands in the pure SDW phase when the FS is not perfectly nested, leaving a hole pocket $E_\beta(\mathbf{k}) = 0$ around $(\pi, 0)$.

In the coexistence phase we specify eigenvalues (13) for the two symmetry classes: $I = (E, O)$ class ($\Delta_{\mathbf{k}}^+ = 0$, or $\Delta_{\mathbf{k}+\mathbf{Q}} = -\Delta_{\mathbf{k}}$) and $II = (E, E)$ class ($\Delta_{\mathbf{k}}^- = 0$, or $\Delta_{\mathbf{k}+\mathbf{Q}} = \Delta_{\mathbf{k}}$),

$$E_{1,2,I,II}^2 = \Gamma_{\mathbf{k}} \pm 2\Lambda_{\mathbf{k}}^{I,II}, \quad \Gamma_{\mathbf{k}} = (\xi_{\mathbf{k}}^+)^2 + (\xi_{\mathbf{k}}^-)^2 + (\Delta_{\mathbf{k}})^2 + M^2$$

$$\Lambda_{\mathbf{k}}^I = [(\xi_{\mathbf{k}}^+ \xi_{\mathbf{k}}^-)^2 + M^2(\xi_{\mathbf{k}}^+)^2]^{\frac{1}{2}}$$

$$\Lambda_{\mathbf{k}}^{II} = [(\xi_{\mathbf{k}}^+ \xi_{\mathbf{k}}^-)^2 + M^2((\xi_{\mathbf{k}}^+)^2 + (\Delta_{\mathbf{k}})^2)]^{\frac{1}{2}}. \quad (14)$$

These dispersion relations have distinctly different characteristics. Spectrum of class I is completely gapped: The lowest energy state

$$E_{2,I}^2 = [\xi_{\mathbf{k}}^+ - \sqrt{(\xi_{\mathbf{k}}^-)^2 + M^2}]^2 + \Delta_{\mathbf{k}}^2 \quad (15)$$

can only be zero when both terms on the RHS are zero, i.e., when nodal lines of $\Delta_{\mathbf{k}}$ intersect Fermi surface in the SDW state, which is impossible in this case. The quasiparticle bands in SDW + $d_{x^2-y^2}$ -SC state are shown in Fig. 2(b).

In the case of (E, E) class (II), the spectrum has symmetry nodes on the SDW Fermi surface for d_{xy} state. But there is also an additional nodal point on the boundary of the RBZ (where $\xi_{\mathbf{k}}^- = 0$) that is not removed by the SC order:

$$\xi_{\mathbf{k}}^- = 0: \quad E_{2,II} = M - \sqrt{(\xi_{\mathbf{k}}^+)^2 + \Delta_{\mathbf{k}}^2} = 0. \quad (16)$$

The nodal point, given by condition $\xi_{\mathbf{k}}^+ = \xi_{\mathbf{k}} = \sqrt{M^2 - \Delta_{\mathbf{k}}^2}$, is robust even in the SC state as long as $\Delta_{\mathbf{k}} < M$. This point is the base of a (anisotropic) Dirac cone, obvious in the inset of

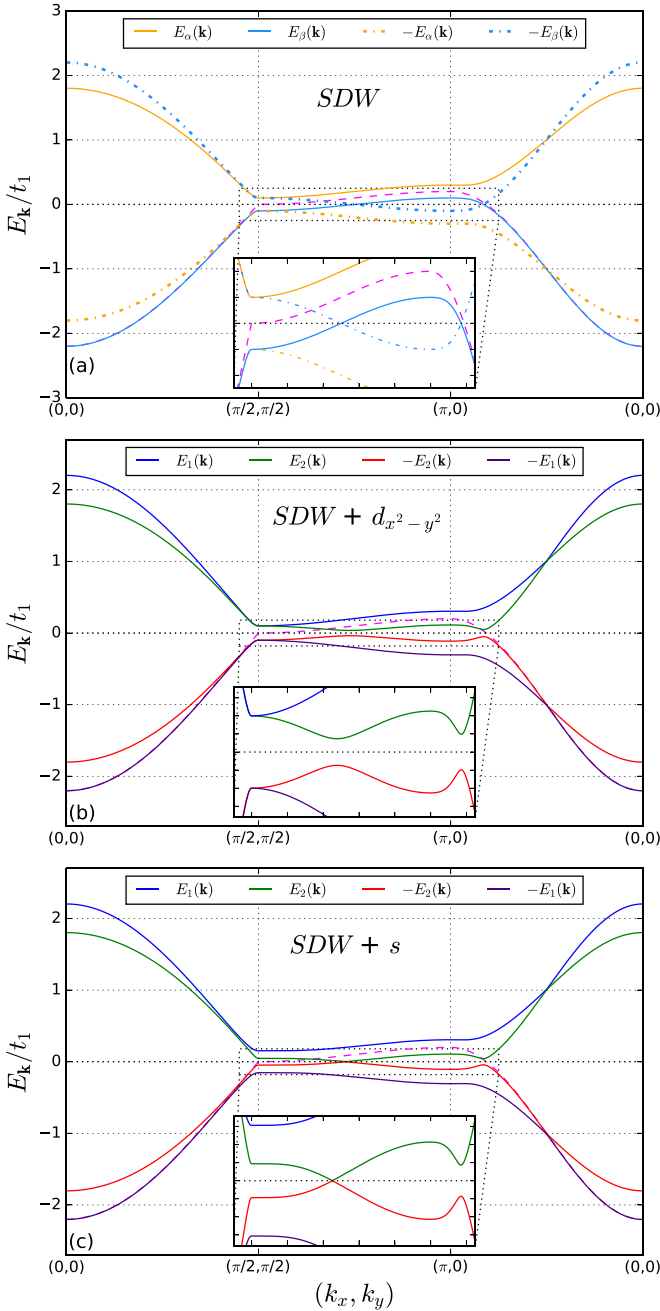


FIG. 2. The quasiparticle energies in the Brillouin zone along the path $(0, 0) \rightarrow (\pi/2, \pi/2) \rightarrow (\pi, 0) \rightarrow (0, 0)$. The normal state band is depicted by the dashed magenta curve. (a) The two bands $E_{\alpha,\beta}$, and their negatives, in the pure SDW phase; (b) the four quasiparticle bands $\pm E_{1,2}(\mathbf{k})$ in the coexisting phase $d_{x^2-y^2}$ -SC and SDW; (c) the four quasiparticle bands in the coexisting phase s -SC and SDW. Insets show the zoomed low energy sector. In the SDW state there remains a hole FS pocket around $(\pi, 0)$. This remaining Fermi surface is completely gapped by emerging $d_{x^2-y^2}$ -SC order. In the co-existing SDW and s -SC a Dirac nodal point remains on the boundary of RBZ. The parameters used for illustration are $t_2/t_1 = 0.2$, $M/t_1 = 0.1$, and $\Delta/t_1 = 0.05$ (the characteristic computed values are $M/t_1 \sim \Delta/t_1 \sim 10^{-3}$).

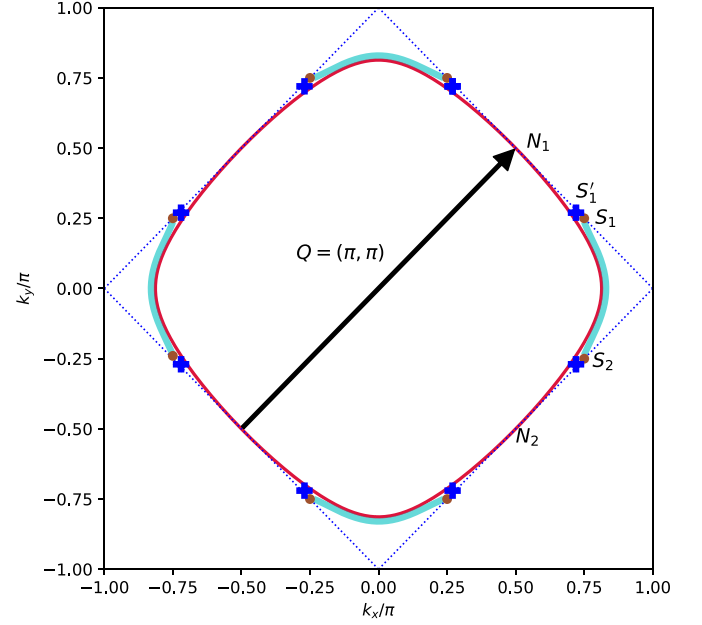


FIG. 3. Location of the extra nodes S'_1 on the boundary of the RBZ in the coexisting SDW and s -SC states shown by the blue crosses. They are the remnants of the FS points S_1 in the pure SDW state. The parameters used for illustration are $t_2/t_1 = 0.2$, $M/t_1 = 0.1$, and $\Delta/t_1 = 0.05$ (the characteristic computed values are $M/t_1 \sim \Delta/t_1 \sim 10^{-3}$).

Fig. 2(c). In our model location of the extra node is given by

$$(k_x, k_y) = \frac{\pi}{2} \pm \arcsin \left[\frac{\sqrt{M^2 - \Delta_{\mathbf{k}}^2}}{t_2} \right]^{1/2} \quad (17)$$

and at the corresponding symmetry points, as shown by the blue crosses in Fig. 3.

As a final remark, we have diagonalized the full Hamiltonian (7) in the RBZ by computing the $\hat{B}_\sigma(\mathbf{k})$ eigenvectors numerically. The Hamiltonian can also be diagonalized by a ‘two-step process’ which is sometimes employed in literature [39]. The methods are equivalent; we explain this in Appendix.

E. Self-consistent equations for SC and SDW

We solve for the mean-fields M , Δ self-consistently, using the Green’s function method [33]. In the reduced Brillouin zone, the Green’s functions required to derive the self consistent equations for $\Delta_{\mathbf{k}}$ are

$$\langle T_\tau c_{-\mathbf{k}-\sigma}^\dagger(\tau) c_{\mathbf{k}\sigma}^\dagger(0) \rangle, \langle T_\tau c_{-\mathbf{k}-\mathbf{Q}-\sigma}^\dagger(\tau) c_{\mathbf{k}+\mathbf{Q}\sigma}^\dagger(0) \rangle$$

and for M

$$\langle T_\tau c_{\mathbf{k}\sigma}(\tau) c_{\mathbf{k}+\mathbf{Q}\sigma}^\dagger(0) \rangle, \langle T_\tau c_{-\mathbf{k}-\mathbf{Q}-\sigma}^\dagger(\tau) c_{-\mathbf{k}-\sigma}(0) \rangle.$$

They are all elements of the following bare Matsubara Green’s function, which we define to be the following 4×4 matrix,

$$\hat{G}(\mathbf{k}, \tau)_{ab} = -\langle T \Psi_{\mathbf{k}\sigma,a}(\tau) \Psi_{\mathbf{k}\sigma,b}^\dagger(0) \rangle, \quad (18)$$

where the indices a, b represent the components of the partial Nambu vector $\Psi_{\mathbf{k}\sigma,a}^\dagger = (c_{\mathbf{k}\sigma}^\dagger, c_{-\mathbf{k}-\sigma}, c_{\mathbf{k}+\mathbf{Q}\sigma}^\dagger, c_{-\mathbf{k}-\mathbf{Q}-\sigma})$. The Green's functions relevant for SC are contained in the diagonal blocks, whereas those relevant for the SDW are contained in the off-diagonal blocks. To obtain them we use the fact that $\hat{G}(\mathbf{k}, \omega_n)$ satisfies the following Dyson equation

$$\hat{G}(\mathbf{k}, \omega_n) = (i\omega_n - \hat{\mathcal{H}}_{\mathbf{k}})^{-1}, \quad (19)$$

where $\omega_n = 2\pi T(n + \frac{1}{2})$ with integer n . Taking the pairing interaction to be of the form $g(\mathbf{k}, \mathbf{k}') = g\eta(\mathbf{k})\eta(\mathbf{k}')$, calculating the relevant Green's functions from the above Dyson equation and substituting them into (3), we arrive at the following self-consistent equations for the two symmetry classes [33].

The (E, O) class: $d_{x^2-y^2}$ with $\Delta_{\mathbf{k}} = \frac{1}{2}\Delta(\cos k_x - \cos k_y)$

$$\begin{aligned} \frac{1}{g} &= T \sum_{\omega_n} \sum_{\mathbf{k} \in \text{FBZ}}^{E_c} \frac{\eta^2(\mathbf{k})}{D_I(\omega_n, \mathbf{k})} (\omega_n^2 + (\xi_{\mathbf{k}}^-)^2 + (\xi_{\mathbf{k}}^+)^2 + M^2 + \Delta_{\mathbf{k}}^2) \\ \frac{1}{U} &= T \sum_{\omega_n} \sum_{\mathbf{k} \in \text{FBZ}}^{E_B} \frac{1}{D_I(\omega_n, \mathbf{k})} (\omega_n^2 + (\xi_{\mathbf{k}}^-)^2 - (\xi_{\mathbf{k}}^+)^2 + M^2 + \Delta_{\mathbf{k}}^2) \\ D_I(\omega_n, \mathbf{k}) &= (\omega_n^2 + (\xi_{\mathbf{k}}^-)^2 + (\xi_{\mathbf{k}}^+)^2 + \Delta_{\mathbf{k}}^2 + M^2) - 4(\xi_{\mathbf{k}}^+)^2((\xi_{\mathbf{k}}^-)^2 + M^2) \\ &= (\omega_n^2 + E_{1,I}^2)(\omega_n^2 + E_{2,I}^2). \end{aligned} \quad (20)$$

The (E, E) class: the isotropic s wave with $\Delta_{\mathbf{k}} = \Delta$ and d_{xy} with $\Delta_{\mathbf{k}} = \Delta \sin k_x \sin k_y$

$$\begin{aligned} \frac{1}{g} &= T \sum_{\omega_n} \sum_{\mathbf{k} \in \text{FBZ}}^{E_c} \frac{\eta^2(\mathbf{k})}{D_{II}(\omega_n, \mathbf{k})} (\omega_n^2 + (\xi_{\mathbf{k}}^-)^2 + (\xi_{\mathbf{k}}^+)^2 - M^2 + \Delta_{\mathbf{k}}^2) \\ \frac{1}{U} &= T \sum_{\omega_n} \sum_{\mathbf{k} \in \text{FBZ}}^{E_B} \frac{1}{D_{II}(\omega_n, \mathbf{k})} (\omega_n^2 + (\xi_{\mathbf{k}}^-)^2 - (\xi_{\mathbf{k}}^+)^2 + M^2 - \Delta_{\mathbf{k}}^2) \\ D_{II}(\omega_n, \mathbf{k}) &= (\omega_n^2 + (\xi_{\mathbf{k}}^-)^2 + (\xi_{\mathbf{k}}^+)^2 + \Delta_{\mathbf{k}}^2 + M^2) - 4(\xi_{\mathbf{k}}^+)^2((\xi_{\mathbf{k}}^-)^2 + M^2) - 4\Delta_{\mathbf{k}}^2 M^2 = (\omega_n^2 + E_{1,II}^2)(\omega_n^2 + E_{2,II}^2), \end{aligned} \quad (21)$$

where $E_{1,2,I,II}$ are the quasiparticle energies for symmetry classes I and II, defined in (14). E_C and E_B are the SC cutoff and the SDW cutoff energies, respectively.

Numerical solution of self-consistent equations

In the following, we solve the self-consistent equations (20) and (21) for band parameters $t_1/2\pi T_{\text{SDW}} = 100$, $t_2/2\pi T_{\text{SDW}} = 10$, $E_C/2\pi T_{\text{SDW}} = 30$, and $E_B/2\pi T_{\text{SDW}} = 60$, and eliminate interactions g and U , to obtain the temperature dependence of the order parameters $\Delta(T)$ and $M(T)$. For perfect nesting with $t_2 = 0$, SDW order gaps the entire FS. This prohibits SC order to open up a gap anywhere on the FS when $T_{C0} < T_{\text{SDW}}$, and the superconductivity never appears in this case. This is verified by numerically solving the self-consistent equations (20) and (21) with $t_2 = 0$. The result is the usual BCS profile [35] for $M(T)$ and $\Delta = 0$.

However, both SC and SDW orders can appear when we go away from the perfect nesting limit. The nature of the coexistence is very different for the (E, O) and (E, E) symmetry classes. Solutions of the self-consistent equations (20) and (21) depend on the parameter $p = \frac{T_{C0}}{T_{\text{SDW}}}$. We show the order parameter profiles later, together with thermal conductivity results, in Sec. III and here summarize the main points.

For the (E, O) class of SDW+ $d_{x^2-y^2}$ -SC, one numerically solves Eqs. (20). In this case SC can naturally coexist with SDW, and in fact below T_C the magnetization M is enhanced compared to the pure SDW state. SC transition temperature is also increased on the SDW background, $T_C > T_{C0}$, see

Figs. 6(a) and 6(c). The SDW→SDW+SC transition is always second order.

For states of (E, E) class the interplay is more complicated. In Figs. 7(a) and 7(c) we show numerical solution of (21) for the d_{xy} pairing state. Depending on the value of T_{C0}/T_{SDW} the SDW→SC transition can be either first or second order. For relatively strong SC order, $p = 0.5$, the SC state completely replaces SDW order via a first-order transition. For a lower $p = 0.35$, SDW survives and allows for a smaller Δ order to appear simultaneously through a second-order transition. This competition comes with suppression of the superconducting transition temperature in the presence of the SDW background, $T_C < T_{C0}$. Behavior for the isotropic s -wave state is similar to the d_{xy} case, Fig. 8.

F. Kinetic method for heat conductivity

We use the Boltzmann kinetic-equation approach to calculate the thermal conductivity for the system with intertwined orders. This method was widely used to compute thermal conductivity, both in s -wave superconductor [2,3], as well as in unconventional superconductors [12,40–42], and for quantum critical systems [43–45]. We begin with the expression of the total heat current carried by the quasiparticles

$$\mathbf{j}_E = 2 \sum_{n=1}^2 \mathbf{j}_n = 2 \sum_{n=1}^2 \int \frac{d^2k}{8\pi^2} E_n(\mathbf{k}) \mathbf{v}_n(\mathbf{k}) f_n(\mathbf{k}). \quad (22)$$

In the above expression we integrate momentum over the FBZ, double counting the states, and therefore require an extra

factor of 2 in the denominator: $2 \times 4\pi^2$. The sum is over the two quasiparticle branches with distinct energies E_1 and E_2 (as given in (13)) and $f_n(\mathbf{k})$ is the distribution function of the respective quasiparticle branches. The factor of two takes care of the spin degeneracy of each branch. The thermal conductivity tensor is the proportionality coefficient between the heat current and temperature gradient.

$$(\mathbf{j}_E)_i = -\kappa_{ij} \nabla_j T \quad (23)$$

The quasiparticle distribution function $f_n(\mathbf{k})$ satisfies the Boltzmann equation

$$\frac{\partial f_n(\mathbf{k})}{\partial t} + \frac{\partial E_n}{\partial \mathbf{k}} \nabla f_n - \nabla E_n \frac{\partial f_n(\mathbf{k})}{\partial \mathbf{k}} = I_n^{\text{coll}}(\mathbf{k}), \quad (24)$$

$I_n^{\text{coll}}(\mathbf{k})$ being the collision integral. We follow the usual process of linearizing the left hand side of (24) by writing $f_n(\mathbf{k}) =$

$f_n^0(\mathbf{k}) + \delta f_n(\mathbf{k})$, where $f_n^0(\mathbf{k}) = \frac{1}{e^{E_n(\mathbf{k})/T} + 1}$ is the equilibrium Fermi-Dirac distribution function. $\delta f_n(\mathbf{k})$ is the deviation from the equilibrium value caused by the presence of the stationary thermal gradient. The linearization yields [40]

$$\frac{\partial \delta f_n(\mathbf{k})}{\partial t} - E_n(\mathbf{k}) \mathbf{v}_n(\mathbf{k}) \frac{\nabla T}{T} \frac{\partial f_n^0(\mathbf{k})}{\partial E_n} = I_n^{\text{coll}}(\mathbf{k}). \quad (25)$$

The quasiparticle velocity is defined as

$$\mathbf{v}_n(\mathbf{k}) = \nabla_{\mathbf{k}} E_n(\mathbf{k}). \quad (26)$$

For a stationary thermal gradient the first term is zero. We now look at the right hand side; the collision integrals in the case of weak disorder are obtained by multiplying the contribution of a single impurity by their concentration N_{imp} :

$$\begin{aligned} I_1^{\text{coll}}(\mathbf{k}) &= N_{\text{imp}} \int \frac{d^2 k'}{(2\pi)^2} [W_{11}(\mathbf{k}, \mathbf{k}')(\delta f_1(\mathbf{k}') - \delta f_1(\mathbf{k})) + W_{12}(\mathbf{k}, \mathbf{k}')(\delta f_2(\mathbf{k}') - \delta f_1(\mathbf{k}))] \\ I_2^{\text{coll}}(\mathbf{k}) &= N_{\text{imp}} \int \frac{d^2 k'}{(2\pi)^2} [W_{22}(\mathbf{k}, \mathbf{k}')(\delta f_2(\mathbf{k}') - \delta f_2(\mathbf{k})) + W_{21}(\mathbf{k}, \mathbf{k}')(\delta f_1(\mathbf{k}') - \delta f_2(\mathbf{k}))], \end{aligned} \quad (27)$$

where $W_{nm}(\mathbf{k}, \mathbf{k}')$ is the rate of elastic scattering between the quasiparticle branches n and m in the FBZ. Therefore we have two coupled kinetic equations for $\delta f_1(\mathbf{k})$ and $\delta f_2(\mathbf{k})$. We can rewrite (25) for $\delta f_n(\mathbf{k})$ as

$$\begin{aligned} E_1(\mathbf{k}) \mathbf{v}_1(\mathbf{k}) \frac{\nabla T}{T} \frac{\partial f_1^0(\mathbf{k})}{\partial E_1} &= -N_{\text{imp}} \left[\int \frac{d^2 k'}{(2\pi)^2} (W_{11}(\mathbf{k}, \mathbf{k}') \delta f_1(\mathbf{k}') + W_{12}(\mathbf{k}, \mathbf{k}') \delta f_2(\mathbf{k}')) \right] + \left(\frac{1}{\tau_{11}} + \frac{1}{\tau_{12}} \right) \delta f_1(\mathbf{k}) \\ E_2(\mathbf{k}) \mathbf{v}_2(\mathbf{k}) \frac{\nabla T}{T} \frac{\partial f_2^0(\mathbf{k})}{\partial E_2} &= -N_{\text{imp}} \left[\int \frac{d^2 k'}{(2\pi)^2} (W_{22}(\mathbf{k}, \mathbf{k}') \delta f_2(\mathbf{k}') + W_{21}(\mathbf{k}, \mathbf{k}') \delta f_1(\mathbf{k}')) \right] + \left(\frac{1}{\tau_{22}} + \frac{1}{\tau_{21}} \right) \delta f_2(\mathbf{k}) \end{aligned} \quad (28)$$

where we have defined the quasiparticle relaxation time as

$$\tau_{nm}^{-1}(\mathbf{k}) = N_{\text{imp}} \int \frac{d^2 k'}{(2\pi)^2} W_{nm}(\mathbf{k}, \mathbf{k}'). \quad (29)$$

The above equations are decoupled by the usual symmetry argument [12,40]. The driving term is odd under spatial inversion since $\mathbf{v}(-\mathbf{k}) = -\mathbf{v}(\mathbf{k})$, whereas the quasiparticle relaxation time is even under spatial inversion $\tau_{nm}^{-1}(-\mathbf{k}) = \tau_{nm}^{-1}(\mathbf{k})$ due to symmetry $W_{nm}(-\mathbf{k}, -\mathbf{k}') = W_{nm}(\mathbf{k}, \mathbf{k}')$, which implies that $\delta f_n(\mathbf{k})$ is odd under $\mathbf{k} \rightarrow -\mathbf{k}$. Thus the first terms on the right in (28) are integrals of odd functions over a symmetric region of integration and therefore go to zero: $[\dots] = 0$, which represents vanishing vertex corrections. Thus the heat current carried by the quasiparticle branches with energies $E_{1,2}(\mathbf{k})$ are

$$\begin{aligned} (\mathbf{j}_1)_i &= \int \frac{d^2 k}{8\pi^2} E_1^2(\mathbf{k}) v_{1i}(\mathbf{k}) v_{1j}(\mathbf{k}) \frac{\nabla_j T}{T} \frac{\partial f_1^0(\mathbf{k})}{\partial E_1} \left(\frac{1}{\tau_{11}} + \frac{1}{\tau_{12}} \right)^{-1} \\ (\mathbf{j}_2)_i &= \int \frac{d^2 k}{8\pi^2} E_2^2(\mathbf{k}) v_{2i}(\mathbf{k}) v_{2j}(\mathbf{k}) \frac{\nabla_j T}{T} \frac{\partial f_2^0(\mathbf{k})}{\partial E_2} \left(\frac{1}{\tau_{22}} + \frac{1}{\tau_{21}} \right)^{-1} \end{aligned} \quad (30)$$

which results in the following expression for the thermal conductivity tensor,

$$\begin{aligned} \kappa_{ij} &= (\kappa_1)_{ij} + (\kappa_2)_{ij} \\ (\kappa_1)_{ij} &= -\frac{2}{T} \int \frac{d^2 k}{8\pi^2} E_1^2(\mathbf{k}) v_{1i}(\mathbf{k}) v_{1j}(\mathbf{k}) \frac{\partial f_1^0(\mathbf{k})}{\partial E_1} \left(\frac{1}{\tau_{11}} + \frac{1}{\tau_{12}} \right)^{-1} \\ (\kappa_2)_{ij} &= -\frac{2}{T} \int \frac{d^2 k}{8\pi^2} E_2^2(\mathbf{k}) v_{2i}(\mathbf{k}) v_{2j}(\mathbf{k}) \frac{\partial f_2^0(\mathbf{k})}{\partial E_2} \left(\frac{1}{\tau_{22}} + \frac{1}{\tau_{21}} \right)^{-1}. \end{aligned} \quad (31)$$

The expression for the scattering rate in the Born limit is given by

$$W_{nm}(\mathbf{k}, \mathbf{k}') = \frac{2\pi}{\hbar} |\langle \mathbf{k}', n | H_{\text{imp}} | \mathbf{k}, m \rangle|^2 \delta(E_n(\mathbf{k}) - E_m(\mathbf{k}')) = \frac{2\pi}{\hbar} |V(\mathbf{k}, \mathbf{k}')|^2 |C_{nm}(\mathbf{k}, \mathbf{k}')|^2 \delta(E_n(\mathbf{k}) - E_m(\mathbf{k}')). \quad (32)$$

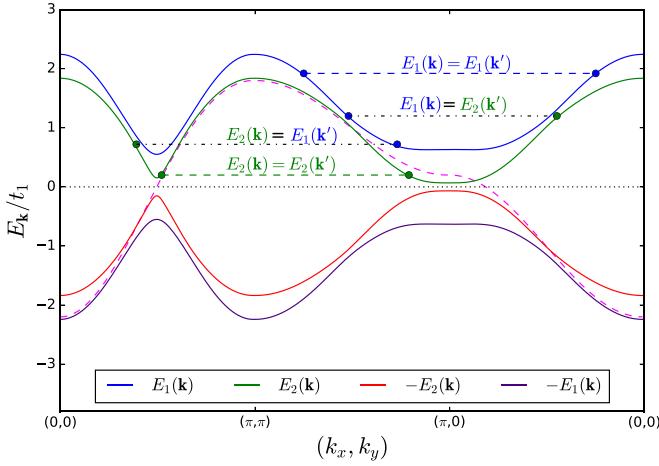


FIG. 4. Schematic representation of the various scattering processes in the full BZ. The band structure is along the path $(0, 0) \rightarrow (\pi, \pi) \rightarrow (\pi, 0) \rightarrow (0, 0)$. The dashed blue and green horizontal lines represent intraband scattering processes; the dash-dotted black horizontal lines represent interband scattering processes. The parameters used for illustration are $t_2/t_1 = 0.2$, $M/t_1 = 0.35$, and $\Delta/t_1 = 0.2$.

The quasiparticle state with momentum \mathbf{k} and energy $E_1(\mathbf{k})$ is defined as $|\mathbf{k}, 1\rangle = a_{1\mathbf{k}}^\dagger |0\rangle$. Similarly the quasiparticle state with momentum \mathbf{k} and energy $E_2(\mathbf{k})$ is defined as $|\mathbf{k}, 2\rangle = a_{2\mathbf{k}}^\dagger |0\rangle$. $|0\rangle$ is the vacuum state with no quasiparticles. $\langle \mathbf{k}', n | H_{\text{imp}} | \mathbf{k}, m \rangle$ is the amplitude for a single impurity to scatter from the particle state \mathbf{k} with energy $E_m(\mathbf{k})$ to the state \mathbf{k}' with energy $E_n(\mathbf{k}')$. The matrix $C_{nm}(\mathbf{k}, \mathbf{k}')$ contains the coherence factors coming from the Bogoliubov transformation between the normal and ordered states. In the following we consider the case of an isotropic scattering amplitude $V(\mathbf{k}, \mathbf{k}') = V = \text{const}$. Therefore the expression (29) for the quasiparticle lifetimes becomes

$$\begin{aligned} \tau_{nm}^{-1}(\mathbf{k}) &= N_{\text{imp}} V^2 \frac{2\pi}{\hbar} \int \frac{d^2 k'}{(2\pi)^2} |C_{nm}(\mathbf{k}, \mathbf{k}')|^2 \delta(E_n(\mathbf{k}) - E_m(\mathbf{k}')). \end{aligned} \quad (33)$$

We evaluate the momentum integral (33) numerically using the high precision sampling method [46]. Using $\tau_{nm}^{-1}(\mathbf{k})$ from (33) we numerically evaluate the momentum integrals in (31) over the FBZ, see Fig. 4. We also numerically compute the values for $\tau_{nm}^{-1}(\mathbf{k})$ and $\kappa(T)$ in the normal state, by setting $\Delta = 0$ and $M = 0$ in equations (33) and (31), respectively, and eliminating the unknown $N_{\text{imp}} V^2$ in favor of normal state relaxation time τ_N that only appears in $\kappa_N(T)$. We assume τ_N^{-1} is small enough and neglect order parameter suppression by impurities. The matrix of coherence factors $C_{nm}(\mathbf{k}, \mathbf{k}')$ is also computed numerically, by first writing the impurity scattering Hamiltonian in the same Nambu basis as (7)

$$\begin{aligned} H_{\text{imp}} &= V \sum_{\mathbf{k}, \mathbf{k}', \sigma} c_{\mathbf{k}'\sigma}^\dagger c_{\mathbf{k}\sigma} \\ &= \frac{V}{4} \sum_{\mathbf{k}, \mathbf{k}' \in \text{FBZ}} \Psi_{\mathbf{k}'\sigma, a}^\dagger \mathcal{S}_{ab} \Psi_{\mathbf{k}\sigma, b} \end{aligned}$$

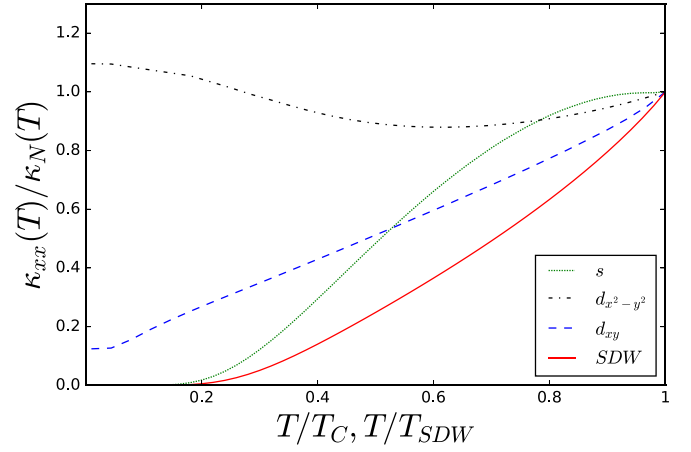


FIG. 5. Thermal conductivity for pure SC states: s -, $d_{x^2-y^2}$ - and d_{xy} -wave (dispersion parameters $t_1/2\pi T_C = 100$, $t_2/2\pi T_C = 10$), or for pure SDW state in perfectly nested regime ($t_1/2\pi T_{\text{SDW}} = 100$, $t_2/2\pi T_{\text{SDW}} = 0$).

$$\mathcal{S}_{ab} = \begin{pmatrix} 1 & 0 & 0 & 0 \\ 0 & -1 & 0 & 0 \\ 0 & 0 & 1 & 0 \\ 0 & 0 & 0 & -1 \end{pmatrix}, \quad (34)$$

where the factor $\frac{1}{4}$ comes from both particle-hole doubling for SC and $(\mathbf{k}, \mathbf{k} + \mathbf{Q})$ doubling for SDW in the FBZ. Upon performing the Bogoliubov transformation (8) on the Nambu vectors, we get

$$H_{\text{imp}} = \frac{V}{4} \sum_{\mathbf{k}, \mathbf{k}' \in \text{FBZ}} A_{\mathbf{k}'a}^\dagger D_{ab}(\mathbf{k}, \mathbf{k}') A_{\mathbf{k}b}, \quad (35)$$

where $A_{\mathbf{k}}^\dagger = (a_{1\mathbf{k}}^\dagger, a_{3\mathbf{k}}, a_{2\mathbf{k}}^\dagger, a_{4\mathbf{k}})$ and the matrix $\hat{D}(\mathbf{k}, \mathbf{k}')$ from which we get the coherence factors

$$\hat{D}(\mathbf{k}, \mathbf{k}') = \hat{B}_\sigma^\dagger(\mathbf{k}') \hat{S} \hat{B}_\sigma(\mathbf{k}). \quad (36)$$

The \mathbf{k} dependence in $\hat{D}(\mathbf{k}, \mathbf{k}')$ comes from $\Delta(\mathbf{k})$ and $\xi(\mathbf{k})$ through the eigenvectors of $\hat{H}_{\mathbf{k}}$, and since we artificially quadruple our bands we only include physically available in-band scattering, so \mathcal{S}_{ab} is diagonal. From the ordering of the $A_{\mathbf{k}}^\dagger$ vector, the intraband coherence factors

$$C_{11}(\mathbf{k}, \mathbf{k}') = D_{11}(\mathbf{k}, \mathbf{k}'), \quad C_{22}(\mathbf{k}, \mathbf{k}') = D_{33}(\mathbf{k}, \mathbf{k}'),$$

and interband

$$C_{12}(\mathbf{k}, \mathbf{k}') = D_{13}(\mathbf{k}, \mathbf{k}'), \quad C_{21}(\mathbf{k}, \mathbf{k}') = D_{31}(\mathbf{k}, \mathbf{k}'),$$

all for scattering inside the FBZ, as shown in Fig. 4.

III. NUMERICAL RESULTS AND DISCUSSION

We begin our discussion by first calculating thermal conductivity of the pure SC or SDW states for our tight binding model. For various pairing, s -, $d_{x^2-y^2}$ -, and d_{xy} -wave, the values of $\Delta(T)$ are obtained by self consistently solving the weak coupling gap equation and neglecting T_c suppression by impurities. The numerical results for κ_{xx} are shown in Fig. 5. We see the characteristic exponential fall in the thermal conductivity for the isotropic fully-gapped s -wave superconductor [2,3]. The general behavior of $\kappa(T)/T$ for the d_{xy} and $d_{x^2-y^2}$ states

also agrees with earlier calculations [12,17], where the low- T regime is dominated by the nodal quasiparticles, producing the finite residual κ/T . However, while for circular FS κ_{xx} is the same for the d_{xy} and $d_{x^2-y^2}$ states, in the case of our anisotropic FS the two symmetries result in very different values of heat conductivity. The $d_{x^2-y^2}$ pairing has nodes on flat parts of the FS with large Fermi velocity and smaller DOS. By gapping the corners of the FS with large DOS, the scattering rate is significantly reduced, producing longer-lived high-velocity nodal quasiparticles that result in heat conductivity exceeding that of the normal state. The d_{xy} state, on the other hand, has nodes where Fermi velocity is small, resulting in much lower κ/T .

For completeness, we note that for strong scattering centers one has to go beyond Born approximation to explain experimental data in cuprates and heavy fermions [12,47]. Also, quasiparticle Boltzmann approach fails at low temperatures when low-energy quasiparticles cannot be well established due to impurity broadening [12].

We also show thermal conductivity for pure SDW state when the Fermi surface is nested perfectly, i.e., $\mu = 0$ and $t_2 = 0$ in our model. The SDW opens a gap along the entire FS. The sharp fall in the thermal conductivity seen in Fig. 5 is often seen in thermal conductivity experiments on spin density wave antiferromagnets [48–50].

The difference between slopes of $\kappa(T)$ just below the transition temperature for s -, d -wave superconductors and SDW can be explained by the difference in coherence factors. For a singlet superconductor,

$$|C_{11}^{\text{SC}}|^2 = \frac{1}{2} \left(1 + \frac{\xi_{\mathbf{k}} \xi_{\mathbf{k}'} - \Delta_{\mathbf{k}} \Delta_{\mathbf{k}'}}{E_1(\mathbf{k}) E_2(\mathbf{k}')} \right), \quad (37)$$

$$|C_{22}^{\text{SC}}|^2 = \frac{1}{2} \left(1 + \frac{\xi_{\mathbf{k}+\mathbf{Q}} \xi_{\mathbf{k}'+\mathbf{Q}} - \Delta_{\mathbf{k}+\mathbf{Q}} \Delta_{\mathbf{k}'+\mathbf{Q}}}{E_2(\mathbf{k}) E_2(\mathbf{k}')} \right) \quad (38)$$

$$|C_{12}^{\text{SC}}|^2 = |C_{21}^{\text{SC}}|^2 = 0 \quad (39)$$

with $E_1(\mathbf{k}) = \sqrt{(\xi_{\mathbf{k}}^-)^2 + \Delta_{\mathbf{k}}^2}$ and $E_2(\mathbf{k}) = \sqrt{(\xi_{\mathbf{k}+\mathbf{Q}})^2 + \Delta_{\mathbf{k}+\mathbf{Q}}^2}$ being the two branches that together count the states of the superconductor in the full BZ. For the SDW state

$$|C_{11}^{\text{SDW}}|^2 = |C_{22}^{\text{SDW}}|^2 = \frac{1}{2} \left(1 + \frac{\xi_{\mathbf{k}}^- \xi_{\mathbf{k}'}^- + M^2}{\Pi_{\mathbf{k}} \Pi_{\mathbf{k}'}} \right), \quad (40)$$

$$|C_{12}^{\text{SDW}}|^2 = |C_{21}^{\text{SDW}}|^2 = \frac{1}{2} \left(1 - \frac{\xi_{\mathbf{k}}^- \xi_{\mathbf{k}'}^- + M^2}{\Pi_{\mathbf{k}} \Pi_{\mathbf{k}'}} \right), \quad (41)$$

$\Pi_{\mathbf{k}} = \sqrt{(\xi_{\mathbf{k}}^-)^2 + M^2}$. For both the s and d wave superconductors, the $\xi_{\mathbf{k}} \xi_{\mathbf{k}'}$ terms vanish after \mathbf{k}' integration in equation (33), due to cancellation of positive and negative $\xi_{\mathbf{k}'}$ contributions. This leaves $\tau_{11}^{-1}(\mathbf{k}) = \tau_N^{-1} \frac{N(E_1(\mathbf{k}))}{N_0} (1 - \frac{\Delta^2}{E_1^2(\mathbf{k})})$ and $\tau_{22}^{-1}(\mathbf{k}) = \tau_N^{-1} \frac{N(E_2(\mathbf{k}))}{N_0} (1 - \frac{\Delta^2}{E_2^2(\mathbf{k})})$ for the s -wave case. For the d -wave states also the $\Delta_{\mathbf{k}} \Delta_{\mathbf{k}'}$ terms vanish on integrating over the directions of \mathbf{k}' in equation (33), resulting in $\tau_{11}^{-1}(\mathbf{k}) = \tau_N^{-1} \frac{N(E_1(\mathbf{k}))}{N_0}$ and $\tau_{22}^{-1}(\mathbf{k}) = \tau_N^{-1} \frac{N(E_2(\mathbf{k}))}{N_0}$ for the d -wave states. $N(E_{1,2}(\mathbf{k}))$ denotes the density of SC states with energies $E_{1,2}(\mathbf{k})$, and N_0 being the normal density of states at the Fermi level. For a SDW with a perfectly nested FS, $\xi_{\mathbf{k}+\mathbf{Q}} = -\xi_{\mathbf{k}}$, so $\xi_{\mathbf{k}}^+ = 0$ and $\xi_{\mathbf{k}}^- = \xi_{\mathbf{k}}$. Thus $E_{\alpha}(\mathbf{k}) = \Pi_{\mathbf{k}}$

and $E_{\beta}(\mathbf{k}) = -\Pi_{\mathbf{k}}$. Again, terms $\xi_{\mathbf{k}}^- \xi_{\mathbf{k}'}^-$ will drop out under the \mathbf{k}' integration in equation (33), leaving $\tau_{11}^{-1}(\mathbf{k}) = \tau_N^{-1} \frac{N(E_{\alpha}(\mathbf{k}))}{N_0} (1 + \frac{M^2}{E_{\alpha}^2(\mathbf{k})})$ and $\tau_{22}^{-1}(\mathbf{k}) = \tau_N^{-1} \frac{N(E_{\beta}(\mathbf{k}))}{N_0} (1 + \frac{M^2}{E_{\beta}^2(\mathbf{k})})$. For perfectly nested FS the two bands do not overlap in energy and thus there is no interband scattering, $\tau_{12}^{-1}(\mathbf{k}) = \tau_{21}^{-1}(\mathbf{k}) = 0$. $N(E_{\alpha,\beta}(\mathbf{k}))$ once again denotes the density of SDW quasiparticle states with energy $E_{\alpha,\beta}(\mathbf{k})$.

Comparing the coherence factors for various states, one can notice that the effective relaxation times in equation (31) have this hierarchy near their transition temperatures

$$\tau_{\text{SDW}} < \tau_d < \tau_s$$

resulting in the observed different slopes in Fig. 5. Finally, we note that the difference in signs inside coherence factors for fully gapped s -SC ($1 - \Delta^2/E^2$) and SDW ($1 + M^2/E^2$), comes from the particle-hole difference in the impurity scattering matrix, $\mathcal{S}_{ab}^{\text{SC}} \propto \text{diag}(1, -1)$ vs $\mathcal{S}_{ab}^{\text{SDW}} \propto \text{diag}(1, 1)$.

A. The (E, O) class

We now turn to the discussion of the pairing states belonging to the various symmetry classes. For all cases below the parameters used for FS are $t_1/2\pi T_{\text{SDW}} = 100$, $t_2/2\pi T_{\text{SDW}} = 10$.

The $d_{x^2-y^2}$ pairing state which belongs to the (E, O) symmetry class is not competitive with the SDW, and below T_C the SC order enhances the SDW order, as shown in Fig. 6. The temperature dependence of the self-consistently determined order parameters $\Delta(T)$ and $M(T)$, and of the thermal conductivity, are presented for two values of the parameter

$$p = \frac{T_{C0}}{T_{\text{SDW}}},$$

where T_{C0} is the transition temperature of the SC order in the absence of the SDW and T_{SDW} is the transition temperature of the SDW in the absence of the SC. The $d_{x^2-y^2}$ pairing state coexists with the SDW order for all values of p . Further, the transition temperature of the SC is enhanced in the presence of the SDW. The onset of the SDW gaps the nested flat parts of the FS (orange shaded regions in the inset of Fig. 6(b)) leading to a weaker metallic state (remaining Fermi surface shown by cyan curves in the inset), causing the gradual fall in the thermal conductivity for $T_C < T < T_{\text{SDW}}$, seen in Figs. 6(b) and 6(d). The nodes of the $d_{x^2-y^2}$ pairing state appear under the SDW gap on nested FS parts and thus do not result in any low-energy excitations. The sharp fall of the thermal conductivity for $T < T_C$, and exponential low- T behavior, is characteristic of the fully gapped FS [2,3] due to the simultaneous coexistence of the SDW and SC orders. Notice that the heat conductivity shows a kink at the coexistence transition.

B. The (E, E) class

The d_{xy} -wave and the isotropic s -wave SC pairing states belong to the (E, E) symmetry class. Behavior of these states, and their signatures in thermal transport, are quite different from those for the (E, O) symmetry class.

We begin by discussing the d_{xy} pairing state in order to contrast its behavior with the $d_{x^2-y^2}$ pairing state. This state does not coexist with the SDW order for all values of relative

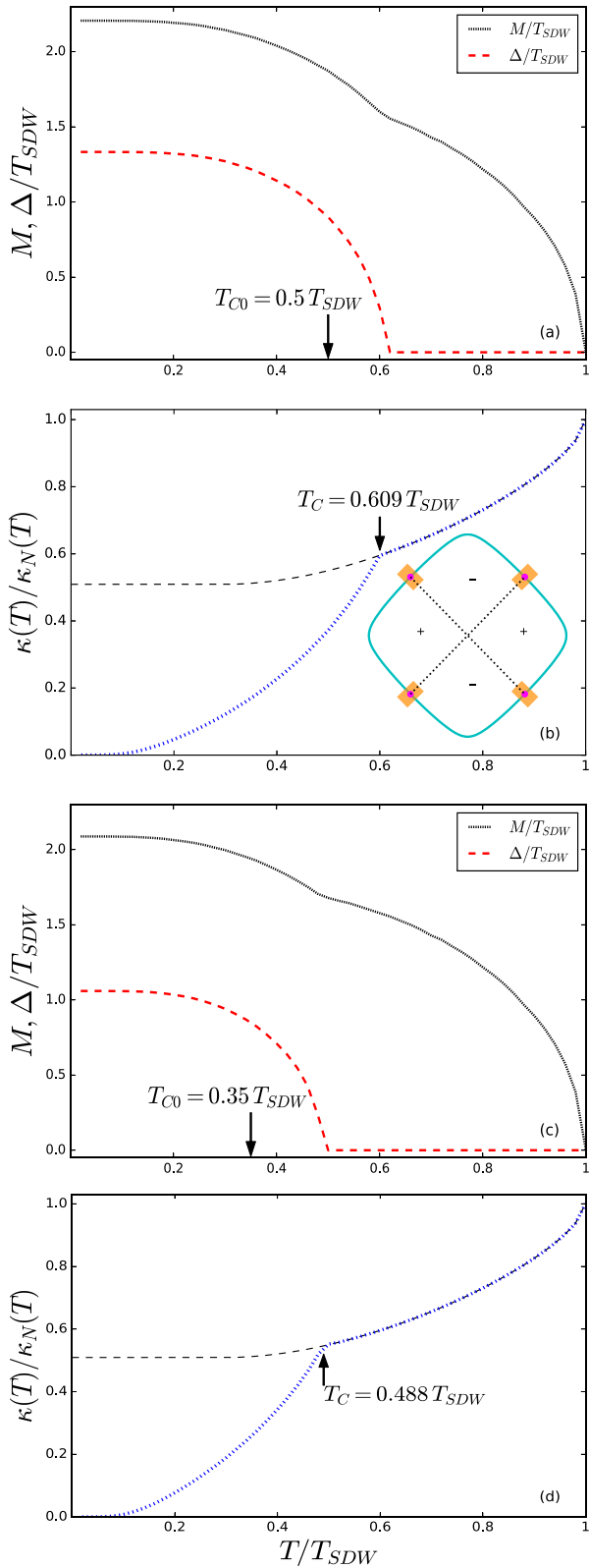


FIG. 6. Coexistence of SDW and $d_{x^2-y^2}$ -SC in (E, O) class. (a), (b) temperature dependence of SDW and SC order parameters and thermal conductivity for $p = 0.5$; (b), (d) same for $p = 0.35$. Inset in (b) shows FS, $d_{x^2-y^2}$ nodal lines, and the SDW-gapped regions. Thermal conductivity in the co-existence phase is shown by the dotted blue curve, and by the black dashed curve in a purely SDW phase. The normal state thermal conductivity is T-linear $\kappa_N(T) = \text{const} \times T$.

temperatures p . In Fig. 7(a) we show that for $p = 0.5$ the SC state appears through a first order phase transition, completely replacing SDW order, whereas for $p = 0.35$ it appears through a second order phase transition, and both SC and SDW order parameters are present (Fig. 7(c)). However, the (E, E) SC states compete with SDW, resulting in suppression of the magnetic order at temperatures below T_C , which itself is reduced.

In the case of the first order phase transition Fig. 7(a), the system goes from a weak metallic phase to a purely superconducting phase. The SDW order M , that gaps only the nested parts of the Fermi surface, is replaced at $T = 0.49T_{SDW}$ with SC gap Δ , that covers more of the Fermi surface, and thus can have a lower value of the free energy, even at a smaller magnitude of the SC gap. This results in a sharp increase in the thermal conductivity. Behavior of the thermal conductivity for $T < T_C$ in this case is the same as that of the d_{xy} pairing state in the absence of the SDW. The dashed red curve is the appropriately scaled thermal conductivity in the pure SC state, from Fig. 5.

When the SC and SDW order can coexist, e.g., for the case of $p = 0.35$ shown in Figs. 7(c) and 7(d), behavior of thermal transport is very unusual. Below T_{SDW} , a part of the FS gets gapped with M , indicated by the shaded orange in the sketch in the inset of 7(d). $\kappa(T)$ drops, but gets saturated at a finite value due to the remaining FS, shown by the cyan lines, which gives a weaker-than-normal metallic state that we denote as SDW-metallic state. One expects that at the onset of d_{xy} order with symmetry nodes (magenta dots) on this FS, the heat conductivity would show a somewhat similar behavior to the one for the pure SC state, as in Fig. 5. This is indeed the case, as can be seen in 7(d). The only quantitative difference is due to appearance of the extra nonsymmetry nodes in the SDW+SC state, discussed in Sec. II D. They arise near the SDW-gapped region, and marked as the blue crosses in the sketch. Since the excitation gap collapses in both symmetry node and the extra node, the SC order parameter $\Delta_{\mathbf{k}}$, although growing in amplitude below T_C , does not efficiently gap the FS between the nodes, resulting in a more gradual reduction of $\kappa(T)/\kappa_N(T)$ below T_C . In the low temperature limit the extra nodes result in relative enhancement of the residual thermal conductivity.

Fully gapped s -wave state shows similar coexistence pattern: it fully replaces SDW order for strong SC pairing, resulting in a sudden jump of physical observables, Figs. 8(a) and 8(b). For $p = 0.35$, the s -wave SC state appears through a second order phase transition, resulting in SDW+SC coexistence, Fig. 8(c). At T_C the emerging SC order gaps the SDW-metallic state resulting in a suppression of κ . Again, the gapless excitations in the additional nodes (blue cross marks in the inset of Fig. 8(d)), at low temperatures result in finite thermal conductivity, eliminating the exponential character of the fully-gapped s -wave heat transport.

IV. CONCLUSION

We have considered a single-band electronic system where spin-singlet superconducting order can appear inside a collinear spin-density-wave phase, at the mean-field level. It is based on a tight-binding model on a square lattice with a

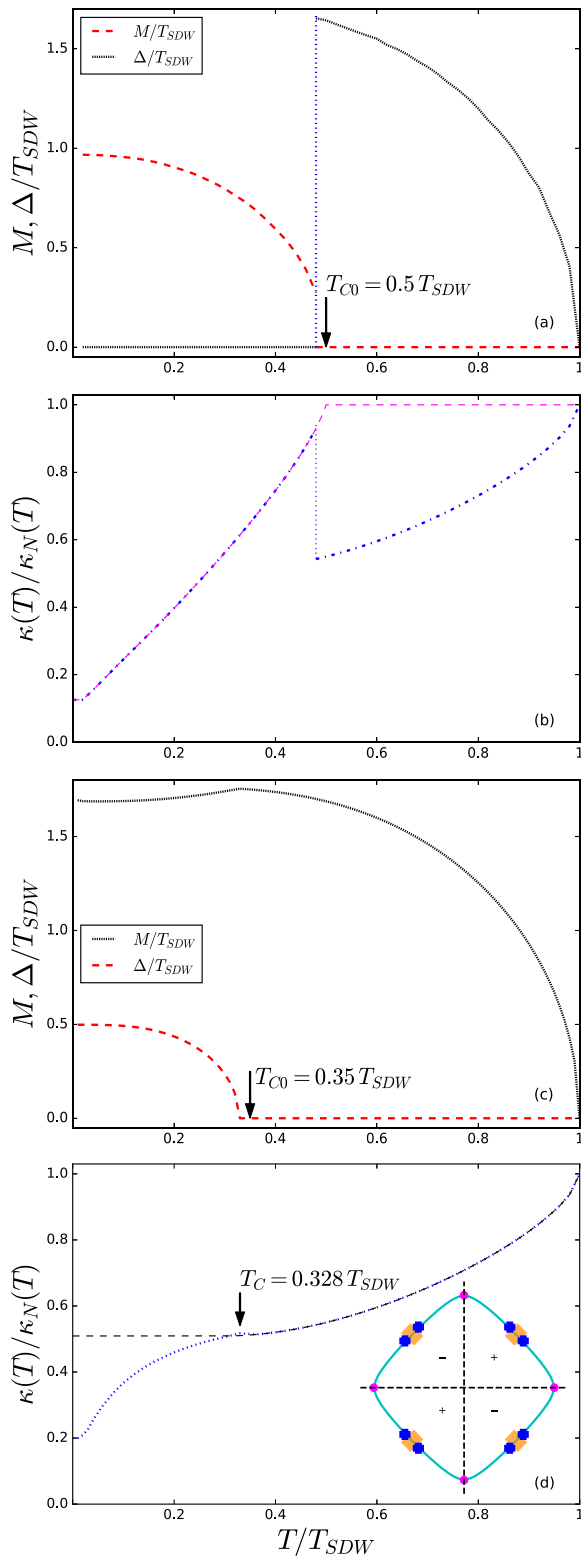


FIG. 7. Same as in Fig. 6 but for interplay of SDW and d_{xy} -SC in (E, E) class. (a), (b) for $p = 0.5$ the SDW and SC states do not coexist, switching through a first order transition. Heat conductivity makes a jump reflecting $\Delta < M$ relation. (c), (d) Coexistence regime, $p = 0.35$; thermal conductivity in the SDW+SC phase behaves significantly different from the pure d_{xy} -SC. Inset in (d) shows the d_{xy} -symmetry nodes (magenta circles) and extra nodes (blue crosses) relative to the FS in k space. See text for details.

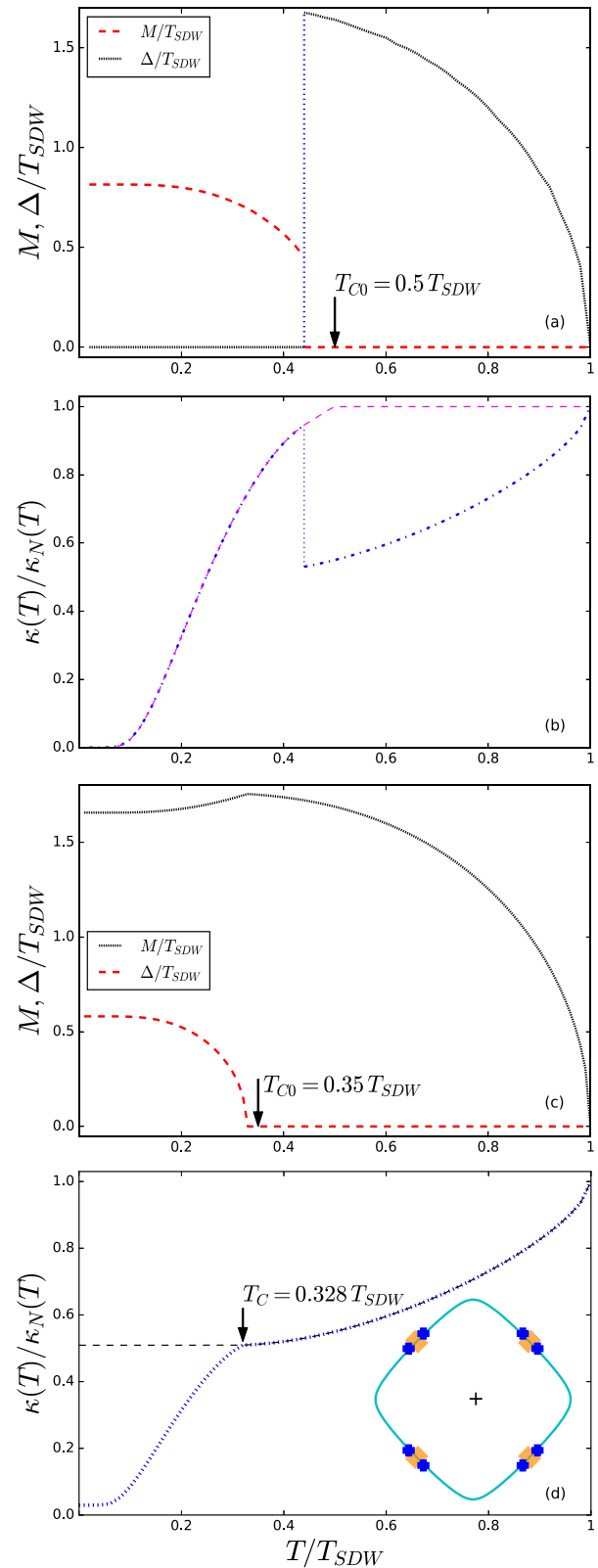


FIG. 8. Interplay of SDW and s -SC (a), (b) temperature dependence of M , Δ , and thermal conductivity when $T_{C0}/T_{SDW} = 0.5$. The SDW and SC states do not coexist, similarly to the d_{xy} case. (c), (d) Coexistence is possible for lower $T_{C0}/T_{SDW} = 0.35$; thermal conductivity at low temperatures reaches a finite value due to the emergent nodes, shown by the blue crosses in the inset of (d). See text for details.

commensurate SDW with ordering vector $\mathbf{Q} = (\pi, \pi)$. Coexistence of the SC and SDW orders is controlled by selecting a band structure with a Fermi surface, such that only a part of it is nested supporting SDW order, leaving the other part for SC. The amplitudes of the SC and SDW orders were determined self-consistently at all temperatures.

The nature of the coexisting phase depends, most importantly, on the properties of the SC order parameter connected by the nesting vector \mathbf{Q} . If the SDW order mixes up pairs with $\Delta_{\mathbf{k}+\mathbf{Q}} = -\Delta_{\mathbf{k}}$, as is the case for the $d_{x^2-y^2}$ SC symmetry, the two orders attract each other and naturally coexist [34]. Mixing states with $\Delta_{\mathbf{k}+\mathbf{Q}} = \Delta_{\mathbf{k}}$ (d_{xy} - or s -wave) results in competition of SDW and SC, although they can still coexist for weak enough SC state arising inside the SDW phase.

One of the most interesting differences between the two versions of SC+SDW mixture is the spectrum of low-energy excitations. For SDW+ $d_{x^2-y^2}$ the nodes of the SC order appear on the nested parts of the FS and thus appear under the SDW gap, resulting in the fully gapped system. On the other hand, in SDW+ d_{xy} the symmetry-protected SC nodes appear on the non-nested part of the Fermi surface. In addition to those, we found an additional set of robust nodes, appearing on the boundary of the folded Brillouin zone. These nodes are the remnants of the SDW-state Fermi surface and exist even in the s -wave superconducting state. They form an anisotropic Dirac cone of low-energy excitations.

Temperature dependence of the electronic heat conductivity in the SDW+SC system was computed using Boltzmann transport equation method, where the impurity scattering collision integral and quasiparticle lifetime were determined (in Born limit) from the correct coherence factors of the coexistence phase. Our numerical analysis shows that there are significant differences in the thermal conductivity behavior that are determined by the symmetry of the order parameter, FS topology, and the nodal structure of the coexistence phase.

For the SDW+ $d_{x^2-y^2}$ combination, the nodal structure of SC order parameter is immersed under the SDW gap producing only gapped excitations that result in the rapid drop of the thermal conductivity below the second-order coexistence transition and typical exponentially-small residual $\kappa(T)/T$. On the other hand, in the SDW+ s , d_{xy} system, the two orders may completely avoid each other, resulting in the trivial first-order jump in heat conductivity. However, the most interesting situation arises when SC does not replace SDW completely at low temperature, and they coexist. The nodal quasiparticles are preserved in this case, and even new Dirac-like excitations appear in both d_{xy} and s -wave systems. These low-energy excitations lead to a finite residual κ/T in the $T \rightarrow 0$ limit for both the SDW+ s , d_{xy} systems.

ACKNOWLEDGMENTS

Numerical work was done on the Pacific Research Platform's Nautilus HyperCluster. S.S.C would like to thank Nazmul Kazi for help with implementation of the numerical analysis.

APPENDIX: TWO-STEP DIAGONALIZATION

We wish to clarify certain aspects of the diagonalization procedure that we have employed in this paper and compare it with previous work done on similar models by several authors [39]. We have diagonalized the full mean field Hamiltonian $\hat{\mathcal{H}}(\mathbf{k})$ in (7) using a unitary Bogoliubov transformation $\hat{B}(\mathbf{k})$ by numerically computing eigenvectors in the RBZ. In literature a 'two-step' procedure is often employed to diagonalize the model Hamiltonian (7), which yields identical results to our case, provided all pairing terms are properly accounted for. Step one of the two-step process involves diagonalizing the first two terms in (2) via a unitary transformation by introducing new quasiparticle operators $\alpha_{\mathbf{k}}, \beta_{\mathbf{k}}$ for the two SDW bands with dispersions $E_{\mathbf{k}}^{\alpha,\beta} = \xi_{\mathbf{k}}^{\pm} \pm \sqrt{(\xi_{\mathbf{k}}^{\mp})^2 + M^2}$. Namely the first two terms in the Hamiltonian are written as

$$H_0 + H_{\text{SDW}} = \sum_{\sigma} \sum_{\mathbf{k} \in \text{RBZ}} \psi_{\mathbf{k}i}^{\dagger} h_{1\mathbf{k}ij} \psi_{\mathbf{k}j} \quad (A1)$$

$$h_{1\mathbf{k}ij} = \begin{pmatrix} \xi_{\mathbf{k}} & \text{sgn}(\sigma)M \\ \text{sgn}(\sigma)M & \xi_{\mathbf{k}+\mathbf{Q}} \end{pmatrix},$$

where $\psi_{\mathbf{k}i}^{\dagger} = (c_{\mathbf{k}\sigma}^{\dagger}, c_{\mathbf{k}+\mathbf{Q}\sigma}^{\dagger})$ defines the Nambu basis. The above Hamiltonian is then diagonalized using the following Bogoliubov transformation

$$c_{\mathbf{k}\sigma} = u_{\mathbf{k}} \alpha_{\mathbf{k}\sigma} - \text{sgn}(\sigma) v_{\mathbf{k}} \beta_{\mathbf{k}\sigma} \quad (A2)$$

$$c_{\mathbf{k}+\mathbf{Q}\sigma} = \text{sgn}(\sigma) v_{\mathbf{k}} \alpha_{\mathbf{k}\sigma} + u_{\mathbf{k}} \beta_{\mathbf{k}\sigma},$$

where $u_{\mathbf{k}} = \sqrt{\frac{1}{2}(1 + \frac{\xi_{\mathbf{k}}}{\Pi_{\mathbf{k}}})}$, $v_{\mathbf{k}} = \sqrt{\frac{1}{2}(1 - \frac{\xi_{\mathbf{k}}}{\Pi_{\mathbf{k}}})}$ with $\Pi_{\mathbf{k}} = \sqrt{(\xi_{\mathbf{k}}^{\pm})^2 + M^2}$. The diagonalization reduces (A1) to

$$H_0 + H_{\text{SDW}} = \sum_{\mathbf{k} \in \text{RBZ}} \sum_{\sigma} E_{\mathbf{k}}^{\alpha} \alpha_{\mathbf{k}\sigma}^{\dagger} \alpha_{\mathbf{k}\sigma} + E_{\mathbf{k}}^{\beta} \beta_{\mathbf{k}\sigma}^{\dagger} \beta_{\mathbf{k}\sigma}. \quad (A3)$$

In step two, the same unitary transformation (A2) is applied to the superconducting term H_{SC} in (2), which when combined with (A3), results in the following mean field Hamiltonian

$$H_0 + H_{\text{SDW}} + H_{\text{SC}} = \frac{1}{2} \sum_{\mathbf{k} \in \text{RBZ}} \gamma_{\mathbf{k}i}^{\dagger} h_{\mathbf{k}ij} \gamma_{\mathbf{k}j} \quad (A4)$$

$$h_{\mathbf{k}ij} = \begin{pmatrix} E_{\mathbf{k}}^{\alpha} & \Delta_{\mathbf{k}}^{\alpha} & 0 & \Delta_{\mathbf{k}}^{\alpha\beta} \\ \Delta_{\mathbf{k}}^{\alpha} & -E_{\mathbf{k}}^{\alpha} & -\Delta_{\mathbf{k}}^{\alpha\beta} & 0 \\ 0 & -\Delta_{\mathbf{k}}^{\alpha\beta} & E_{\mathbf{k}}^{\beta} & \Delta_{\mathbf{k}}^{\beta} \\ \Delta_{\mathbf{k}}^{\alpha\beta} & 0 & \Delta_{\mathbf{k}}^{\beta} & -E_{\mathbf{k}}^{\beta} \end{pmatrix},$$

where $\gamma_{\mathbf{k}i}^{\dagger} = (\alpha_{\mathbf{k}\uparrow}^{\dagger}, \alpha_{-\mathbf{k}\downarrow}, \beta_{\mathbf{k}\uparrow}^{\dagger}, \beta_{-\mathbf{k}\downarrow})$ defines the Nambu basis. The superconducting order parameters dressed by the SDW coherence factors are given by $\Delta_{\mathbf{k}}^{\alpha} = u_{\mathbf{k}}^2 \Delta_{\mathbf{k}} - v_{\mathbf{k}}^2 \Delta_{\mathbf{k}+\mathbf{Q}}$, $\Delta_{\mathbf{k}}^{\beta} = u_{\mathbf{k}}^2 \Delta_{\mathbf{k}+\mathbf{Q}} - v_{\mathbf{k}}^2 \Delta_{\mathbf{k}}$, and $\Delta_{\mathbf{k}}^{\alpha\beta} = u_{\mathbf{k}} v_{\mathbf{k}} (\Delta_{\mathbf{k}} + \Delta_{\mathbf{k}+\mathbf{Q}})$. If one neglects the off-diagonal blocks in the above Hamiltonian, i.e., interband pairing terms of the form $\langle \alpha_{\mathbf{k}\uparrow}^{\dagger} \beta_{-\mathbf{k}\downarrow}^{\dagger} \rangle$ etc., then (A4) can be diagonalized by two independent Bogoliubov transformations which yield the energy dispersions [39] $\mathcal{E}_{\mathbf{k}}^{\gamma} = \sqrt{(E_{\mathbf{k}}^{\gamma})^2 + (\Delta_{\mathbf{k}}^{\gamma})^2}$ where $\gamma = (\alpha, \beta)$. We do not neglect the

interband pairing terms of the form $\langle \alpha_{\mathbf{k}\uparrow}^\dagger \beta_{-\mathbf{k}\downarrow}^\dagger \rangle$ when diagonalizing (A4). If we diagonalize (A4) keeping the off diagonal terms [51], we get the following dispersion relation

$$E_{1,2}^2 = \frac{1}{2}(\Xi_{\mathbf{k}} \pm \Sigma_{\mathbf{k}})$$

$$\Xi_{\mathbf{k}} = [(E_{\mathbf{k}}^\alpha)^2 + (E_{\mathbf{k}}^\beta)^2 + (\Delta_{\mathbf{k}}^\alpha)^2 + (\Delta_{\mathbf{k}}^\beta)^2 + 2\Delta_{\mathbf{k}}^{\alpha\beta}]$$

$$\Sigma_{\mathbf{k}} = [\Pi_{\mathbf{k}}^2 - 4((E_{\mathbf{k}}^\beta)^2 (\Delta_{\mathbf{k}}^\alpha)^2 + 2E_{\mathbf{k}}^\alpha E_{\mathbf{k}}^\beta (\Delta_{\mathbf{k}}^{\alpha\beta})^2 + ((\Delta_{\mathbf{k}}^{\alpha\beta})^2 + \Delta_{\mathbf{k}}^\alpha \Delta_{\mathbf{k}}^\beta)^2 + (E_{\mathbf{k}}^\alpha)^2 ((E_{\mathbf{k}}^\beta)^2 + (\Delta_{\mathbf{k}}^\beta)^2))]^{\frac{1}{2}}. \quad (\text{A5})$$

Upon substituting the expressions for $\Delta_{\mathbf{k}}^\alpha$, $\Delta_{\mathbf{k}}^\beta$, $\Delta_{\mathbf{k}}^{\alpha\beta}$, $E_{\mathbf{k}}^\alpha$, and $E_{\mathbf{k}}^\beta$, one recovers the eigenvalues given in (13).

-
- [1] J. Ziman, *Electrons and Phonons* (Clarendon Press, Oxford, 1960).
- [2] J. Bardeen, G. Rickayzen, and L. Tewordt, *Phys. Rev.* **113**, 982 (1959).
- [3] B. T. Geilikman, *JETP* **7**, 721 (1958).
- [4] C. Pfeleiderer, *Rev. Mod. Phys.* **81**, 1551 (2009).
- [5] D. J. Van Harlingen, *Rev. Mod. Phys.* **67**, 515 (1995).
- [6] C. C. Tsuei and J. R. Kirtley, *Rev. Mod. Phys.* **72**, 969 (2000).
- [7] L. Taillefer, *Annu. Rev. Condens. Matter Phys.* **1**, 51 (2010).
- [8] D. F. Agterberg, J. S. Davis, S. D. Edkins, E. Fradkin, D. J. Van Harlingen, S. A. Kivelson, P. A. Lee, L. Radzihovsky, J. M. Tranquada, and Y. Wang, *Annu. Rev. Condens. Matter Phys.* **11**, 231 (2020).
- [9] H.-H. Wen and S. Li, *Annu. Rev. Condens. Matter Phys.* **2**, 121 (2011).
- [10] G. R. Stewart, *Rev. Mod. Phys.* **83**, 1589 (2011).
- [11] A. Chubukov, *Annu. Rev. Condens. Matter Phys.* **3**, 57 (2012).
- [12] B. Arfi and C. J. Pethick, *Phys. Rev. B* **38**, 2312 (1988).
- [13] P. Hirschfeld, D. Vollhardt, and P. Wölfle, *Solid State Commun.* **59**, 111 (1986).
- [14] K. Scharnberg, D. Walker, H. Monien, L. Tewordt, and R. A. Klemm, *Solid State Commun.* **60**, 535 (1986).
- [15] H. Monien, K. Scharnberg, and D. Walker, *Solid State Commun.* **63**, 263 (1987).
- [16] A. C. Durst and P. A. Lee, *Phys. Rev. B* **62**, 1270 (2000).
- [17] M. J. Graf, S.-K. Yip, J. A. Sauls, and D. Rainer, *Phys. Rev. B* **53**, 15147 (1996).
- [18] Y. Matsuda, K. Izawa, and I. Vekhter, *J. Phys.: Condens. Matter* **18**, R705 (2006).
- [19] H. Shakeripour, C. Petrovic, and L. Taillefer, *New J. Phys.* **11**, 055065 (2009).
- [20] B. Lake, H. M. Rønnow, N. B. Christensen, G. Aeppli, K. Lefmann, D. F. McMorrow, P. Vorderwisch, P. Smeibidl, N. Mangkorntong, T. Sasagawa, M. Nohara, H. Takagi, and T. E. Mason, *Nature (London)* **415**, 299 (2002).
- [21] N. D. Mathur, F. M. Grosche, S. R. Julian, I. R. Walker, D. M. Freye, R. K. W. Haselwimmer, and G. G. Lonzarich, *Nature (London)* **394**, 39 (1998).
- [22] S. Badoux, W. Tabis, F. Laliberté, G. Grissonnanche, B. Vignolle, D. Vignolles, J. Béard, D. A. Bonn, W. N. Hardy, R. Liang *et al.*, *Nature (London)* **531**, 210 (2016).
- [23] D. Y. Kim, S.-Z. Lin, F. Weickert, M. Kenzelmann, E. D. Bauer, F. Ronning, J. D. Thompson, and R. Movshovich, *Phys. Rev. X* **6**, 041059 (2016).
- [24] N. Doiron-Leyraud, P. Auban-Senzier, S. René de Cotret, C. Bourbonnais, D. Jérôme, K. Bechgaard, and L. Taillefer, *Phys. Rev. B* **80**, 214531 (2009).
- [25] A. C. Durst and S. Sachdev, *Phys. Rev. B* **80**, 054518 (2009).
- [26] P. R. Schiff and A. C. Durst, *Phys. Rev. B* **81**, 054504 (2010).
- [27] X. F. Sun, S. Ono, X. Zhao, Z. Q. Pang, Y. Abe, and Y. Ando, *Phys. Rev. B* **77**, 094515 (2008).
- [28] S. Chatterjee, S. Sachdev, and A. Eberlein, *Phys. Rev. B* **96**, 075103 (2017).
- [29] M. J. Graf, S.-K. Yip, and J. A. Sauls, *J. Low Temp. Phys.* **102**, 367 (1996).
- [30] M. Graf, S.-K. Yip, and J. Sauls, *Phys. B: Condens. Matter* **280**, 176 (2000).
- [31] B. Lussier, B. Ellman, and L. Taillefer, *Phys. Rev. B* **53**, 5145 (1996).
- [32] K. Machida, *J. Phys. Soc. Jpn.* **50**, 2195 (1981).
- [33] K. Machida and M. Kato, *Phys. Rev. Lett.* **58**, 1986 (1987).
- [34] M. Kato and K. Machida, *Phys. Rev. B* **37**, 1510 (1988).
- [35] J. E. Hirsch, *Phys. Rev. B* **31**, 4403 (1985).
- [36] M. Kato, K. Machida, and M. aki Ozaki, *Jpn. J. Appl. Phys.* **26**, 1245 (1987).
- [37] A. B. Vorontsov, M. G. Vavilov, and A. V. Chubukov, *Phys. Rev. B* **81**, 174538 (2010).
- [38] R. M. Fernandes, D. K. Pratt, W. Tian, J. Zarestky, A. Kreyssig, S. Nandi, M. G. Kim, A. Thaler, N. Ni, P. C. Canfield, R. J. McQueeney, J. Schmalian, and A. I. Goldman, *Phys. Rev. B* **81**, 140501(R) (2010).
- [39] J.-P. Ismer, I. Eremin, E. Rossi, D. K. Morr, and G. Blumberg, *Phys. Rev. Lett.* **105**, 037003 (2010).
- [40] V. P. Mineev and K. Samokin, *Introduction to Unconventional Superconductivity* (Gordon and Breach Science Publishers, Amsterdam, 1998).
- [41] B. Arfi, *Phys. Rev. B* **47**, 523 (1993).
- [42] L. Fritz and S. Sachdev, *Phys. Rev. B* **80**, 144503 (2009).
- [43] K. Damle and S. Sachdev, *Phys. Rev. B* **56**, 8714 (1997).
- [44] S. Sachdev, *Phys. Rev. B* **57**, 7157 (1998).
- [45] T. Senthil, M. Vojta, and S. Sachdev, *Phys. Rev. B* **69**, 035111 (2004).
- [46] M. Methfessel and A. T. Paxton, *Phys. Rev. B* **40**, 3616 (1989).
- [47] C. J. Pethick and D. Pines, *Phys. Rev. Lett.* **57**, 118 (1986).
- [48] M. S. Kim, Z. P. Yin, L. L. Zhao, E. Morosan, G. Kotliar, and M. C. Aronson, *Phys. Rev. B* **84**, 075112 (2011).
- [49] T. A. Sayles, W. M. Yuhasz, J. Paglione, T. Yanagisawa, J. R. Jeffries, M. B. Maple, Z. Henkie, A. Pietraszko, T. Cichorek, R. Wawryk *et al.*, *Phys. Rev. B* **77**, 144432 (2008).
- [50] F. Steckel, S. Rodan, R. Hermann, C. G. F. Blum, S. Wurmehl, B. Büchner, and C. Hess, *Phys. Rev. B* **90**, 134411 (2014).
- [51] A. T. Rømer, I. Eremin, P. J. Hirschfeld, and B. M. Andersen, *Phys. Rev. B* **93**, 174519 (2016).

CONCLUSION

In this thesis the problem of coexistence of Spin Density Waves and singlet superconductivity was studied. We considered a single-band electronic system where spin-singlet Superconducting order can appear inside a collinear Spin-density-wave phase. We treat both the orders on the same footing within the mean-field approximation. It is based on a tight-binding model on a square lattice with a commensurate SDW with ordering vector $\mathbf{Q} = (\pi, \pi)$. Coexistence of the SC and SDW orders is controlled by selecting a band structure with a Fermi surface, such that only a part of it is nested supporting SDW order, leaving the other part for SC.

Firstly the the SC states were classified based on the the combined symmetry operations of parity: $\Delta_{-\mathbf{k}} = \pm\Delta_{\mathbf{k}}$ (even or odd) and translation by the nesting vector: $\Delta_{\mathbf{k}+\mathbf{Q}} = \pm\Delta_{\mathbf{k}}$ (even or odd). Then the self consistent gap equations were derived under the assumption that the pure SDW transition temperature T_{SDW} is greater than the pure SC transition temperature T_{C0} and then solved numerically. It was found that the symmetry classification has important consequences for the coexistence problem: If the SDW order mixes up pairs with $\Delta_{\mathbf{k}+\mathbf{Q}} = -\Delta_{\mathbf{k}}$, as is the case for the $d_{x^2-y^2}$ SC symmetry, the two orders cooperate with each other and naturally coexist. On the other hand mixing states with $\Delta_{\mathbf{k}+\mathbf{Q}} = \Delta_{\mathbf{k}}$ as in the case of d_{xy} - or s -wave, results in competition of SDW and SC, although they can still coexist for weak enough SC state arising inside the SDW phase.

Then the nature of the low energy excitations in the coexistence phase for the s - or d -wave SC states were analysed in detail. It was found that a combination of (π, π) -SDW and the $d_{x^2-y^2}$ pairing state results in fully gapped excitations. This is because the nodes of the SC order appear on the nested parts of the FS and thus appear under the SDW gap. On the other hand, in SDW+ d_{xy} the usual SC nodes appear on the non-nested part the Fermi surface and thus are not gapped by the SDW order. In addition to those, it was shown that

there are additional set of robust nodes, appearing on the boundary of the folded Brillouin zone. These nodes are the remnants of the SDW-state Fermi surface which are not gapped by the SC order and exist even in the s -wave superconducting state. They form an anisotropic Dirac cone of low-energy excitations.

Then the electronic thermal conductivity was calculated within the framework of the Boltzmann kinetic theory, using Born approximation for the impurity scattering collision integral. It was found that the heat transport signatures of various SC states emerging from collinear SDW order are quite distinct. The $d_{x^2-y^2}$ pairing state, where the Fermi surface is fully gapped results in a sharp fall of the thermal conductivity for $T < T_C$ and an exponential low- T behaviour. In the case of d_{xy} or s -wave pairing states, Dirac like excitations are present and hence lead to a finite residual thermal conductivity in the $T \rightarrow 0$ limit. The main result of the thesis is the different heat transport signatures of the various SC states emerging from the SDW background. As has been stated before, coexistent magnetic and superconducting states have been discovered in cuprates, iron-based superconductors, and heavy-fermion superconductors, therefore this theoretical study may be useful for identifying order parameter symmetry of such compounds.

One of the aims of this thesis was to emphasize the effects that arise from interplay of different orders, taking the coexistence SC and the SDW orders as a case study. Obviously one can study along similar lines, the interplay of other orders like nematicity [20, 31] relevant to iron based superconductors [22] and pair-density waves [2, 24] which may be relevant to the the Q - phase [1] of CeCoIn_5 . It would be interesting to see if the heat transport signatures of various SC states emerging from such orders have any special characteristic features. One of the drawbacks of our calculation is that for strong scattering centers one has to go beyond Born approximation [5, 75] to explain experimental data in cuprates and heavy fermions. The Boltzmann approach fails at low temperatures when low-energy quasiparticles cannot be well established due to impurity broadening [75]. As the energy states relevant to studying

transport phenomena lie within a thin shell around the Fermi surface, one can use the quasi-classical technique [37, 66] and derive quantum kinetic equations [79] to study thermal transport beyond the Boltzmann semi-classical method. It would be possible if the such a theory can be worked out, to study effects beyond the Born approximation, especially the unitary limit of resonant scattering [37].

REFERENCES CITED

- [1] D. F. Agterberg, M. Sigrist, and H. Tsunetsugu. Order parameter and vortices in the superconducting q phase of CeCoIn_5 . *Phys. Rev. Lett.*, 102:207004, May 2009.
- [2] Daniel F. Agterberg, J.C. Séamus Davis, Stephen D. Edkins, Eduardo Fradkin, Dale J. Van Harlingen, Steven A. Kivelson, Patrick A. Lee, Leo Radzihovsky, John M. Tranquada, and Yuxuan Wang. The physics of pair-density waves: Cuprate superconductors and beyond. *Annual Review of Condensed Matter Physics*, 11(1):231–270, 2020.
- [3] L. Alff, Y. Krockenberger, B. Welter, M. Schonecke, R. Gross, D. Manske, and M. Naito. A hidden pseudogap under the ‘dome’ of superconductivity in electron-doped high-temperature superconductors. *Nature*, 422(6933):698–701, Apr 2003.
- [4] Alexandros Aperis, Georgios Varelogiannis, and Peter B. Littlewood. Magnetic-field-induced pattern of coexisting condensates in the superconducting state of CeCoIn_5 . *Phys. Rev. Lett.*, 104:216403, May 2010.
- [5] B. Arfi and C. J. Pethick. Thermal conductivity and ultrasonic attenuation in heavy-fermion superconductors. *Phys. Rev. B*, 38:2312–2325, Aug 1988.
- [6] N. P. Armitage, P. Fournier, and R. L. Greene. Progress and perspectives on electron-doped cuprates. *Rev. Mod. Phys.*, 82:2421–2487, Sep 2010.
- [7] N. W. Ashcroft and N. D. Mermin. *Solid State Physics*, pages 346–348. Holt-Saunders, 1976.
- [8] J. Ashkenazi, C. G. Kuper, and Amiram Ron. Microscopic theory of coexistence of superconductivity and antiferromagnetism. *Phys. Rev. B*, 28:418–421, Jul 1983.
- [9] A. F. Bangura, J. D. Fletcher, A. Carrington, J. Levallois, M. Nardone, B. Vignolle, P. J. Heard, N. Doiron-Leyraud, D. LeBoeuf, L. Taillefer, S. Adachi, C. Proust, and N. E. Hussey. Small fermi surface pockets in underdoped high temperature superconductors: Observation of Shubnikov–de Haas oscillations in $\text{YBa}_2\text{Cu}_4\text{O}_8$. *Phys. Rev. Lett.*, 100:047004, Feb 2008.
- [10] J. Bardeen, L. N. Cooper, and J. R. Schrieffer. Theory of superconductivity. *Phys. Rev.*, 108:1175–1204, Dec 1957.
- [11] J. Bardeen, G. Rickayzen, and L. Tewordt. Theory of the Thermal Conductivity of Superconductors. *Phys. Rev.*, 113(4):982–994, 1959.
- [12] D. N. Basov and Andrey V. Chubukov. Manifesto for a higher T_c . *Nature Physics*, 7(4) : 272 – 276, Apr 2011.

- [13] J. G. Bednorz and K. A. Müller. Possible high- T_c superconductivity in the BaLaCuO system. *Zeitschrift für Physik B Condensed Matter*, 64(2):189–193, Jun 1986.
- [14] V I Belinicher and B I Sturman. The photogalvanic effect in media lacking a center of symmetry. *Soviet Physics Uspekhi*, 23(3):199–223, mar 1980.
- [15] E. Berg, C-C. Chen, and S. A. Kivelson. Stability of nodal quasiparticles in superconductors with coexisting orders. *Phys. Rev. Lett.*, 100:027003, Jan 2008.
- [16] N. N. Bogoliubov, V. V. Tolmachev, D. V. Shirkov, and R. Bruce Lindsay. A New Method in the Theory of Superconductivity. *Physics Today*, 13(5):44, January 1960.
- [17] Cristina Buzea and Kevin Robbie. Assembling the puzzle of superconducting elements: a review. *Superconductor Science and Technology*, 18(1):R1–R8, nov 2004.
- [18] Sudip Chakravarty, R. B. Laughlin, Dirk K. Morr, and Chetan Nayak. Hidden order in the cuprates. *Phys. Rev. B*, 63:094503, Jan 2001.
- [19] Shubhayu Chatterjee, Subir Sachdev, and Andreas Eberlein. Thermal and electrical transport in metals and superconductors across antiferromagnetic and topological quantum transitions. *Phys. Rev. B*, 96:075103, Aug 2017.
- [20] Xiao Chen, S. Maiti, R. M. Fernandes, and P. J. Hirschfeld. Nematicity and superconductivity: Competition versus cooperation. *Phys. Rev. B*, 102:184512, Nov 2020.
- [21] Sourav Sen Choudhury and Anton B. Vorontsov. Thermal transport in superconductors with coexisting spin density wave order. *Phys. Rev. B*, 103:104501, Mar 2021.
- [22] Amalia I. Coldea and Matthew D. Watson. The key ingredients of the electronic structure of fese. *Annual Review of Condensed Matter Physics*, 9(1):125–146, 2018.
- [23] L. L. Daemen and A. W. Overhauser. Superconductivity and charge-density waves. *Phys. Rev. B*, 40:124–128, Jul 1989.
- [24] Tanmoy Das. Nodeless superconducting gap induced by odd parity pair density wave in underdoped cuprates. *Annals of Physics*, 420:168251, 2020.
- [25] Adam C. Durst and Patrick A. Lee. Impurity-induced quasiparticle transport and universal-limit wiedemann-franz violation in d-wave superconductors. *Phys. Rev. B*, 62:1270–1290, Jul 2000.
- [26] Adam C. Durst and Subir Sachdev. Low-temperature quasiparticle transport in a d -wave superconductor with coexisting charge order. *Phys. Rev. B*, 80:054518, Aug 2009.
- [27] G. M. Eliashberg. Interactions between Electrons and Lat-tice Vibrations in a Superconductor. *JETP (U.S.S.R.)*, 11:696–702, 1960.

- [28] G. M. Eliashberg. Temperature Green's Function for Electrons in a Superconductor. *JETP (U.S.S.R.)*, 12:1000–1002, 1961.
- [29] Eric Fawcett. Spin-density-wave antiferromagnetism in chromium. *Rev. Mod. Phys.*, 60:209–283, Jan 1988.
- [30] Patrick Fazekas. *Lecture Notes on Electron Correlation and Magnetism*. WORLD SCIENTIFIC, 1999.
- [31] Eduardo Fradkin, Steven A. Kivelson, Michael J. Lawler, James P. Eisenstein, and Andrew P. Mackenzie. Nematic fermi fluids in condensed matter physics. *Annual Review of Condensed Matter Physics*, 1(1):153–178, 2010.
- [32] Eduardo Fradkin, Steven A. Kivelson, and John M. Tranquada. Colloquium: Theory of intertwined orders in high temperature superconductors. *Rev. Mod. Phys.*, 87:457–482, May 2015.
- [33] B. T. Geilikman. Thermal Conduction in Superconductors. *JETP (U.S.S.R.)*, 7(4):721, 1958.
- [34] P. G. De Gennes. *Superconductivity of Metals and Alloys*. W.A. Benjamin, New York, 1966.
- [35] B B Goodman. The thermal conductivity of superconducting tin below 1 k. *Proceedings of the Physical Society. Section A*, 66(3):217–227, mar 1953.
- [36] L. P. Gorkov. Energy Spectrum of Superconductors. *JETP (U.S.S.R.)*, 7:505, 1961.
- [37] M. J. Graf, S-K. Yip, J. A. Sauls, and D. Rainer. Electronic thermal conductivity and the Wiedemann-Franz law for unconventional superconductors. *Phys.Rev.*, 53(22):15147–15161, 1996.
- [38] Richard L. Greene, Pampa R. Mandal, Nicholas R. Poniatowski, and Tarapada Sarkar. The strange metal state of the electron-doped cuprates. *Annual Review of Condensed Matter Physics*, 11(1):213–229, 2020.
- [39] P. D. Grigoriev. Properties of superconductivity on a density wave background with small ungapped fermi surface parts. *Phys. Rev. B*, 77:224508, Jun 2008.
- [40] G. Grüner. The dynamics of charge-density waves. *Rev. Mod. Phys.*, 60:1129–1181, Oct 1988.
- [41] J. E. Hirsch. Two-dimensional hubbard model: Numerical simulation study. *Phys. Rev. B*, 31:4403–4419, Apr 1985.
- [42] Ryusuke Ikeda, Yuhki Hatakeyama, and Kazushi Aoyama. Antiferromagnetic ordering induced by paramagnetic depairing in unconventional superconductors. *Phys. Rev. B*, 82:060510, Aug 2010.

- [43] J.-P. Ismer, Ilya Eremin, Enrico Rossi, Dirk K. Morr, and G. Blumberg. Theory of multiband superconductivity in spin-density-wave metals. *Phys. Rev. Lett.*, 105:037003, Jul 2010.
- [44] Yoichi Kamihara, Takumi Watanabe, Masahiro Hirano, and Hideo Hosono. Iron-based layered superconductor LaFeAs with $T_c = 26\text{K}$. *Journal of the American Chemical Society*, 130(11):3296–3297, Mar 2008.
- [45] H. J. Kang, Pengcheng Dai, J. W. Lynn, M. Matsuura, J. R. Thompson, Shou-Cheng Zhang, D. N. Argyriou, Y. Onose, and Y. Tokura. Antiferromagnetic order as the competing ground state in electron-doped $\text{Nd}_{1.85}\text{Ce}_{0.15}\text{CuO}_4$. *Nature*, 423(6939):522–525, May 2003.
- [46] Masaru Kato and Kazushige Machida. Superconductivity and spin-density waves: Application to heavy-fermion materials. *Phys. Rev. B*, 37:1510–1519, Feb 1988.
- [47] Masaru Kato, Kazushige Machida, and Masa aki Ozaki. Stable superconducting state in the presence of spin density waves in URuSi₂. *Japanese Journal of Applied Physics*, 26(S3-2):1245, jan 1987.
- [48] Yasuyuki Kato, C. D. Batista, and I. Vekhter. Antiferromagnetic order in pauli-limited unconventional superconductors. *Phys. Rev. Lett.*, 107:096401, Aug 2011.
- [49] Takafumi Kita. Introduction to Nonequilibrium Statistical Mechanics with Quantum Field Theory. *Progress of Theoretical Physics*, 123(4):581–658, 04 2010.
- [50] G. Knebel, D. Aoki, D. Braithwaite, B. Salce, and J. Flouquet. Coexistence of antiferromagnetism and superconductivity in CeRhIn₅ under high pressure and magnetic field. *Phys. Rev. B*, 74:020501, Jul 2006.
- [51] Georg Knebel, Dai Aoki, Jean-Pascal Brison, and Jacques Flouquet. The quantum critical point in cerhin5: A resistivity study. *Journal of the Physical Society of Japan*, 77(11):114704, 2008.
- [52] A. A. Kordyuk. Pseudogap from arpes experiment: Three gaps in cuprates and topological superconductivity (review article). *Low Temperature Physics*, 41(5):319–341, 2015.
- [53] Pengcheng Li, F. F. Balakirev, and R. L. Greene. High-field hall resistivity and magnetoresistance of electron-doped $\text{Pr}_{2-x}\text{Ce}_x\text{CuO}_{4-\delta}$. *Phys. Rev. Lett.*, 99:047003, Jul 2007.
- [54] Kazushige Machida. Spin Density Wave and Superconductivity in Highly Anisotropic Materials. *Journal of the Physical Society of Japan*, 50(7):2195–2202, 1981.
- [55] Kazushige Machida and Masaru Kato. Inherent spin-density-wave instability in heavy-fermion superconductivity. *Phys. Rev. Lett.*, 58:1986–1988, May 1987.
- [56] Kazushige Machida, Kazuo Nokura, and Takeo Matsubara. New pairing state and partial destruction of pairing in antiferromagnetic superconductors. *Phys. Rev. Lett.*, 44:821–823, Mar 1980.

- [57] Saurabh Maiti and Andrey V. Chubukov. Superconductivity from repulsive interaction. *AIP Conference Proceedings*, 1550(1):3–73, 2013.
- [58] Y Matsuda, K Izawa, and I Vekhter. Nodal structure of unconventional superconductors probed by angle resolved thermal transport measurements. *Journal of Physics: Condensed Matter*, 18(44):R705–R752, oct 2006.
- [59] H. Matsui, K. Terashima, T. Sato, T. Takahashi, S.-C. Wang, H.-B. Yang, H. Ding, T. Uefuji, and K. Yamada. Angle-resolved photoemission spectroscopy of the antiferromagnetic superconductor $\text{Nd}_{1.87}\text{Ce}_{0.13}\text{CuO}_4$. *Phys. Rev. Lett.*, 94:047005, Feb 2005.
- [60] Bernd T. Matthias, E. Corenzwit, J. M. Vandenberg, and H. E. Barz. High superconducting transition temperatures of new rare earth ternary borides. *Proceedings of the National Academy of Sciences*, 74(4):1334–1335, 1977.
- [61] W. L. McMillan. Landau theory of charge-density waves in transition-metal dichalcogenides. *Phys. Rev. B*, 12:1187–1196, Aug 1975.
- [62] Amal Medhi, Saurabh Basu, and C. Y. Kadolkar. Coexistence of magnetism and superconductivity in a t – j bilayer. *Phys. Rev. B*, 76:235122, Dec 2007.
- [63] H. Miao, G. Fabbris, R. J. Koch, D. G. Mazzone, C. S. Nelson, R. Acevedo-Esteves, G. D. Gu, Y. Li, T. Yilmaz, K. Kaznatcheev, E. Vescovo, M. Oda, T. Kurosawa, N. Momono, T. Assefa, I. K. Robinson, E. S. Bozin, J. M. Tranquada, P. D. Johnson, and M. P. M. Dean. Charge density waves in cuprate superconductors beyond the critical doping. *npj Quantum Materials*, 6(1):31, Mar 2021.
- [64] V. P. Mineev and K.V. Samokin. *Introduction to Unconventional Superconductivity*. Gordon and Breach Science Publishers, Amsterdam, 1998.
- [65] Eun Gook Moon and Subir Sachdev. Competition between spin density wave order and superconductivity in the underdoped cuprates. *Phys. Rev. B*, 80:035117, Jul 2009.
- [66] A. Moor, A. F. Volkov, and K. B. Efetov. Quasiclassical description of a superconductor with a spin density wave. *Phys. Rev. B*, 83:134524, Apr 2011.
- [67] M. J. Nass, K. Levin, and G. S. Grest. Bardeen-Cooper-Schrieffer pairing in antiferromagnetic superconductors. *Phys. Rev. Lett.*, 46:614–617, Mar 1981.
- [68] M. J. Nass, K. Levin, and G. S. Grest. Impurity and spin-fluctuation effects in antiferromagnetic superconductors. *Phys. Rev. B*, 25:4541–4561, Apr 1982.
- [69] Zaira Nazario and David I. Santiago. Coexistence of spin-density wave and d-wave superconducting order parameter. *Phys. Rev. B*, 70:144513, Oct 2004.
- [70] Michael R. Norman. The challenge of unconventional superconductivity. *Science*, 332(6026):196–200, 2011.

- [71] A. W. Overhauser. Spin density waves in an electron gas. *Phys. Rev.*, 128:1437–1452, Nov 1962.
- [72] Johnpierre Paglione and Richard L. Greene. High-temperature superconductivity in iron-based materials. *Nature Physics*, 6(9):645–658, Sep 2010.
- [73] D. Parker, M. G. Vavilov, A. V. Chubukov, and I. I. Mazin. Coexistence of superconductivity and a spin-density wave in pnictide superconductors: Gap symmetry and nodal lines. *Phys. Rev. B*, 80:100508, Sep 2009.
- [74] R. Peierls. Zur theorie der elektrischen und thermischen leitfähigkeit von metallen. *Annalen der Physik*, 396(2):121–148, 1930.
- [75] C. J. Pethick and David Pines. Transport processes in heavy-fermion superconductors. *Phys. Rev. Lett.*, 57:118–121, Jul 1986.
- [76] D. K. Pratt, W. Tian, A. Kreyssig, J. L. Zarestky, S. Nandi, N. Ni, S. L. Bud’ko, P. C. Canfield, A. I. Goldman, and R. J. McQueeney. Coexistence of competing antiferromagnetic and superconducting phases in the underdoped $\text{Ba}(\text{Fe}_{0.953}\text{Co}_{0.047})_2\text{As}_2$ compound using x-ray and neutron scattering techniques. *Phys. Rev. Lett.*, 103:087001, Aug 2009.
- [77] Cyril Proust and Louis Taillefer. The remarkable underlying ground states of cuprate superconductors. *Annual Review of Condensed Matter Physics*, 10(1):409–429, 2019.
- [78] T. V. Ramakrishnan and C. M. Varma. Pairbreaking in superconductors near and below antiferromagnetic transitions. *Phys. Rev. B*, 24:137–143, Jul 1981.
- [79] Jørgen Rammer. *Quantum Field Theory of Non-equilibrium States*. Cambridge University Press, 2007.
- [80] A. T. Rømer, I. Eremin, P. J. Hirschfeld, and B. M. Andersen. Superconducting phase diagram of itinerant antiferromagnets. *Phys. Rev. B*, 93:174519, May 2016.
- [81] D. J. Scalapino. Superconductivity and spin fluctuations. *Journal of Low Temperature Physics*, 117(3):179–188, Nov 1999.
- [82] Philip R. Schiff and Adam C. Durst. Effect of coexisting order of various form and wave vector on low-temperature thermal conductivity in d -wave superconductors. *Phys. Rev. B*, 81:054504, Feb 2010.
- [83] J. R. Schrieffer. *Theory of Superconductivity*. Westview Press, Boulder, 1999.
- [84] H Shakeripour, C Petrovic, and Louis Taillefer. Heat transport as a probe of superconducting gap structure. *New Journal of Physics*, 11(5):055065, May 2009.

- [85] Z.-X. Shen, D. S. Dessau, B. O. Wells, D. M. King, W. E. Spicer, A. J. Arko, D. Marshall, L. W. Lombardo, A. Kapitulnik, P. Dickinson, S. Doniach, J. DiCarlo, T. Loeser, and C. H. Park. Anomalously large gap anisotropy in the a-b plane of $\text{Bi}_2\text{Sr}_2\text{CaCu}_2\text{O}_{8+\delta}$. *Phys. Rev. Lett.*, 70:1553–1556, Mar 1993.
- [86] S. Shimizu, H. Mukuda, Y. Kitaoka, A. Iyo, Y. Tanaka, Y. Kodama, K. Tokiwa, and T. Watanabe. Uniform mixing of antiferromagnetism and high-temperature superconductivity in electron-doped layers of four-layered $\text{Ba}_2\text{Ca}_3\text{Cu}_4\text{O}_8\text{F}_2$. *Phys. Rev. Lett.*, 98:257002, Jun 2007.
- [87] Manfred Sigrist. Introduction to unconventional superconductivity. *AIP Conference Proceedings*, 789(1):165–243, 2005.
- [88] F. Steglich, J. Aarts, C. D. Bredl, W. Lieke, D. Meschede, W. Franz, and H. Schäfer. Superconductivity in the presence of strong pauli paramagnetism: CeCu_2Si_2 . *Phys. Rev. Lett.*, 43:1892–1896, Dec 1979.
- [89] X. F. Sun, S. Ono, X. Zhao, Z. Q. Pang, Yasushi Abe, and Yoichi Ando. Doping dependence of phonon and quasiparticle heat transport of pure and dy-doped $\text{Bi}_2\text{Sr}_2\text{CaCu}_2\text{O}_{8+\delta}$ single crystals. *Phys. Rev. B*, 77:094515, Mar 2008.
- [90] Michael Tinkham. *Introduction to Superconductivity*. Dover Publications, 2nd edition, 2004.
- [91] Dirk van Delft and Peter Kes. The discovery of superconductivity. *Physics Today*, 63(9):38–43, 2010.
- [92] A. B. Vorontsov, M. G. Vavilov, and A. V. Chubukov. Superconductivity and spin-density waves in multiband metals. *Phys. Rev. B*, 81:174538, May 2010.
- [93] M. K. Wu, J. R. Ashburn, C. J. Torng, P. H. Hor, R. L. Meng, L. Gao, Z. J. Huang, Y. Q. Wang, and C. W. Chu. Superconductivity at 93 k in a new mixed-phase y-ba-cu-o compound system at ambient pressure. *Phys. Rev. Lett.*, 58:908–910, Mar 1987.
- [94] W. Yu, J. S. Higgins, P. Bach, and R. L. Greene. Transport evidence of a magnetic quantum phase transition in electron-doped high-temperature superconductors. *Phys. Rev. B*, 76:020503, Jul 2007.
- [95] Yubo Zhang, Christopher Lane, James W. Furness, Bernardo Barbiellini, John P. Perdew, Robert S. Markiewicz, Arun Bansil, and Jianwei Sun. Competing stripe and magnetic phases in the cuprates from first principles. *Proceedings of the National Academy of Sciences*, 117(1):68–72, 2020.